SYNTHESIS AND EVALUATION OF NOVEL TRI-ARYL PHOSPHONIUM DERIVATIVES AS POTENTIAL ANTI-CANCER AGENTS

A THESIS

SUBMITTED TO THE FACULTY OF

UNIVERISITY OF MINNESOTA

BY

ZACHARY GARDNER

IN PARTIAL FULFILLMENT OF THE REQUIREMENTS

FOR THE DEGREE OF

MASTER OF SCIENCE

Advisor: Venkatram R. Mereddy

January 2020

ACKNOWLEDGEMENTS

First, I would like to thank my advisor Dr. Venkatram R. Mereddy for all of his guidance, teaching, creativity, and bolstering affect throughout my master's degree at UMD. I am thankful for his continuous support and professional leadership over the years with the development as a research scientist. I would also like to thank Dr. Jon Holy for his support with biological aspects of this thesis, and Dr. Paul Kiprof for the guidance and investigation within my projects during my undergraduate and graduate careers at UMD.

I would like to acknowledge the Department of Chemistry and Biochemistry, College of Pharmacy, School of Medicine at University of Minnesota Duluth for their support and help at every step of the way, and all of my professor's time and knowledge who contributed to my overall education experience.

I would also like to thank my excellent lab members, who were not only mentors and colleagues, but also friends that helped with the daily tasks these past years, Shirisha Jonnalagadda, Sravan Jonnalagadda, Grady Nelson, Conor Ronayne, Lucas Solano, Erica Lueth, Tanner Schumacher, and Greeshma Kumpati. I would like to acknowledge Dr. Akira Yoshimura for his experimental and instrumental knowledge that assisted numerous times with compounds.

Lastly, I would like to acknowledge my family, friends and players, who supported me through the ups and downs through this journey.

ABSTRACT

The metabolic properties of cancer cells differ significantly from those of normal cells due to their high demand for energy for rapid proliferation and the need to produce anabolic building blocks for increasing cell mass. In fact, altered metabolism has been recognized as one of the critical hallmarks of cancer, and tumors characteristically exhibit aggressive glycolysis even in the presence of sufficient amounts of oxygen. Several recent studies have revealed additional levels of complexity and also recognized the importance of mitochondrial OxPhos to generate a large portion of ATP in cancer cells. OxPhos also plays an important role in cancer cell survival, drug resistance, relapse, and metastasis. OxPhos intermediates are utilized in the Kreb's cycle and many of which are shuttled into numerous biosynthetic pathways including fatty acids, amino acids, and nucleotides. Selective inhibition of OxPhos will lead to severe ATP depletion and dysfunction of the TCA cycle, starving cancer cells of critical components for cell survival and proliferation. In this regard, we designed, synthesized and evaluated mitochondrial OxPhos inhibitors with therapeutically relevant features. We undertook a structure-activity study using triphenylphosphine as a structural template. For this purpose, several modified phosphonium salts conjugated to α-halomethylacrylate template with high potential for reactivity within the mitochondria were synthesized. In this thesis, the design, synthesis, *in vitro* cell proliferation inhibition, mitochondrial activity, systemic toxicity in mice and *in vitro* fluorescence microscopy studies will be presented.

TABLE OF CONTENTS

LIST OF SCHEMES

LIST OF FIGURES

LIST OF ABBREVIATIONS

OxPhos	oxidative phosphorylation
ATP	adenosine triphosphate
NADH or NAD^+	nicotinamide adenine dinucleotide
$FADH_2$ or FADH	flavin adenine dinucleotide
TCA	tricarboxylic acid cycle
μmol	micromoles
μL	microliters
PBS	phosphate buffered saline
IC_{50}	inhibition of 50% of the activity or cell growth
SRB	sulforhodamine-B
mM	millimolar
3-BPA	3-bromopyruvic acid
nM	nanomolar
mg/Kg	dosage in milligram per kilogram of mouse
^1H NMR	proton (^1H) nuclear magnetic resonance spectrum
SAR	structure activity relationship
OH	hydroxy
OMe	methoxy
MTT	3-(4,5-dimethylthiazol-2-yl)-2,5-diphenyltetrazolium bromide
SEM	standard error of the mean
ECAR	extracellular acidification rate
OCR	oxygen consumption rate

FCCP	carbonyl cyanide-4-(trifluoromethoxy)phenylhydrazone
DMSO	dimethyl sulfoxide
CO_2	carbon dioxide
ETC	electron transport chain
ADP	adenosine diphosphate
TPP or TPP^+ or PPh_3	triphenylphosphonium cation
DCA	dichloracetate
PDK	pyruvate dehydrogenase kinase
EEDQ	N-ethoxycarbonyl-2-ethoxy-1,2-dihydroquinoline
AMPK	5’ AMP-activated protein kinase
DMF	dimethylformamide
STAT3	signal transducer and activator of transcription 3
A*k*t	protein kinase B
ERK	extracellular signal-regulated kinase
DOX	doxorubicin
PARP	poly (ADP-ribose) polymerase
DCC	N,N’-dicyclohexylcarbodiimide
NHS	N-hydroxysuccinide
DIPEA	N,N-diisopropylethylamine
HBTU	N,N,N’,N’-tetramethyl-*O*-(1H-benzotriazol-1-yl)uranium hexafluorophosphate

CHAPTER 1: INTRODUCTION

1A. Cellular and Cancer Metabolism

Cancer is one of the leading causes of mortality in humans. According to the American Cancer Society, it is estimated that in 2019, over 1.7 million new cases of cancer will be reported and over 600,000 patients will pass away from the fight with cancer[1]. Standard treatment options for cancer involve surgery, cytotoxic chemotherapies, and/or radiation therapy[1]. Modern cancer treatment strategies involve development of targeted therapeutic agents with small molecules, monoclonal antibodies, or immune-therapeutics to halt the tumor growth with decreased side effects when compared to classical non-selective and cytotoxic chemotherapy[2–11]. These targeted strategies take advantage of upregulated physiological processes in cancer, and recently reprogrammed energy metabolism of cancer cells may offer a selective targeting mechanism for new generation therapeutics. Solid tumors are able to use metabolic pathways at an upregulated rate to sustain growth. These metabolic pathways are chemical reactions that involve the breakdown of food to yield energy. Major sources of energy include carbohydrates, lipids, amino acids and other micronutrients present within what humans ingest. These energy sources are vital in the energetic and biosynthetic pathways that support cancer progression, and numerous metabolic pathways are reprogrammed and overexpressed to meet the needs of uncontrolled and rapid cell proliferation[12]. Specifically, glycolysis and mitochondrial oxidative phosphorylation (OxPhos) are processes that produce the majority of cellular energy[13–18]. Glycolysis is a 10-step enzymatic pathway that breaks down glucose into pyruvate and generates 2 molecules of ATP within the cytosol of the cell. Pyruvate will then be shuttled into the mitochondria and converted into acetyl CoA[12]. Once inside the mitochondrial matrix, pyruvate is converted to acetyl CoA which initiates the citric acid cycle. The citric acid cycle is an eight steps enzymatic pathway that generates molecules of 6 NADH, 2 $FADH_2$ and 26 ATP per one glucose molecule[16,17]. These energy transfer molecules will go through the oxidative phosphorylation (OxPhos) within the mitochondria producing energy. With numerous steps within the mitochondria and energy production possibilities, targeting the mitochondria with chemotherapeutic agents is a new important drug design for cancer treatment.

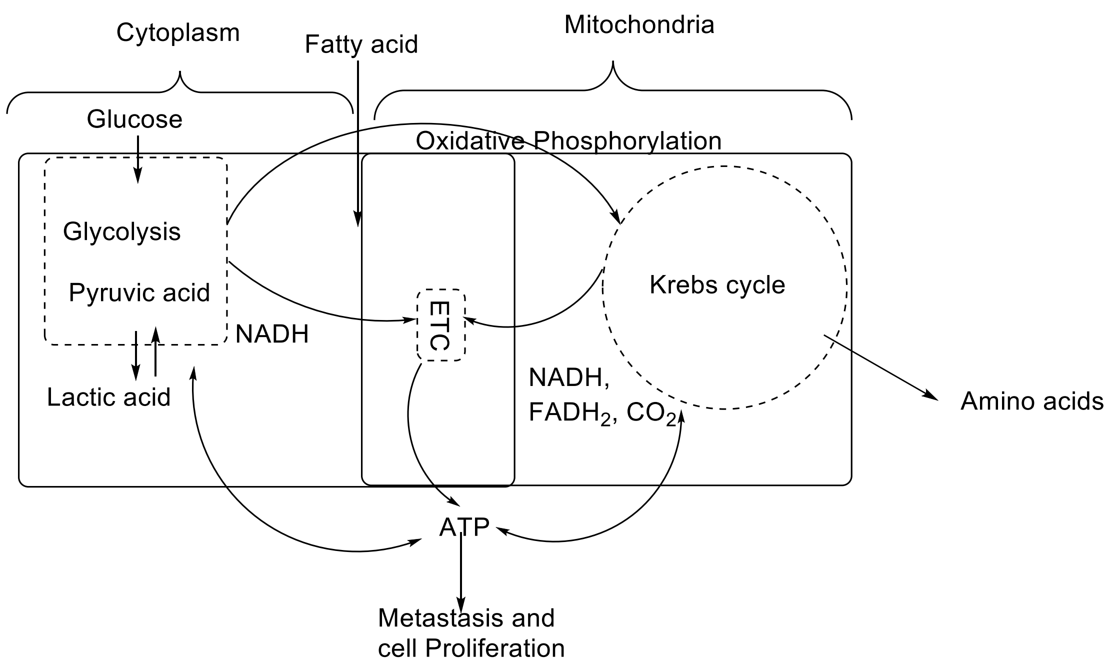

Figure 1.1: Cancer cell metabolism involving glycolysis and mitochondrial oxidative phosphorylation.

Due to there being over 200 types of cancers diagnoses possible with further subsection of those cancers based off the morphology and genetic makeup, disrupting the energetic pathways of cancers has become an important course of treatment. When a cell becomes malignant, the upregulation of energetic pathways occurs and possible metastasis invasion to other neighboring cell types growing the disease[15,18–20]. Cancer cells pursuing this idea of metastasis, grow based off the supply of oxygenation, pH levels, and the catabolic molecules for energy production[21]. Interestingly, cancer cells exhibit phenotypic changes that support both glycolysis and OxPhos to sustain enhanced proliferation and metastasis. With the buildup of glycolysis the end products, cancer cells reorganize their metabolic needs and undergo a shift of energy generation within the high oxygenated OxPhos process[16]. Once in the electron transport chain, TCA cycle metabolites in combination with cofactors, NADH, and $FADH_2$, will be able to create energy in the form of ATP that can be utilized for malignant cell functions including invasion and metastasis to other cells[20,22,23].

With tumor metabolism demanding a high amount of energy to support the rapid cell proliferation, altering the energy production is part of the hallmarks of cancer[18,24]. Primarily, tumors exhibit the ability to adapt to glycolytic cells to generate energy present within an oxygenated rich area (Warburg Effect)[15,17,18,25]. Recent studies have shown the ability to shift to a more mitochondrial oxidative phosphorylation (OxPhos) to generate high amounts of ATP in cancer cells. Disrupting the mitochondrial function will lead to the starving of the cellular components, causing cell death[26–28].

Due to the heterogenetic tumor microenvironments present within cancer, tumor pockets can be found in many locations with high and poor nutrient levels. The mitochondrial function is best in high levels of nutrients, but with minimal oxygen levels the electron transport chain can function[27–29]. With this heterogenous environment, cancer cells require high levels of mitochondrial biogenesis to be able to fuel the cancer growth. This mitochondrial function has the ability to adapt to produce a higher amount of mitochondrial mass[30,31]. Mitochondrial OxPhos presence within cancer cells oxidize lactate, the end product of glycolysis, into pyruvate causing a symbiotic metabolic plasticity with the glycolytic cancer cell. With the ability to pursue both pathways within the plasticity, cells increase the mitochondrial mass when proliferation is needed[32–34]. The increase of the mitochondrial mass establishes a mitochondrial membrane potential ($\Delta\psi_m$) that exploits a lipophilic cationic barrier and controls nutritional needs for cancer cells over normal cells[33,34].

1B. Triphenyl Phosphonium (TPP^+)

The mitochondrial membrane potential is established by the outer and inner membranes that shuttle several small molecules through. With the mitochondrial matrix having a negative membrane potential on the inner compartment, recent studies have used cationic molecules to be shuttled through. For this reason, triphenylphosphonium (TPP^+) based cations having a large ionic radius with the hydrophobic surface is an option for diffusion into the inner membrane (**Figure 1.2**). TPP^+ do not require any specific transporters for the mitochondrial translocation and have been shown to be inside the mitochondria compared to the cytoplasm[32–34].

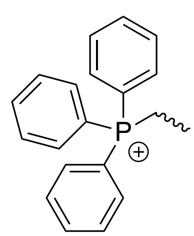

Triphenylphosphonium cation

Figure 1.2: Chemical structure of triphenylphosphonium cation(TPP^+)

With the inner mitochondrial membrane having a potential between -30 and -60 mV, the delocalized lipophilic cationic character of the TPP^+ can transport readily through the inner membrane[35]. Cancer cells usually have a higher membrane potential within the mitochondria compared to normal cells. With a higher membrane potential in cancer cells, the possibility of accumulation of TPP cations in the membrane is increased disrupting the membrane's overall function. The interaction of the TPP molecule with the mitochondria is based off the dynamics of the lipophilicity of the cation. Some of the represented examples of the TPP^+ conjugates are described below.

1B.1. Synthesis of TPP^+ Alkylation with simple hydrocarbon chains

To increase the hydrophobicity, Ross *et al.* used different carbon length alkyl chains to alkylate TPP, creating a more lipophilic TPP^+ molecules that would lead to faster mitochondrial uptake. They also combined the prototypical mitochondria-targeted antioxidant, MitoQ, with the elongated carbon-chain to the TPP cation (**Figure 1.3**)[33,36].

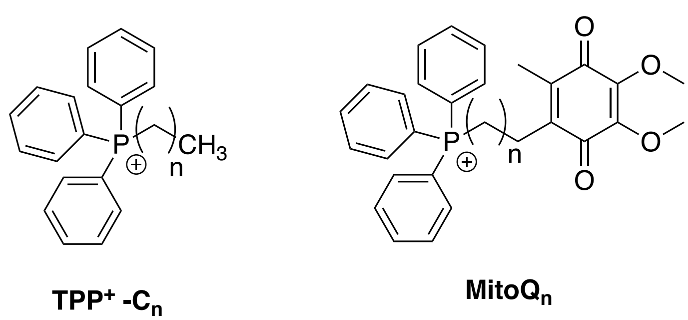

Figure 1.3: Example of alkylating TPP^+ with carbon chains and MitoQ

With increasing the lipophilicity with the carbon chain and MitoQ, Ross *et al.* showed that the cationic efflux rate increased, that lowered the energy barrier within the phospholipid bilayer, allowing for more lipophilic compounds transportation inside the mitochondrial membrane. The accumulation of alkyl-TPP^+ and MitoQ-TPP^+ within the mitochondrial membrane was shown from the simplest single carbon chain to 10-carbon chain. Longer carbon chain lengths was found to be more efficient delivery the TPP^+ into the mitochondria[36].

The TPP cationic character with an anti-cancer drug conjugate, there is a clear potential for selectively targeting the mitochondria of cancerous cells[37]. Numerous chemotherapy agents and/or potential chemotherapeutics that are being studied have this TPP^+ moiety to increase the mitochondrial interaction.

1B.2. Synthesis of TPP^+ with dichloroacetate (DCA)

Dichloroacetate (DCA) is a small molecule, which is a pyruvate dehydrogenase kinase inhibitor (PDK), present in numerous clinical trials for different cancers. With the phosphorylation of pyruvate kinase by PDK, pyruvate is promoted to stay within glycolysis and is not utilized within the mitochondria. With DCA present, inhibition of PDK allows for the increased pyruvate within the mitochondria inducing apoptotic signals within cancerous cells. Pathak *et al*. merged the DCA with the TPP^+ moiety to see if the presence of DCA is increased within the mitochondria (**Scheme 1.1**)[38–40].

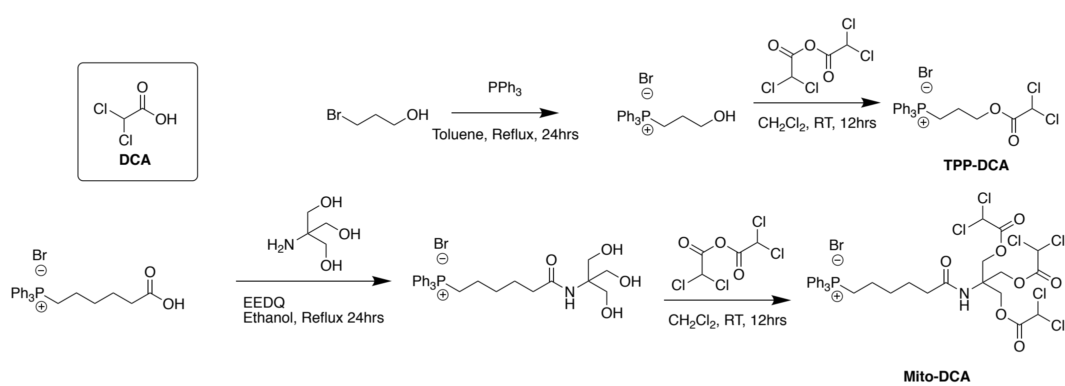

Scheme 1.1: Synthesis of DCA based molecules with TPP^+ moiety

Both these molecules with the TPP+ moiety showed an increased mitochondrial metabolism and downregulated glycolysis. The mitochondrial membrane potential and intracellular ATP levels increased as well and decreased the lactic acid levels intracellularly[33,40].

1B.3. Synthesis of TPP+ with metformin

Boukalova *et al.* synthesized derivatives with the most commonly used antidiabetic drug, metformin[41,42]. Metformin's ability to interact with the mitochondria allow for inhibition of mitochondrial respiration, leading to AMPK activation and bioenergetic reprogramming[43–45]. With metformin's abilities, the TPP+ cation was linked together with different carbon lengths in between (**Scheme 1.2**). With the increased carbon length, there was a decrease in mitochondrial respiration and proliferation of pancreatic cancer cells[42].

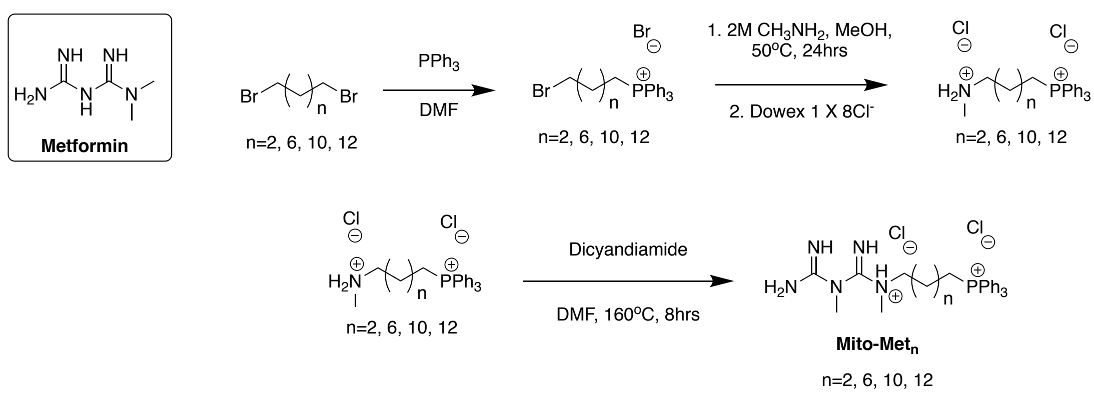

Scheme 1.2: Synthesis of metformin-based molecules with TPP+ moiety

1B.4. Synthesis of TPP+ with resveratrol

Biasutto *et al*. used a plant-based polyphenol, Resveratrol, that demonstrates anti-proliferative and pro-apoptotic effects in different cancerous cell lines[33,46]. The derivatives with the TPP$^+$ moiety, either the hydroxy group or acetylation group, showed an increased antiproliferative activity against colon tumor cells (**Scheme 1.3**). These derivatives show anticancer effects within the mitochondria due to the generation of H_2O_2, that is formed from superoxide formation within the mitochondrial complex I and III, and have shown results of being a mitochondrial uncoupler[33].

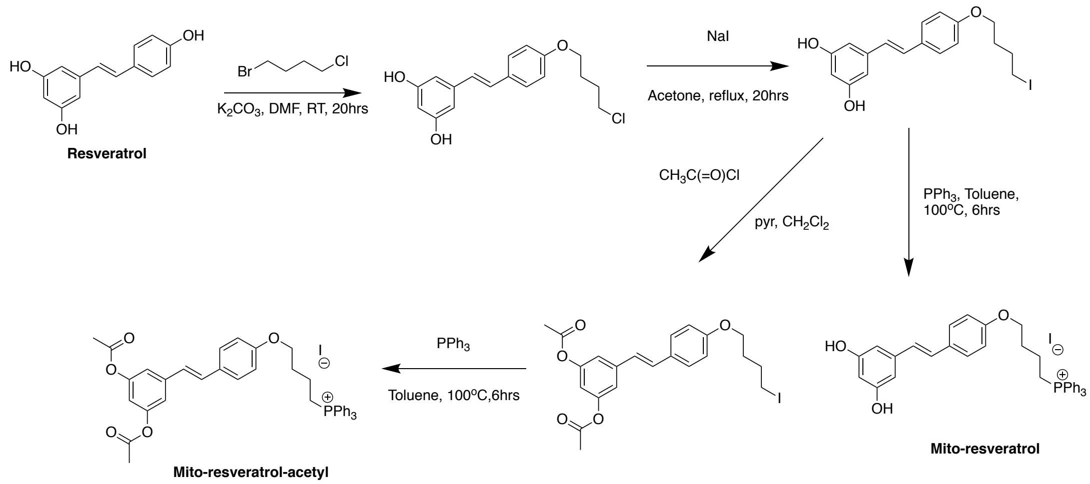

Scheme 1.3: Synthesis of resveratrol-based molecules with TPP$^+$ moiety

1B.5. Synthesis of TPP$^+$ with curcumin

Previous studies show that curcumin exhibits anti-inflammatory, antimutagenic, anticancer and antioxidant properties. Curcumin has shown anti-cancer effects in various cancer cell types, but limited efficacy, even at high doses, due to low bioavailability. Reddy *et at*. synthesized curcumin derivatives with the TPP$^+$ moiety (**Scheme 1.4**) to increase the bioavailability within the body[33,47].

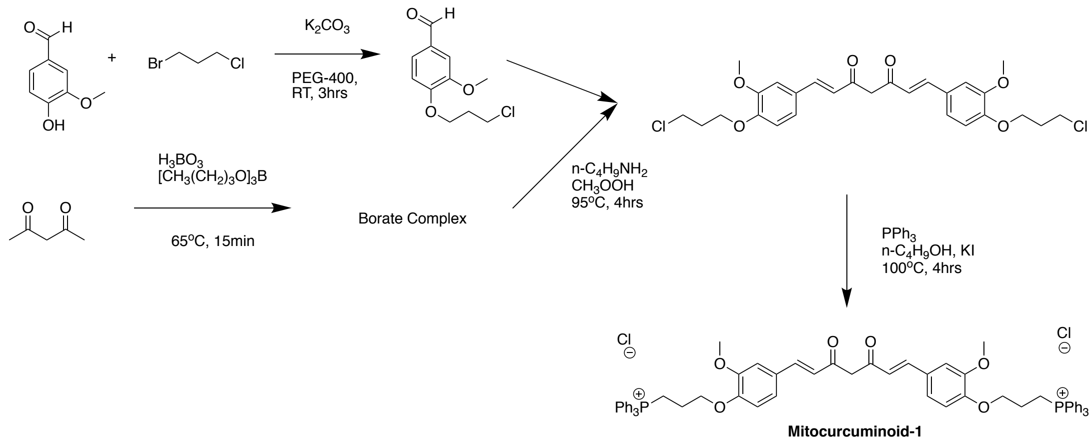

Scheme 1.4: Synthesis of curcumin-based molecules with TPP^+ moiety

The mitocurcuminoids demonstrated antiproliferative effects in various cancer cells lines. The cancerous damage was due to induction of mitochondrial superoxide formation, inhibition of STAT3 and A*k*t phosphorylation, enhanced ERK phosphorylation, and upregulation of proapoptotic BNIP3 expression[33].

1B.6. Synthesis of TPP^+ with doxorubicin

Cancerous cells have the ability to become resistant to treatment within the course of treatment. Doxorubicin (DOX) is an antitumor agent that is widely used for the treatment of various cancers. During the course of treatment, cancerous cells develop drug resistance to DOX. Han *et al*. used the TPP^+ moiety with DOX to synthesis a prodrug that could be evaluated with minimal drug-resistance(**Scheme 1.5**)[48].

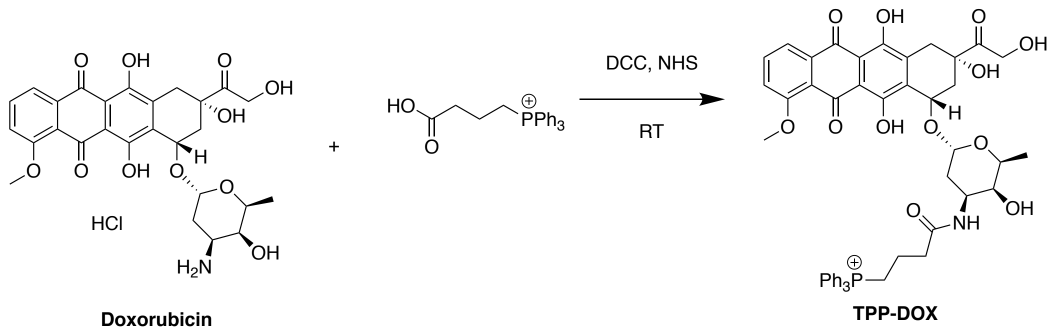

Scheme 1.5: Synthesis of doxorubicin-based molecules with TPP$^+$ moiety

TPP-DOX was evaluated for the toxicity against breast cancer cells and DOX-resistant cell lines. TPP-DOX compared to DOX was evaluated to accumulate higher within the DOX-resistant cell lines and was more potent. TTP-DOX with the DOX-resistant cancer cells also induced the cleavage of caspace-3, PARP, and apoptosis[33].

1B.7. Synthesis of TPP$^+$ with chlorambucil

Chlorambucil, a nitrogen mustard class of DNA alkylating agents, is usually used for leukemia, lymphomas, macroglobulinemia, and solid tumors[34,49]. The issue with chlorambucil is the drug's stability, selectivity, and resistance within the cell. Millard *et al*. synthesized chlorambucil with the TPP$^+$ moiety to interact with the mitochondrial function (**Scheme 1.6**)[33,34].

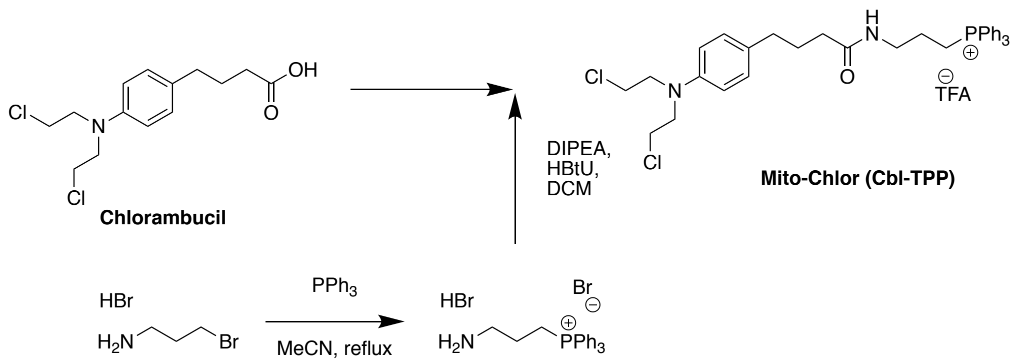

Scheme 1.6: Synthesis of chlorambucil-based molecules with TPP^+ moiety

The TPP^+-linked chlorambucil was evaluated against breast and pancreatic cancer cells showing 80-fold more potent. The compound also was potent within leukemia and pancreatic cancer tumor mouse models[33].

1C. Baylis-Hillman Reaction

The Baylis-Hillman (BH) reaction is an important C-C bond forming reaction in synthetic organic chemistry to obtain densely functionalized alcohols and amines in one step. This simple reaction requires 3 components: an activated alkene, electrophile, and a tertiary amine. This reaction is carried out by mixing the electrophilic aldehyde/aldimines/activated ketones with α, β unsaturated esters, ketones, or nitriles, in the presence of a catalytic amount of nucleophilic base, 1,4-diazabicyclo[2.2.2]octane (DABCO) to result in functionalized allyl alcohols in one step (**Scheme 1.7**)[50–57]. This reaction typically does not require usage of any solvents, heat, or any special reaction conditions and usually provides high yields of the functionalized alcohols. The BH alcohols can then be converted into a leaving group, such as an acetate in the presence of different nucleophiles in S_N2' fashion or converted into an allyl bromide by reacting them with HBr/H_2SO_4 or PBr_3 (**Scheme 1.8**).

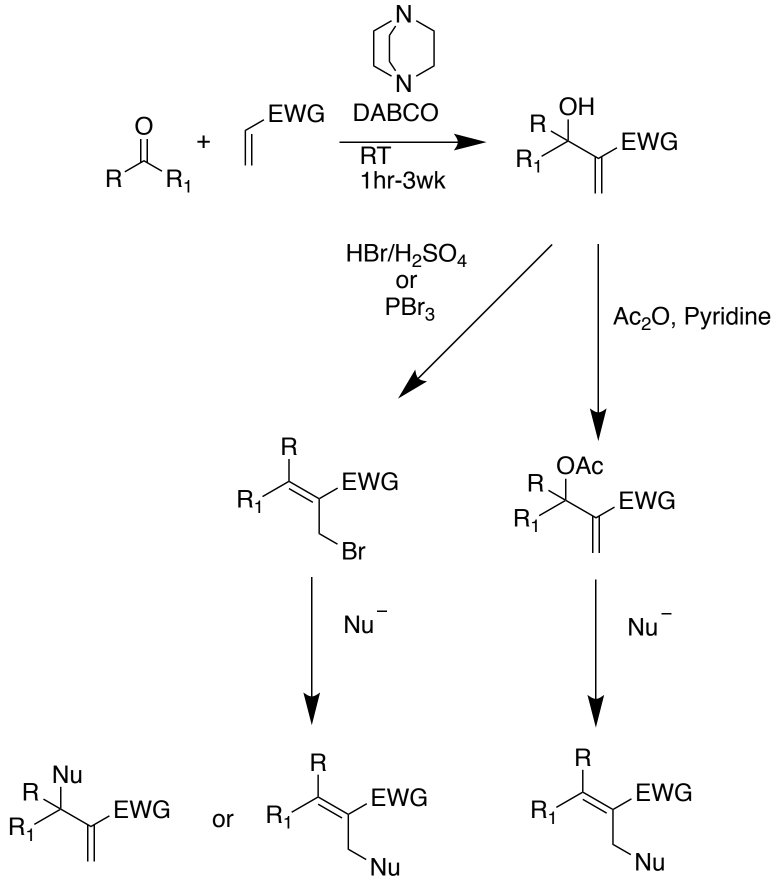

R and R_1= aliphatic, aromatic
EWG= CO_2R, CN, CH_3COCH_3, CONR

Scheme 1.7: General scheme of the Baylis-Hillman reaction and nucleophilic isomerization.

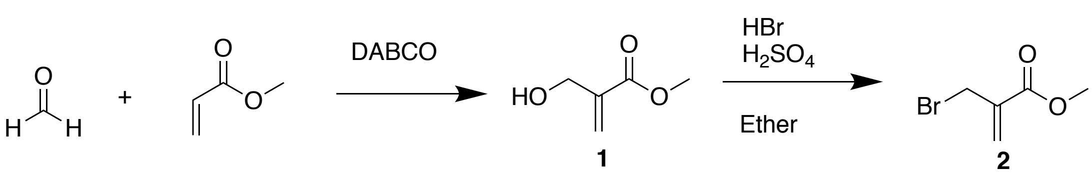

Scheme 1.8: Synthesis of BH alcohol and bromide from formaldehyde.

The BH bromide (**2**) allows for three different reactive opportunities for nucleophilic substitutions to occur. The BH bromide (**2**) can be involved in a direct S_N2 attack, S_N2' attack with allylic rearrangement, or a simple 1,4-addition to provide functionalized synthetic intermediates by a wide variety of nucleophiles containing C, O, S, and N atoms (**Scheme 1.9**)[58,59].

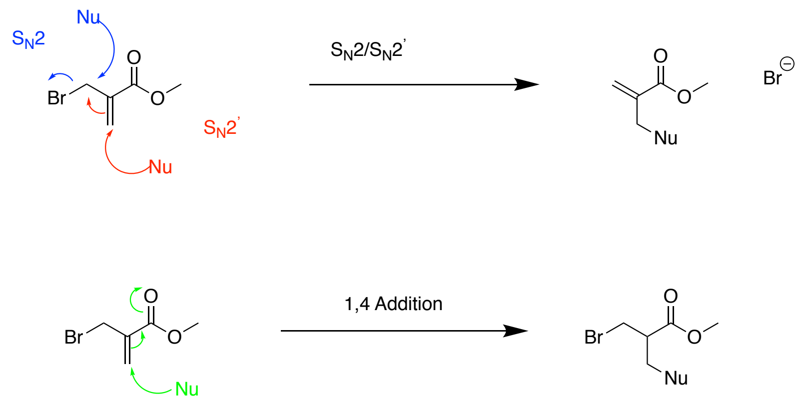

Scheme 1.9: S_N2, S_N2', and 1,4-addition capabilities of Baylis-Hillman bromides

1C.1. Synthesis of α-carboxycarbonyl allyl esters

Previous small molecule therapeutics using the BH reaction by our group has shown interesting results allowing for this BH bromide as an excellent starting material for anticancer drug development. The bromide was replaced with benzoates and the synthesized molecules retained there leaving group compacity and exhibited good *in vitro* and *in vivo* activity

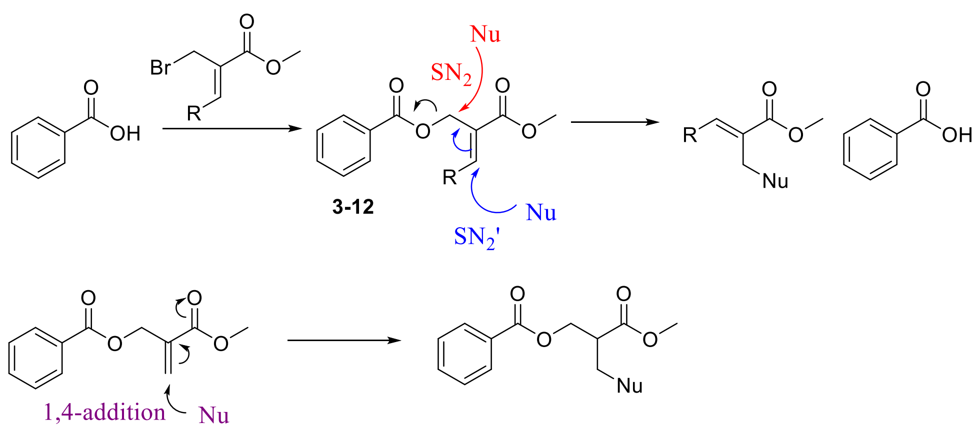

Scheme 1.10: S_N2, S_N2' and 1,4-addition reactions of synthesized α-carboxycarbonyl allyl esters

These synthesized compounds were evaluated by the cell proliferation inhibition studies on breast and pancreatic cancerous cell lines. The structure-activity relationship

(SAR) study determined that aromatic compounds resulted in an increased cell proliferation inhibition compared to aliphatic carboxylic acids. Substituted aromatic, electron donating or electron withdrawing, had minimal effect on the cell proliferation inhibition. The methoxy ester was determined to be the best structural moiety allowing for the S_N2/S_N2' mechanism to occur. The IC_{50} values of the α-carboxycarbonyl allyl esters **3-12** were within the 3- >100 μM range (**Figure 1.4**)[50,60,61].

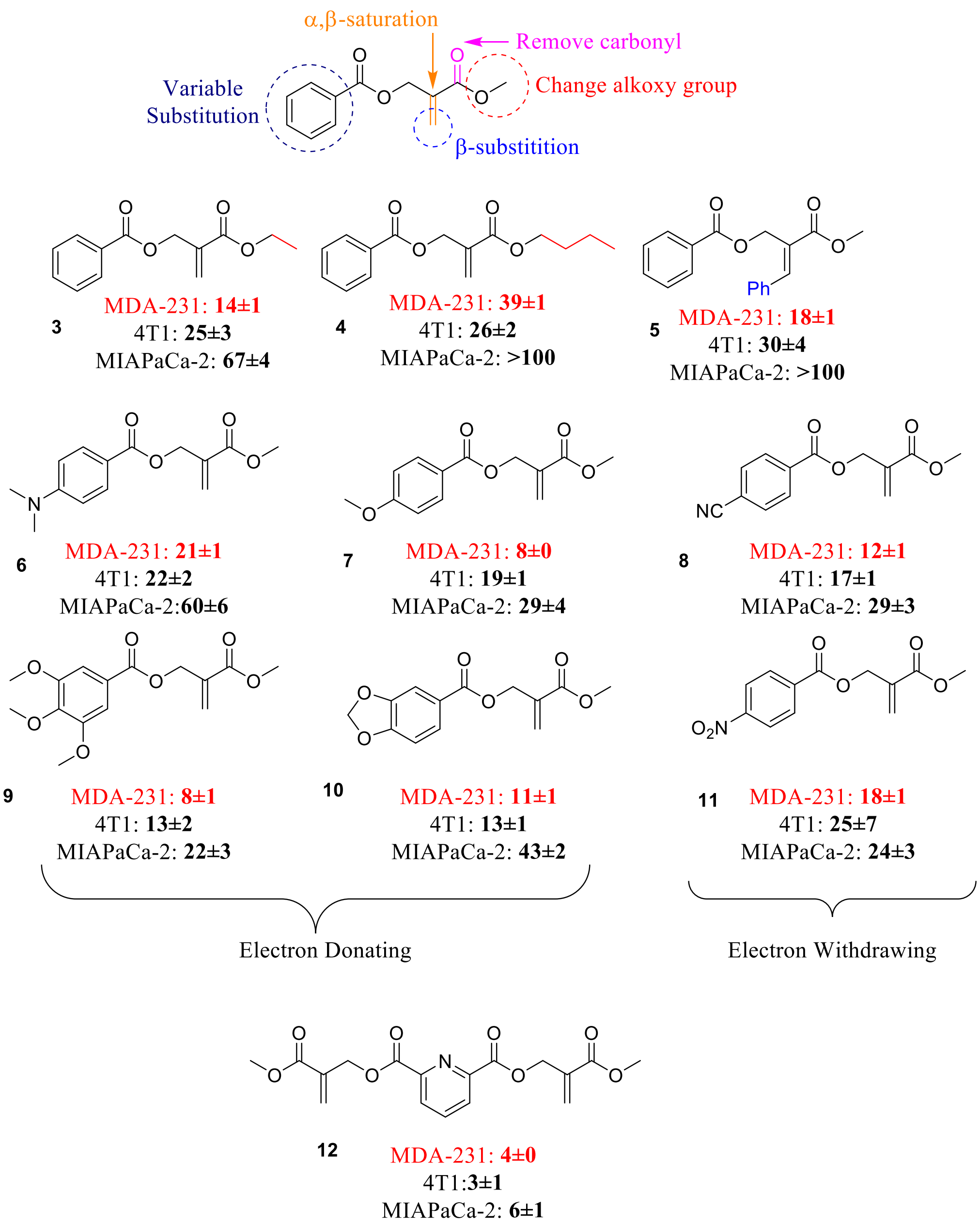

Figure 1.4: Cell proliferation IC_{50} values of α-carboxycarbonyl allyl esters

We hypothesized that conjugating BH bromides with aryl phosphines would lead to phosphonium salts that can be targeted to the mitochondria to develop them as anticancer agents. We also envisioned that these phosphonium salts upon nucleophilic addition in S_N2, S_N2' and 1,4 addition fashion with phosphine acting as a leaving group (**Figure 1.5).** In this regard, these agents have the potential to alkylate intramitochondrial components, disrupt energetic and biosynthetic pathways, and ultimately halt tumor growth.

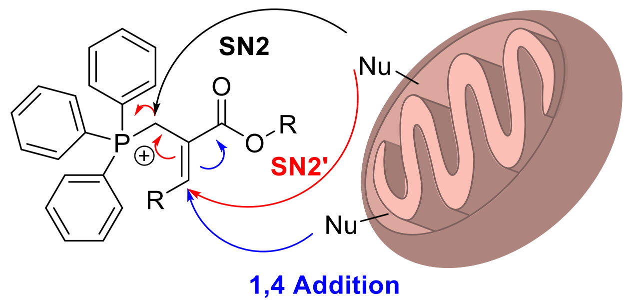

Figure 1.5: Hypothesized mechanism of action of intramitochondrial interaction potential of phosphonium BH hybrids.

CHAPTER 2: RESULTS AND DISCUSSION

As described in the introduction, targeting energetic pathways in cancer has potential means to treat the disease. Numerous literature reports indicate that targeting tumor metabolism is an effective form of cancer treatment. In particular, recent evidence illustrates the importance of mitochondrial metabolism in aggressive and resistant cancer cell populations, and hence potent and selective mitochondrial targeting agents are highly important. The lipophilic cationic molecule triphenylphosphonium (TPP) has been extensively studied as a mitochondrial targeting agent due to its ability to both diffuse cellular and organelle membranes, and to accumulate based on the charge gradient within the mitochondrial membranes and matrix. In highly oxidative cancer cells, the mitochondrial TCA cycle and electron transport chain are working at high levels; resulting in proton gradients that offer a biophysical means of drug delivery to the mitochondrial matrix. In this regard, we sought to investigate the anticancer properties of synthetic TPP hybrids with previously investigated cytotoxic 2-alkoxycarbonylallyl esters. Although phosphonium salts and alkoxycarbonylallyl esters have been independently used as potential anti-cancer agents, molecular hybridization of the templates has not been investigated. These agents exhibit dual mitochondrial targeting ability of the TPP subunit, and the capability of the alkoxycarbonylallyl ester to interact with the intracellular nucleophilic components either in S_N2, S_N2', or 1,4-addition fashion as we have illustrated previously **(Figure 1.5).** In the present work, we hypothesized that conjugating alkoxycarbonylallyl esters with phosphonium salts would lead to new generation mitochondrial targeting agents with potent cell proliferation inhibition properties.

2A. Synthesis, *in vitro* and *in vivo* biological evaluation of aryl phosphoniums

To synthesize 2-(methoxycarbonyl)-allyl-TPP conjugates, we utilized Baylis Hillman bromides synthesized in two steps, whereas for TPPs, we used commercially available aryl phosphines. We decided to use an unsubstituted triphenyl phosphine, metabolically stable fluoro substituted tris(4-fluorophenyl)phosphine, electron donating group containing tri-*p*-tolylphosphine and tris(4-methoxyphenyl)phosphine and cyclohexyldiphenylphosphine, which represented a cyclic alkane group with two phenyl rings. The Baylis-Hillman alcohol **1** was synthesized by formaldehyde and methyl acrylate in the presence of DABCO followed by bromination of the BH alcohol with HBr/H_2SO_4. The resulting crude BH bromide was vacuum distilled to obtain the pure bromide **2** in 57% yield. Treatment of **2** with arylphosphines in acetonitrile resulted in the 2-(methoxycarbonyl)-allyl-TPP conjugates **13-18** (**Scheme 2.1**) (**Figure 2.1**).

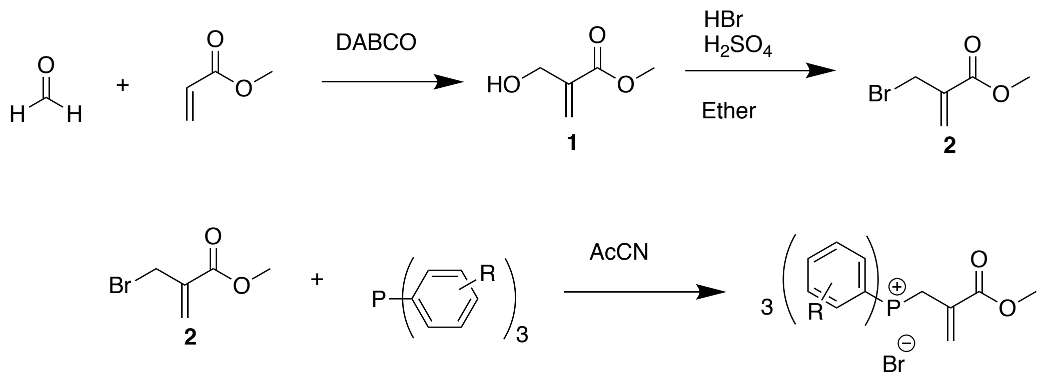

Scheme 2.1: Synthesis of 2-(methoxycarbonyl)-allyl phosphonium bromides

All the synthesized compounds were evaluated for their *in vitro* cell proliferation inhibition properties by utilizing the 3-(4,5-dimethylthiazol-2-yl)-2,5-diphenyltetrazolium bromide (MTT) cell viability assay. Human breast cancer MCF7, human triple-negative breast cancer MDA-MB-231, human pancreatic cancer MIAPaCa-2, human colorectal adenocarcinoma WiDr, murine metastatic breast cancer 4T1, and murine breast cancer 67NR cell lines were utilized. Cells cultured in 96-well plates were incubated with the test compounds for 72 h, and absorbance values expressed as percent of vehicle-only (control) wells. MTT is reduced to formazan through mitochondrial reductase with an absorbance at 570 nm. The IC_{50} value was calculated for each compound as the dose required to suppress the MTT signal to 50% of control values. These assays were carried out in a minimum of three trials and the IC_{50} values were calculated using GraphPad Prism 6 Software (**Figure 2.1)**.

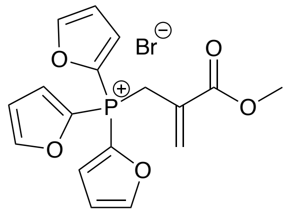

13

MCF-7 : >100
MDA-MB-231 : >100
MiaPaca-2 : 87.9 ± 4.5
WiDr : >100
4T1 : >100
67NR : >100

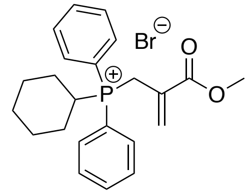

14

MCF-7 : 15.7 ± 7.0
MDA-MB-231 : 56.2 ± 7.0
MiaPaca-2 : 19.8 ± 0.7
WiDr : 14.3 ± 9.2
4T1 : 8.9 ± 2.0
67NR : 67.1 ± 6.2

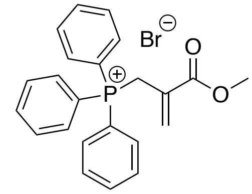

15

MCF-7 : 19.9 ± 3.3
MDA-MB-231 : 28.9 ± 12.7
MiaPaca-2 : 27.4 ± 5.0
WiDr : 7.74 ± 2.1
4T1 : 14.8 ± 4.8
67NR : 58.4 ± 11.6

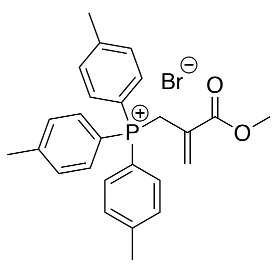

16

MCF-7 : 2.43 ± 0.4
MDA-MB-231 : 3.79 ± 0.2
MiaPaca-2 : 2.66 ± 0.2
WiDr : 1.48 ± 0.3
4T1 : 1.78 ± 0.4
67NR : 5.34 ± 1.2

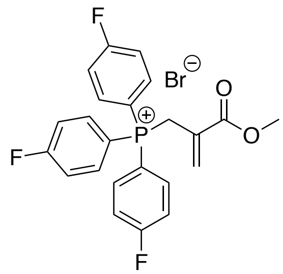

17

MCF-7 : 47.0 ± 5.6
MDA-MB-231 : 91.1 ± 2.8
MiaPaca-2 : >100
WiDr : 19.0 ± 3.3
4T1 : 61.9 ± 6.5
67NR : 73.9 ± 13.0

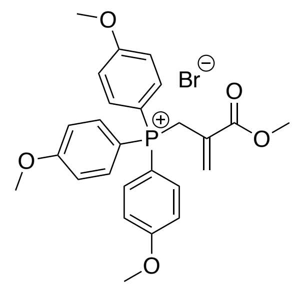

18

MCF-7 : 2.78 ± 0.6
MDA-MB-231 : 4.87 ± 0.8
MiaPaca-2 : 3.60 ± 0.5
WiDr : 1.62 ± 0.2
4T1 : 1.85 ± 0.2
67NR : 10.6 ± 1.5

Figure 2.1: Derivatives from the BH bromide with aryl phosphines **13-18** with the MTT values.

From the cell proliferation inhibition studies (MTT assay) on compounds **13-18**, we found that the tris-(4-methylphenyl)phosphine **16** and tris-(4-methoxyphenyl)phosphine **18** exhibited a higher biological potency on all cells lines tested. The electron donating character of the tolyl and methoxy groups may stabilize the cation, enabling enhanced ability of compounds **16** and **18** to diffuse down their charge gradient into the mitochondrial matrix, leading to higher mitochondrial accumulation and biological potency.

To further understand the SAR of these compounds, the α-carboxy allyl ester unit was the next synthetic modification that was carried out. The alkoxyester group was first modified by replacing the methyl group with t-butyl and N-N-dimethyl groups. The reaction of t-butyl acrylate and N,N-dimethyl acrylamide with formaldehyde in the presence of DABCO, followed by bromination of the resulting BH alcohols using HBr/H_2SO_4 provided the corresponding BH bromides **19** and **20** (**Scheme 2.2**). The pure **19** and **20** were obtained via silica gel column chromatography with hexane elution. The reaction of triphenyl phosphine and tris(4-methoxyphenyl)phosphine with BH bromides **19** and **20** in acetonitrile, followed by precipitation in ether gave the corresponding (2-(tert-butoxy/N,N-dimethylcarbonyl)-allyl)triphenyl phosphonium bromides **21, 22** and **23** respectively in good yields (**Scheme 2.2**).

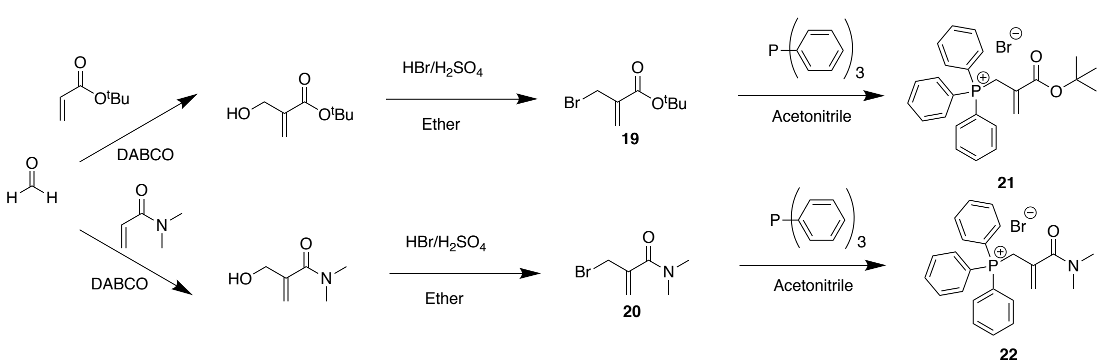

Scheme 2.2: Synthesis of (2-(tert-butoxy/N,N-dimethylcarbonyl)-allyl)triphenylphosphonium bromides.

Cell proliferation inhibition studies of **21** and **23** showed an increase in potency within the tert-butyl substitution compared to methyl group. Enhanced carbon content and lipophilic nature of the t-butyl group may allow for better tissue diffusion and biological potency. Although metabolically stable, N,N-dimethyl amide derivatives are less reactive than the corresponding esters due to nitrogen lone pair delocalization and resonance. Reduced reactivity in this regard may explain the reduced biological potency; further illustrating that the ester moiety is necessary for reactivity with intracellular nucleophiles and subsequent biological activity. In this regard, tert-butyl BH bromide was reacted with tris(4-methoxyphenyl)phosphine and precipitated out in ether to result in the (2-(tert-butoxycarbonyl)allyl)tris(4-methoxyphenyl)phosphonium bromide **23**. This compound showed even further enhancement in cell proliferation inhibition due to a combination enhanced lipophilicity and better cationic stabilization due to methoxy groups (**Figure 2.2**).

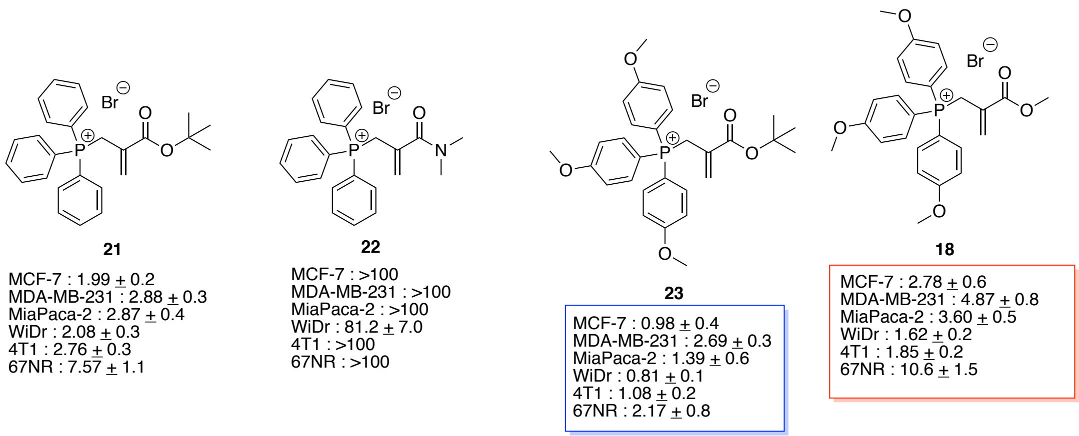

Figure 2.2: Derivatives from the tert-butyl/N,N-dimethyl BH bromide with aryl phosphines with the MTT values.

Encouraged by the biological activity and structural characteristics of these molecules, further structural activity relationship studies (SAR) were carried out. To create β-substituted Baylis-Hillman alcohols, a variety of different aromatic aldehydes were used. Various substituted aromatic aldehydes including benzaldehyde (**24**), 4-fluorobenzaldehyde (**25**), 4-chlorobenzaldehyde (**26**), and 4-bromobenzaldehyde (**27**) were used in the synthesis of the corresponding BH alcohols. Similarly, electron donating groups including *p*-tolyl (**28**), and 4-methoxyphenyl (**29**) BH alcohols, and electron withdrawing groups 4-nitrophenyl (**30**) and 4-cyanophenyl (**31**) aldehydes were utilized. BH alcohols **24-31** were obtained under standard BH reaction conditions with methyl acrylate in the presence of DABCO (**Schemes 2.3, 2.4** and **2.5)**. The BH alcohols **24-31** obtained from the substituted aromatic aldehydes were subjected to bromination using phosphorus tribromide (PBr_3) to obtain the corresponding Z-substituted BH bromides **32-39** (**Schemes 2.3, 2.4** and **2.5)**.

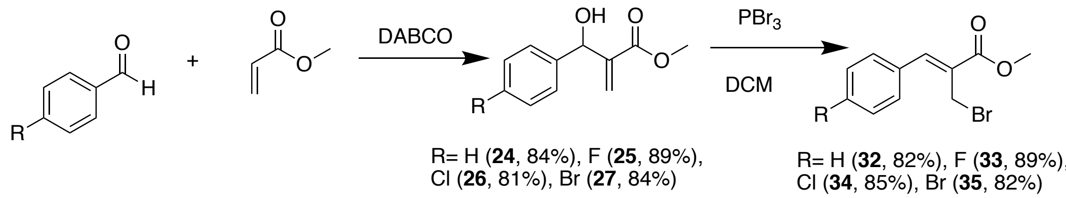

Scheme 2.3: Synthesis of methyl (Z)-2-(bromomethyl)-3-phenylacrylate.

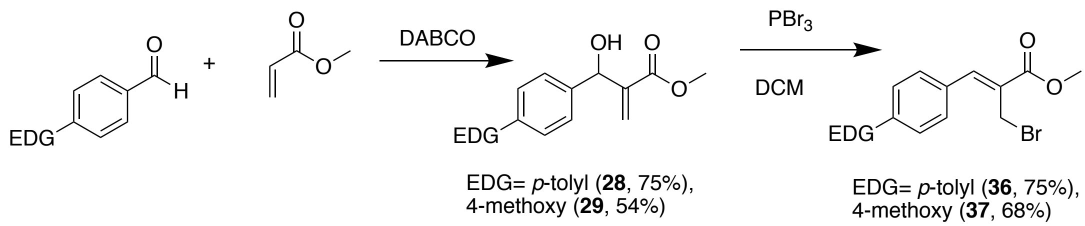

Scheme 2.4: Synthesis of methyl (Z)-2-(bromomethyl)-3-phenylacrylate derived from EDG substituted aromatic aldehydes.

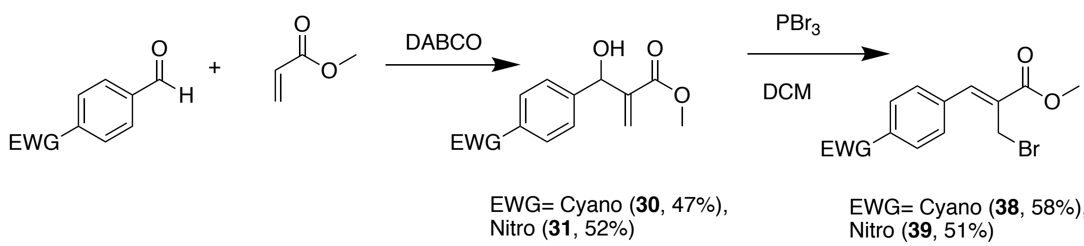

Scheme 2.5: Synthesis of methyl (Z)-2-(bromomethyl)-3-phenylacrylate derived from EWG substituted aromatic aldehydes.

When compared to the similarly potent tris(4-methylphenyl)phosphine **16**, tris(4-methoxyphenyl)phosphine **18** exhibits higher metabolic stability as tolyl groups are especially susceptible to CYP450 benzylic oxidation and fast clearance rates. Hence, the SAR of β-substitution included the tris(4-methoxyphenyl)phosphine in the following examples. To synthesize a library of phosphonium salts, the corresponding BH bromides **32-39** were reacted with tris(4-methoxyphenyl)phosphine in acetonitrile, and the phosphonium salts were precipitated out by trituration with ether resulting in the pure phosphonium salts **40-47** in good yields (**Scheme 2.6**).

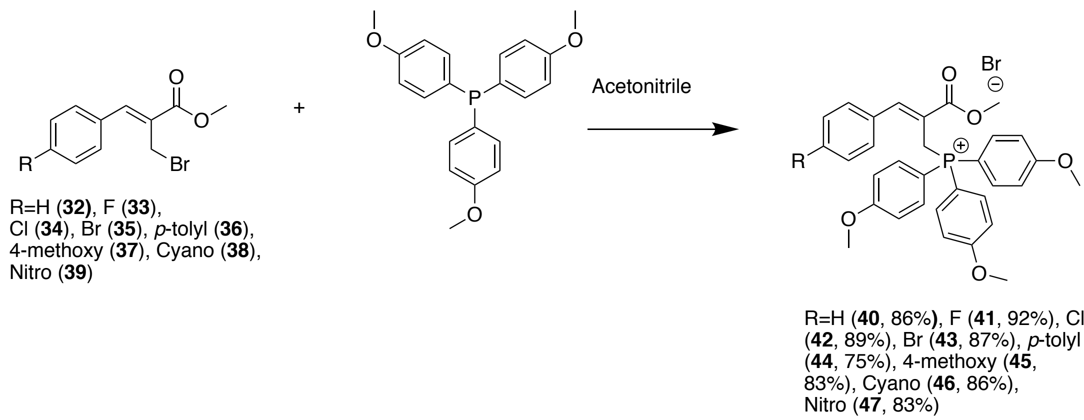

Scheme 2.6: Synthesis of the phosphonium salts with the β-substituted BH bromides.

We then carried out cell proliferation inhibition studies (MTT assay) on compounds **40-47** on various cancer cell lines (**Figure 2.3**). These studies indicated that aromatic substituted BH bromides with the tris(4-methoxyphenyl)phosphine exhibited increased potency when compared to the β-unsubstituted examples **18** and **23** against the tested cell lines (**Figure 2.2**). Specifically, the derivatives **43** and **45** were the most potent and were designated as first generation lead molecules.

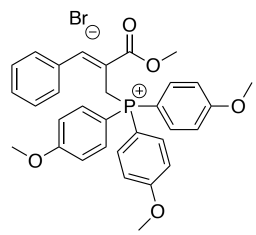

40

MCF-7 : 2.67 ± 0.7
MDA-MB-231 : 9.27 ± 1.4
MiaPaca-2 : 4.59 ± 3.1
WiDr : 2.74 ± 0.9
4T1 : 7.20 ± 4.9
67NR : 4.87 ± 1.8

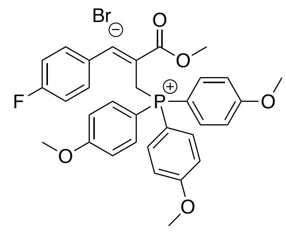

41

MCF-7 : 1.42 ± 0.3
MDA-MB-231 : 7.41 ± 1.6
MiaPaca-2 : 1.29 ± 0.1
WiDr : 2.14 ± 0.4
4T1 : 4.57 ± 2.2
67NR : 5.14 ± 1.1

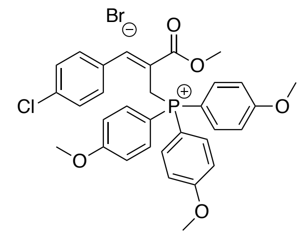

42

MCF-7 : 1.37 ± 0.2
MDA-MB-231 : 3.01 ± 0.5
MiaPaca-2 : 0.59 ± 0.2
WiDr : 1.32 ± 0.4
4T1 : 0.98 ± 0.1

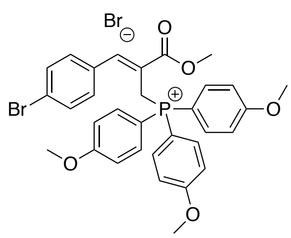

43

MCF-7 : 1.24 ± 0.5
MDA-MB-231 : 1.91 ± 0.4
MiaPaca-2 : 0.73 ± 0.1
WiDr : 0.90 ± 0.4
4T1 : 1.21 ± 0.2
67NR : 2.9 ± 0.4

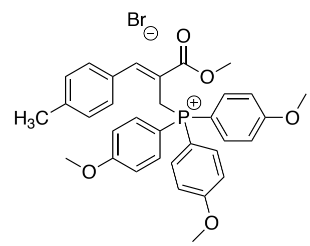

44

MCF-7 : 7.47 ± 3.3
MDA-MB-231 : 9.79 ± 2.0
MiaPaca-2 : 0.34 ± 0.2
WiDr : 2.58 ± 1.2
4T1 : 5.23 ± 2.5
67NR : 2.78 ± 1.1

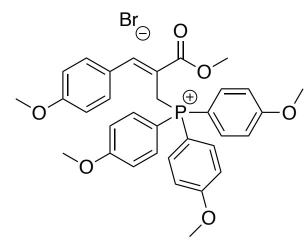

45

MCF-7 : 1.40 ± 0.4
MDA-MB-231 : 3.70 ± 0.7
MiaPaca-2 : 1.37 ± 0.3
WiDr : 1.14 ± 0.2
4T1 : 3.36 ± 2.3
67NR : 4.59 ± 0.2

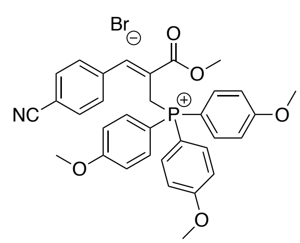

46

MCF-7 : 4.49 ± 0.4
MDA-MB-231 : 12.5 ± 1.3
MiaPaca-2 : 7.86 ± 1.7
WiDr : 4.87 ± 1.3
4T1 : 20.4 ± 7.2
67NR : >100

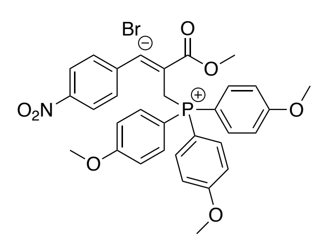

47

MCF-7 : 8.83 ± 3.0
MDA-MB-231 : 8.29 ± 0.5
MiaPaca-2 : 5.59 ± 1.3
WiDr : 5.95 ± 1.1
4T1 : 4.73 ± 0.5
67NR : 28.7 ± 17.7

Figure 2.3: Synthesized compounds **40-47** and corresponding cell proliferation inhibition (IC_{50}) values of the phosphonium bromide salts with β-substituted BH bromides.

We then carried out further synthetic modifications by substituting the methyl ester with a tert-butyl ester to investigate the importance of carbon content on the ester group for biological activity (**Scheme 2.7**). Interestingly, similar to our earlier observed results with tert-butyl derivative **21** and **23**, it was found that tert-butyl derived tris(4methoxyphenyl)phosphine **50**, exhibited enhanced biological potency against all of the cell lines tested. (**Figure 2.4**).

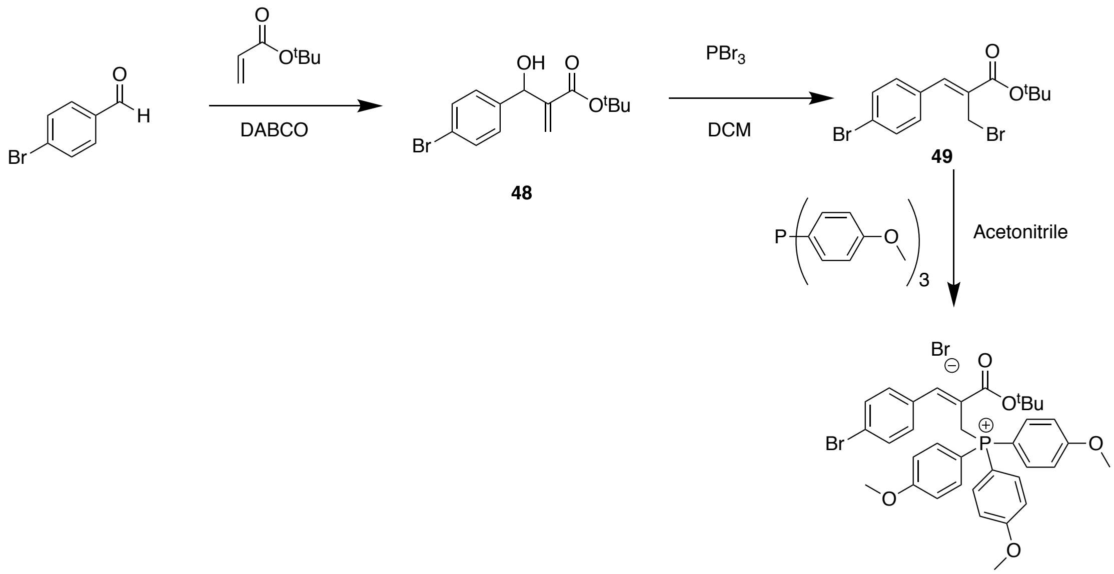

Scheme 2.7: Synthesis of butyl (Z)-2-(bromomethyl)-3-(4-bromophenyl) phosphonium salt **50** (82%) with tris(4-methoxyphenyl)phosphine.

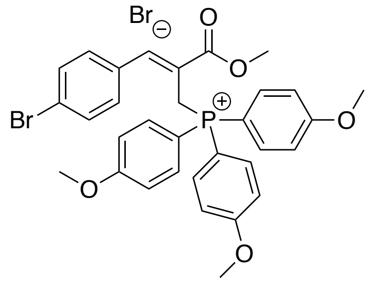

43

MCF-7 : 1.24 ± 0.5
MDA-MB-231 : 1.91 ± 0.4
MiaPaca-2 : 0.73 ± 0.1
WiDr : 0.90 ± 0.4
4T1 : 1.21 ± 0.2
67NR : 2.9 ± 0.4

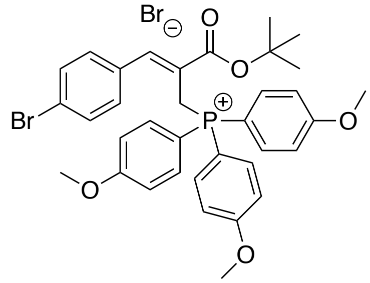

50

MCF-7 : 0.64 ± 0.4
MDA-MB-231 : 2.05 ± 0.3
MiaPaca-2 : 0.36 ± 0.1
WiDr : 0.95 ± 0.1
4T1 : 0.86 ± 0.2
67NR : 0.62 ± 0.1

Figure 2.4: Cell proliferation inhibition (IC_{50}) values comparing phosphonium bromide salts utilizing the MTT assay.

Since compounds **43, 45,** and **50** exhibited potent cell proliferation within the MTT assay at low micromolar and nanomolar concentrations, these compounds were also evaluated using another cell proliferation method called sulforhodamine-B (SRB) assay[62]. The MTT assay is an assay that needs mitochondrial function within the plate to use mitochondrial reductase to reduce the MTT to formazan where then the absorbance can represent the compounds cell viability potential. Due to these compounds being mitochondrial targeting with the phosphonium character, the MTT results may be a result of a false positive – showing mitochondrial function as a surrogate of cell proliferation. Due to this, the SRB assay can be incorporated to confirm the cell proliferation inhibition properties of these molecules. The SRB assay allows for the evaluation of cell proliferation based on the cellular protein content – a more direct measure of protein content than mitochondrial viability. To perform this assay, 5×10^4 cells/mL were cultured within a 48-well plate for each cell line. Compound **43, 45,** and **50** were dissolved in DMSO (final concentration of DMSO <0.1%) and were added to the cultured wells in serial dilution fashion in duplicate and incubated for 72 hours. Following incubation, growth media was removed, and the wells were washed with 1X PBS and dried to fix the cells. SRB (0.5% w/v in 1% acetic acid) was added to bind to cellular protein and incubated for 30-45 minutes. The wells were washed 3 times with 1% acetic acid and dried to remove background SRB. The cellular protein was dissolved in tris base (10mM, pH 10.2) and absorbance was recorded at 540 nm. The percent survival values were calculated for each compound based off the absorbance of the test compound divided by the absorbance of the control wells multiplied by 100. These assays were carried out a minimum of three trials and the IC_{50} values were calculated using GraphPad Prism 6 Software (**Figure 2.5**).

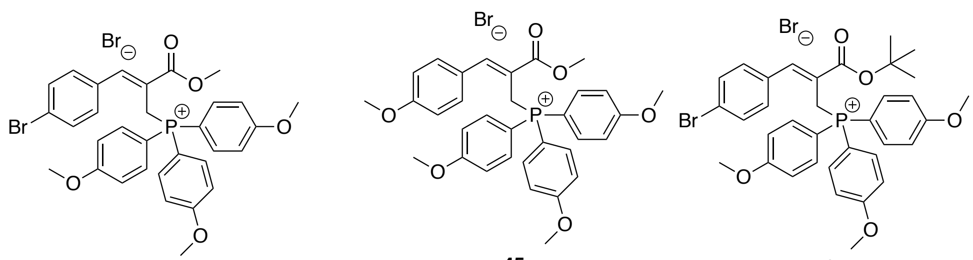

43
MCF-7 : 0.17 ± 0.1
MDA-MB-231 : 0.94 ± 0.4
MiaPaca-2 : 0.29 ± 0.1
WiDr : 0.81 ± 0.2
4T1 : 1.25 ± 0.2
67NR : 1.78 ± 0.3

45
MCF-7 : 0.17 ± 0.1
MDA-MB-231 : 2.19 ± 0.4
MiaPaca-2 : 0.31 ± 0.1
WiDr : 0.76 ± 0.2
4T1 : 1.83 ± 0.2
67NR : 2.56 ± 0.4

50
MCF-7 : 0.06 ± 0.1
MDA-MB-231 : 0.58 ± 0.1
MiaPaca-2 : 0.20 ± 0.1
WiDr : 0.14 ± 0.1
4T1 : 0.50 ± 0.1
67NR : 0.47 ± 0.1

Figure 2.5: Cell proliferation inhibition (IC_{50}) values of the phosphonium bromide salts from the SRB assay.

These results indicated that compounds **43, 45,** and **50** derived from the 4-bromobenzaldehyde and 4-methoxybenzaldehyde with the tris-(4-methoxyphenyl)phosphine had retained comparable cell proliferation inhibition properties and were confirmed as the lead candidate compounds based on potent inhibition properties as reported by both MTT and SRB assays.

Due to the mitochondrial targeting potential of the phosphonium based compounds **43** and **45**, further metabolic assays were performed. In this regard, mitochondrial function of cancer cells treated with TPP based compounds **43** and **45** was evaluated using widely employed Seahorse XFe96® based mitochondrial stress test. Here, cells treated with test compound, followed by the successive addition of oligomycin, carbonyl cyanide-p-trifluoromethoxyphenylhydrazone (FCCP), and rotenone + antimycin A respectively, and changes in oxygen consumption rates (OCR) are recorded in real time to allow for calculating numerous parameters of mitochondrial respiratory function including ATP production, proton leak, maximal respiration, and spare respiratory capacity (**Figure 2.6** and **2.7**)[63]. Oligomycin is an ATP synthase inhibitor, and changes in OCR following acute exposure give rise to the amount of oxygen utilized by cells to produce ATP. By observing differences in control and treated cultures in the presence of oligomycin, the ability of test compound to decrease mitochondrial ATP synthesis can be evaluated[63,64]. FCCP is a mitochondrial membrane uncoupling agent that diminishes the proton gradient across the inner mitochondrial membrane and matrix. Acute exposure of FCCP induces a maximal respiratory state where OCR in combination with TCA cycle and other processes are heightened to retain the cells desired proton gradient. The ability of FCCP to stimulate maximum respiration in this regard can be observed in (acute) compound treated and control cultures to realize potential mitochondrial targeting[63]. Spare respiratory capacity illustrates the ability of cells to increase mitochondrial respiration under physiological stress (ie FCCP stimulation) and can also be calculated and compared between control and compound treated cultures under these conditions[63].

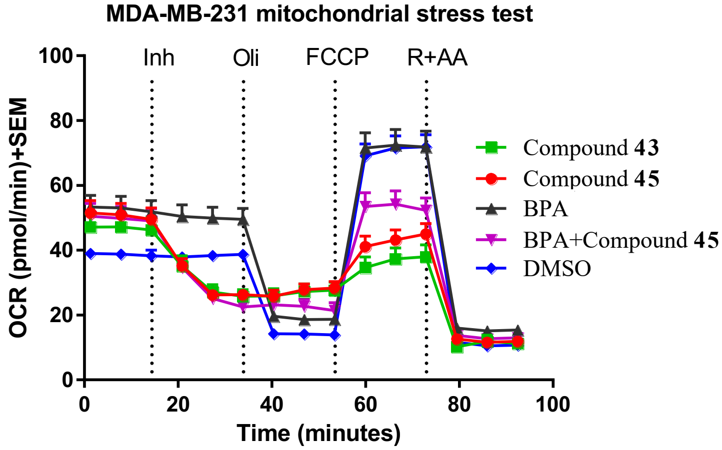

Figure 2.6: Mitochondrial stress test profile using compound **43** and **45** in MDA-MB-231 cell line. MST was performed on Seahorse XFe96® analyzer. The compound **43** and **45** were tested at 10 μM concentration and DMSO was used in control wells. Test compound (10 μM), oligomycin (1 μM), FCCP (0.25μM), and rotenone + antimycin A (0.5 μM each) were added with drug delivery ports at indicated time points.

Hence, within a mitochondrial stress test, successive injections of test compound and known inhibitors shut down different electron transport chain and oxidative processes allowing for the evaluation of the effect of test compound on mitochondrial function. In this regard, MDA-MB-231 cells (20,000 cells/well) were plated on Seahorse XFe96 well plates and incubated overnight. Prior to the assay, growth media was replaced with serum free XF DMEM assay media supplemented with important metabolic substrates glucose, glutamine, and sodium pyruvate at concentrations equal to that of the growth media. The test compounds (**43** and **45**) were injected first followed by the injection of oligomycin which inhibits ATP synthase, also known as mitochondrial complex V, within OxPhos[63,65]. The third injection was FCCP, an inhibitor of the membrane uncoupler of the oxygen consumption from the ATP production[63,66]. The last injection was rotenone and antimycin

A, where rotenone interferes with the electron transports chain within mitochondria by inhibiting electrons from iron-sulfur center in mitochondrial complex I[63,67], and antimycin A inhibits oxidative phosphorylation by binding to cytochrome c reductase within mitochondrial complex III, which inhibits some of the oxidative processes[63,68,69]. The resulting mitochondrial respiratory profile was plotted in real time, and the effect of compound treatment on numerous parameters was evaluated.

Based off of **Figure 2.6**, the initial injection of compound **43** and **45** exhibited a significant decrease in ATP production. With the second injection, ATP synthase is inhibited allowing for the proton gradient differences. The mitochondria require the proton gradient across the inner membrane for this ATP synthase to function. If this proton gradient is not present within the cell, the cells undergo severe energy crisis and redirect the metabolic macromolecules towards pursuing glycolysis. Mitochondrial damage and loss of membrane integrity can result in protons leaking across the mitochondrial membranes. Maintenance of membrane integrity allows for compartmentalization of protons that are ultimately used as the motive for oxidative phosphorylation of ADP. Hence, Proton leakage across the membrane usually results in the decrease in ATP production. With injection of drug of the cells, there is a decrease in ATP production without the ATP synthase inhibitor (**Figure 2.6 and 2.7**), showing the possibility that there is a proton leak across the membrane potential. With the addition of oligomycin, there is no difference present, showing that the mitochondrial membrane proton gradient is damaged. The maximum mitochondrial respiration and spare respiratory capacity in control cells can be induced using the membrane uncoupler such as FCCP. With the addition of FCCP, there is an increase in the OCR but just to the basal respiration (**Figure**

2.7). This means that the mitochondrial function is damaged, and the metabolic substrates are not able to be oxidized. Within MDA-MB-231 cell line, a decreased maximal respiration shows that the cells are unable to reach their maximum OCR compared to the control (**Figure 2.7**). These compounds could be potential proton uncouplers with the ability to inhibit the oxidation of other substrates and/or the electron transport chain. These compounds also reduced the spare respiratory capacity within the MDA-MB-231 cell line. This result shows that the energy demands of the cell are not met.

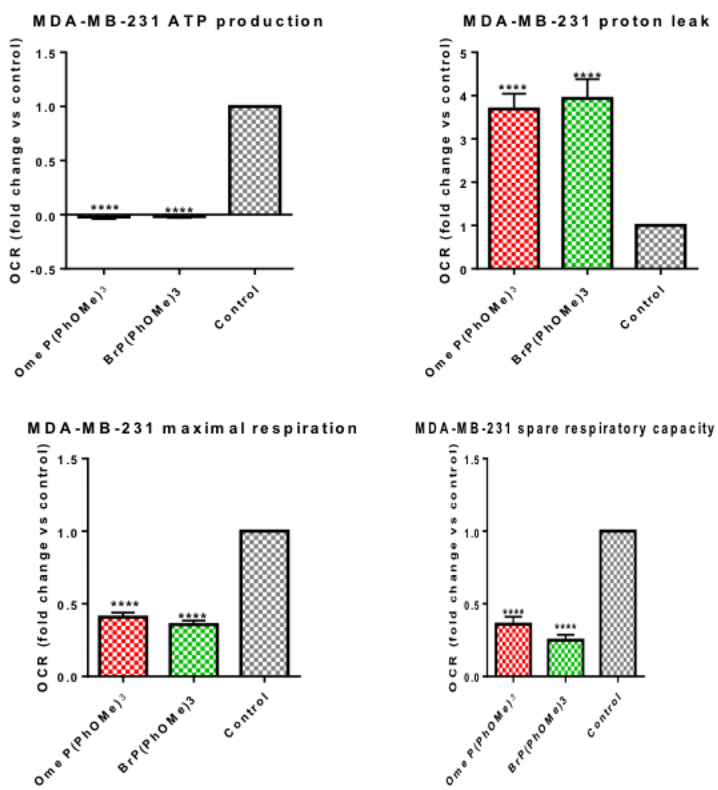

Figure 2.7: Mitochondrial stress test of compound **43** and **45** in MDA-MB-231. The graphs represent mitochondrial parameters: ATP production (top left), Proton leak (top right), Maximal respiration (bottom left), and Spare respiratory capacity (bottom right).

To further understand the function of metabolism within cancer cells with compounds **43** and **45**, the combination treatment of these compounds with bromopyruvic acid (BPA) (**Figure 2.8**), a known glycolytic inhibitor, was evaluated. The combination of the compounds **43** and **45** with BPA was to evaluate the heterogeneity of cancerous cells by targeting the glycolytic pathway with BPA and the mitochondria with the compounds. The idea of stalling tumor growth production by removing the major energy pathways would halt the cancer cell growth.

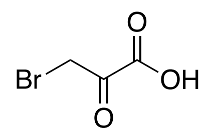

Bromopyruvic Acid (BPA)

Figure 2.8: Structure of bromopyruvic acid (BPA)

Encouraged by preliminary evidence of mitochondrial targeting by compounds **43** and **50**, fluorescence microscopy was conducted on these lead molecules using a mitochondrial targeted fluorescent probe MitotrackerRedCMXROS (MTR). MTR is a unique probe that binds and accumulates in mitochondria as a function of membrane potential and hence, allows for the evaluation of compound effects on both morphology and mitochondrial viability. In **Figure 2.9**, the top row is the control images of breast cancer cell line 4T1 at 2 hours treatment time period. With the use of MTR, the results indicate that the mitochondria of control cultures exhibit a healthy branched mitochondrial network (**Figure 2.9**). With the use of compound **43**, the mitochondria appear to be less branched with an increase in punctate mitochondria. The organized tubular mitochondrial network observed in the control is less abundant, and the mitochondria are becoming broken apart from each other (**Figure 2.9**). With the use of compound **50** at 1μM (t-BuTPPBr) after 2 hours has a diffuse and dim mitochondrial fluorescence. This diffuse morphology may be a result of mitochondrial membrane damage, allowing for MTR leakage into the cytoplasm, and dim fluorescence as a result of low mitochondrial membrane potential and vitality. Interestingly, over the time frame tested (2hr) the t-butyl compound **50** exhibited more drastic mitochondrial perturbations than the corresponding methyl ester. This finding may further support the claim that increased carbon content and lipophilic character of these compounds lead to enhanced membrane diffusion and accumulation in the mitochondria.

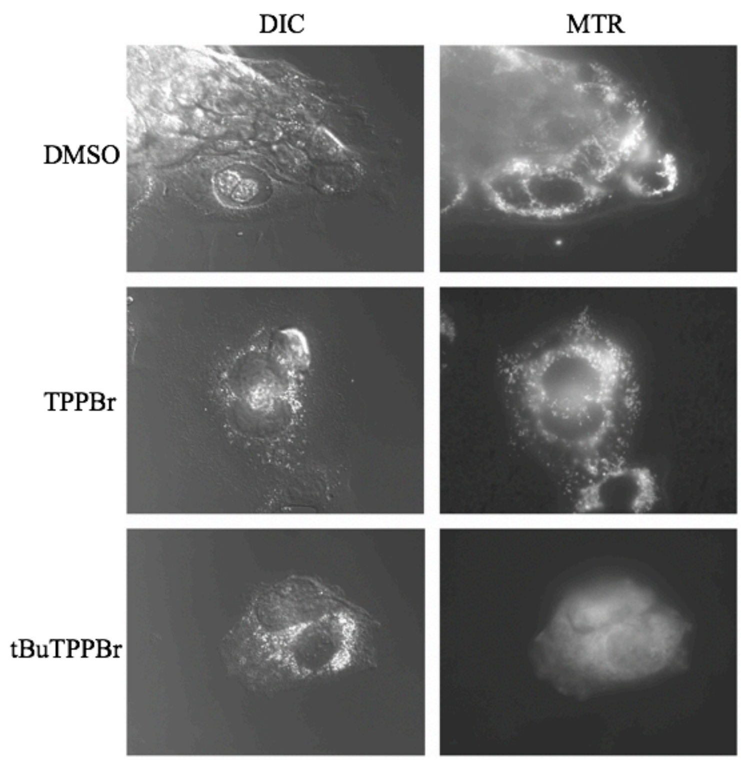

Figure 2.9: Representative fluorescence microscopy images of 4T1 cells treated with compound **43** and **50** and labeled with mitotracker red.

Based on these results, compounds **43** and **45** were designated as the lead candidate compounds for further *in vivo* studies of systemic toxicity and chemotherapeutic efficacy based on its *in vitro* cell proliferation inhibition described above. Initially, compounds **45** were examined for its systemic toxicity in CD1 mice. 12 healthy CD-1 mice were divided into two groups (n=6): Group 1 was administered compound **45** (10mg/kg) and group 2 was administered vehicle only (control) intraperitoneally once daily six days a week for a total of 14 days. This study indicated that compound **45** was well tolerated with no apparent side effects at acceptable therapeutic dose regimens based on normal weight gains and behavior when compared to control group (**Figure 2.10**).

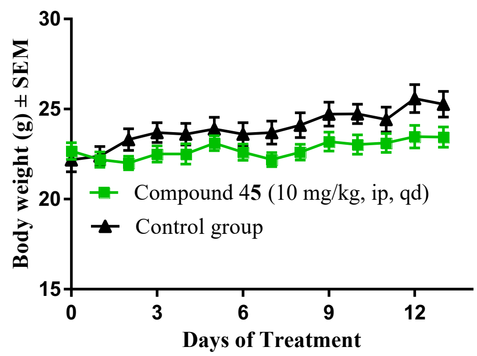

Figure 2.10: Systemic toxicity study of compound **35** in CD-1 mice

After observing minimal *in vivo* systemic toxicity in healthy mice as a single agent, we sought to explore the idea of using a combination protocol for inhibition of the glycolytic and mitochondrial action would terminate cancer tumor growth. MN-D2, a compound developed in our lab is a dual monocarboxylate 1 and 4 (MCT1 and 4) inhibitor, and also a potent inhibitor of glycolysis (**Figure 2.11**). Hence, we envisioned a combination strategy employing compound **45** and MN-D2 for potential cancer treatment. We first examined systemic toxicity in CD1 mice. Inhibition of both glycolytic and mitochondrial function has the potential to be toxic to test subjects so we first optimized the tolerated doses for *in vivo* studies. 12 healthy CD-1 mice were divided into two groups (n=6): Group 1 was administered compound **45** (10mg/kg) and MN-D2 (25mg/kg) every other day and group 2 was administered vehicle only (control) intraperitoneally once daily six days a week for a total of 14 days. This study indicated that compound **45** and MN-D2 was well tolerated with no apparent side effects at acceptable therapeutic dose regimens based on normal weight gains and behavior when compared to control group (**Figure 2.12**).

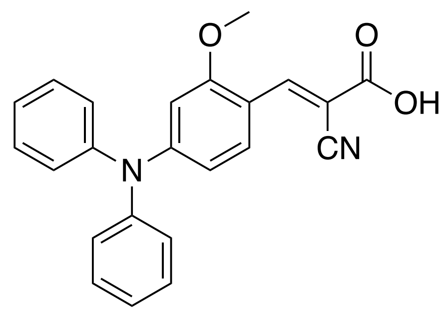

MN-D2

Figure 2.11: Structure of MN-D2, an MCT 1 and 4 inhibitor, and glycolytic inhibitor

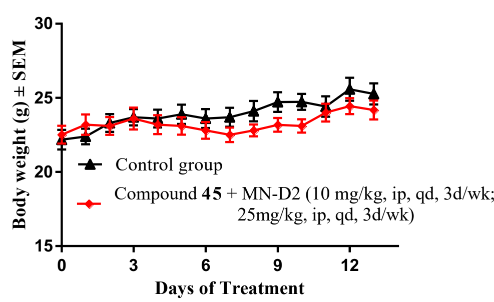

Figure 2.12: Systemic toxicity of a combination of compound **45** and MN-D2.

To further investigate such combinatorial studies, other glycolysis inhibitors were employed. For this study compounds **43** and **45** and bromopyruvic acid (BPA), the glycolytic inhibitor, were examined for their systemic toxicity in CD-1 mice. 30 healthy CD-1 mice were divided into five groups (n=6): Group 1 was administered compound **43**

(10mg/kg), group 2 was administered compound **43** (10mg/kg) plus BPA (2mg/kg) (**Figure 2.13**), group 3 was administered compound **45** (10mg/kg), group 4 was administered compound **45** (10mg/kg) plus BPA (2mg/kg) (**Figure 2.14**), and group 5 was administered vehicle only (control) intraperitoneally once daily six days a week for a total of 14 days. The combination groups were injected intraperitoneally every other day for the study. After 4 days of treatment, the dosage was increased for compounds **43** and **45** to 12mg/kg. This study indicated that compounds **43** and **45** as a single agent and combination treatment was well tolerated until the dosage increase, and the MTD was determined to be 10mg/kg. There were no apparent side effects at this acceptable therapeutic dose regimen based on normal weight gains and behavior when compared to control group with compounds **43** and **45** (**Figure 2.13** and **2.14**).

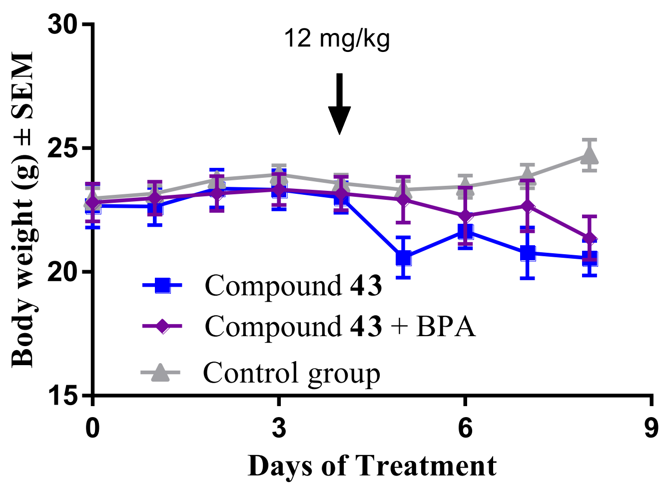

Figure 2.13: Systemic toxicity of a combination of compound **43** and BPA.

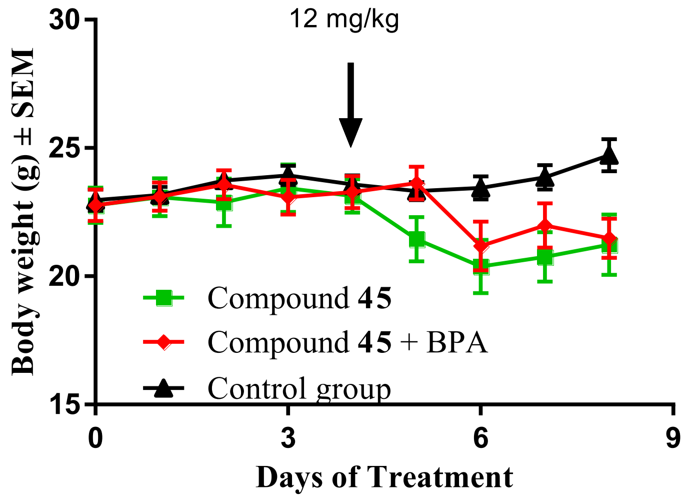

Figure 2.14: Systemic toxicity of a combination of compound **45** and BPA.

2B. Conclusion and Future Directions

In conclusion, several phosphonium salts were synthesized based on different BH bromides and chlorides. Initial studies indicated that the tris-(4-methoxyphenyl)phosphine was the optimal phosphine compared to the other aryl phosphines. Further SAR studies indicated that 4-bromo and electron donating groups present on β-substituted aromatic rings with either a methyl and tert-butyl ester present in the acrylate enhanced the biological activity. The cell proliferation inhibition evaluations by the MTT assay showed that several derivatives exhibited inhibition at low micromolar, and nanomolar concentrations. Due to the MTT assay needing the mitochondria reductase to convert MTT to formazan, and the phosphonium salts ability to damage mitochondria, we confirmed the cell proliferation inhibition by SRB assay, which confirmed that lead compounds exhibited cell proliferation inhibition at low micromolar to nanomolar concentrations. Preliminary *in vitro* studies indicated that the phosphonium salts inhibit the production of ATP within the mitochondria, lead to increase in proton leak within the mitochondrial membrane and there could be a possibility that these compounds are proton uncouplers and not allowing the oxidation of substrates to happen which inhibits the tumor growth ability. Finally, systemic toxicity studies indicate that compounds **43** and **45** were well tolerated in healthy CD-1 mice in numerous studies. Compounds **43** and **45** were also tested with combination studies with glycolytic inhibitors, MN-D2 and BPA, that were tolerated in healthy CD-1 mice.

The future directions of this project will involve mechanistic studies of the lead molecules. These compounds will also be evaluated for anticancer efficacy studies in mice tumor models using 4T1 metastatic breast cancer cell line with a tail-vein injection.

CHAPTER 3: EXPERIMENTAL SECTION

3.1 Materials and Methods

Triphenylphosphine (Sigma-Aldrich), Tris(4-fluorophenyl)phosphine (Sigma-Aldrich), Tri(2-furyl)phosphine (Sigma-Aldrich), Tris(4-methoxyphenyl)phosphine (Sigma-Aldrich), Tri(*p*-tolyl)phosphine (Sigma-Aldrich), formaldehyde (Sigma-Aldrich), methyl acrylate (Sigma-Aldrich), benzaldehyde (Sigma-Aldrich), 4-bromo-benzaldehyde (Sigma-Aldrich), anisaldehyde (Sigma-Aldrich). Other chemical reagents were high grade quality and purchase from Sigma-Aldrich (St. Louis, MO).

The ^{1}H- and ^{13}C-NMR spectra were plotted on a Varian Oxford-500 and Bruker Ascend^{TM} 400 spectrometers. High resolution mass spectra (HRMS) were recorded with a Bruker micrOTOP-Q III ESI mass spectrometer.

3.2 General procedure for synthesis of 2-(bromomethyl)acrylate-phosphonium salts

A mixture of respective aryl-phosphine (1.0 eq, 2mmol) and 2-(bromomethyl) acrylate in 25mL acetonitrile was stirred at room temperature for 3 hours. After it was confirmed that the reaction was completed using a TLC (10% EtOAc/Hexane), reaction vessel was placed under vacuum for removal of organic layer. Following alkylation of the aryl-phosphine, 20mL of ether was added into the reaction vessel and stirred for 3 hours. The solid obtained was filtered and washed with ether, obtaining the final products in 75-92 percent yields. The minor Z-isomer being removed with repeated washings and recrystallizations in ether.

3.3 Cell Culture

MCF-7 cells (ATCC) were grown in α-MEM supplemented with FBS (5%), non-essential aminoacids (0.1 mM), insulin (10 μg/ml), sodium pyruvate (1mM), EGF (100 ng/mL), hydrocortisone (10 μg/ml), HEPES (10 mM), and penicillin-streptomycin (50U/ml-50μg/ml). MDA-MB-231 cells (ATCC) were grown in DMEM supplemented with 10% FBS and penicillin-streptomycin (50U/ml-50μg/ml). MIAPaCa-2 cells (ATCC) were cultured in DMEM supplemented with 10% FBS, 2.5% Horse Serum and penicillin-streptomycin (50U/ml-50μg/ml). WiDr cells (ATCC) were grown in MEM supplemented with 10% FBS and penicillin-streptomycin (50U/ml-50μg/ml). 4T1 cells (ATCC) were cultured in RPMI-1640 supplemented with 10% FBS and penicillin-streptomycin (50U/ml-50μg/ml). 67NR cells (ATCC) were cultured in RPMI-1640 supplemented with 10% FBS and penicillin-streptomycin (50U/ml-50μg/ml).

3.4 Cell Proliferation Inhibition Assay (MTT)

Cells were seeded ($5x10^3$cells/well) in 96 well plates and incubated overnight (37°C, 5%CO_2). Test compounds were then exposed to cells in duplicate in serial dilution fashion and were incubated for an additional 72 hours (37°C, 5%CO_2). 3-(4,5-dimethylthiazol-2-yl)-2,5-diphenyltetrazolium bromide (MTT, 0.5mg/ml) was added and was incubated for four hours. Resulting formazan precipitate was then solubilized (SDS 10%w/v, 0.01N HCl) and incubated for four more hours. Absorbance readings at 570nm of each well were then recorded and concentrations at which 50% of cell growth was inhibited (IC_{50}) were tabulated, using control (untreated) wells as 100% cell survival.

3.5 Cell Proliferation Inhibition Assay (SRB)

Cells were seeded ($2x10^4$cells/well) in 48 well plates and incubated overnight (37°C, 5%CO_2). Test compounds were then exposed to cells in duplicate in serial dilution fashion and were incubated for an additional 72 hours (37°C, 5%CO_2). Media was then aspirated, and cells were washed three times with PBS and were left overnight to dry-fix. 100µL Sulforhodamine B (SRB, 0.5%w/v in 1% acetic acid) was added to each well and was incubated at 37°C for 1hr. SRB was rinsed with 1% acetic acid solution and dried. Dyed cells were then lysed with Tris (10mM, pH 10) and absorbance readings were recorded at 540nm of each well. Concentrations at which 50% of cell growth was inhibited (IC_{50}) were tabulated, using control (untreated) wells as 100% cell survival.

3.6 Statistical Analysis

Statistics were computed using GraphPad Prism version 6.0. Mann-Whitney test was used to compare the compound-treated and control groups for *in vivo* tumor xenograft studies. A P-value of < 0.05 was considered significant.

3.7 Ethical Considerations

The experimental procedures involving animals were conducted on the University of Minnesota Duluth campus that was compliant with the U.S. National Institutes of Health Guide for Care and Use of Laboratory Animals and approved by the Institutional Animal Care and Use Committee (IACUC). Studies with protocols 1311-31063A (systemic toxicity, **Figure 3.10**).

3.8 *In vivo* systemic toxicity in CD-1 mice

Five-week-old CD-1 mice (Charles River) were obtained and acclimatized for one week before initial treatment. Mice (n=6) were grouped randomly based on average body weight. Group-1 was administered with compound X (10mg/kg) while group-2 was administered with vehicle intraperitoneally once daily, six days a week for a total of 14 days of treatment. Mice body weights were recorded daily, and euthanized according to IACUC guidelines at the end of the study. A graph of days of treatment versus body weight±SEM was generated using GraphPad software (**Figure 3.13 and 3.14)**.

3.9 Spectral Characterization

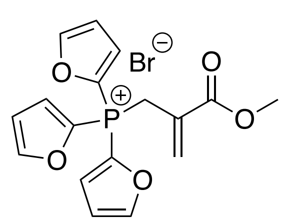

Tri(furan-2-yl)(2-(methoxycarbonyl)allyl)phosphonium bromide

^{1}H NMR (500MHz, $CDCl_3$): δ 8.13-8.12 (m, 3H), 7.99-7.98 (m, 3H), 6.82-6.81(m, 3H), 6.67 (d, *J*=6.5 Hz, 1H), 6.56 (d, *J*=6.0 Hz, 1H), 5.19 (d, *J*=16 Hz, 2H), 3.58 (s, 3H)

^{13}C NMR (125MHz, CDCl$_3$): δ 165.41 (d, J_{CP}=2.9 Hz), 153.27 (d, J_{CP}=8.5 Hz), 136.33 (d, J_{CP}=11.4 Hz), 131.87 (d, J_{CP}=22 Hz), 130.26 (d, J_{CP}=140.1 Hz), 126.14 (d, J_{CP}=11.5 Hz), 113.50 (d, J_{CP}=10.5 Hz), 52.71, 27.17 (d, J_{CP}=57.6 Hz)

HRMS (ESI) m/z: calc'd for $C_{17}H_{16}O_5P$ $[M]^+$: 331.0730, found 331.0733

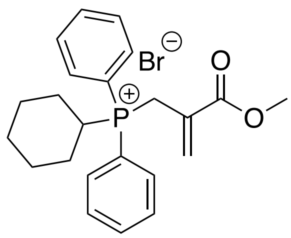

Cyclohexyl(2-(methoxycarbonyl)allyl)diphenylphosphonium bromide

^{1}H NMR (500MHz, CDCl$_3$): δ 7.91-7.87 (m, 4H), 7.79-7.76 (m, 2H), 7.69-7.65 (m, 4H), 6.23-6.21 (m, 2H), 4.69 (d, J=15.0 Hz, 2H), 4.06 (m, 1H), 3.45 (s, 3H), 2.16 (m, 2H), 1.81 (m, 2H), 1.74-1.67 (m, 4H), 1.01-0.96 (m, 3H)

^{13}C NMR (125MHz, CDCl$_3$): δ 166.15 (d, J_{CP}=1.9 Hz), 135.24 (d, J_{CP}=9.5 Hz), 134.64 (d, J_{CP}=2.9 Hz), 134.48 (d, J_{CP}=8.6 Hz), 129.79 (d, J_{CP}=12.4 Hz), 128.00 (d, J_{CP}=9.6 Hz), 115.15 (d, J_{CP}=80 Hz), 52.29, 32.04 (d, J_{CP}=44.9 Hz), 25.57, 25.55, 25.52, 25.42, 25.28, 23.26 (d, J_{CP}=46.6 Hz)

HRMS (ESI) m/z: calc'd for $C_{23}H_{28}O_2P$ $[M]^+$: 367.1821, found 367.1839

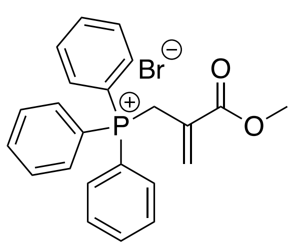

(2-(methoxycarbonyl)allyl)triphenylphosphonium bromide

^{1}H NMR (500MHz, CDCl$_3$): δ 7.75 (m, 6H), 7.69 (m, 3H), 7.58 (m, 6H), 6.39 (s, 2H), 5.09 (d, *J*=15 Hz, 2H) 3.26 (s, 3H)

^{13}C NMR (125MHz, CDCl$_3$): δ 165.74 (d, J_{CP}=2.9 Hz), 135.90 (d, J_{CP}=9.5 Hz), 135.09 (d, J_{CP}=2.8 Hz), 134.20 (d, J_{CP}=9.6 Hz), 130.27 (d, J_{CP}=13.3 Hz), 127.38 (d, J_{CP}=9.5 Hz), 117.70 (d, J_{CP}=85.9 Hz), 52.35, 26.02 (d, J_{CP}=50.5 Hz)

HRMS (ESI) m/z: calc'd for $C_{23}H_{22}O_2P$ [M]$^+$: 361.1352, found 361.1363

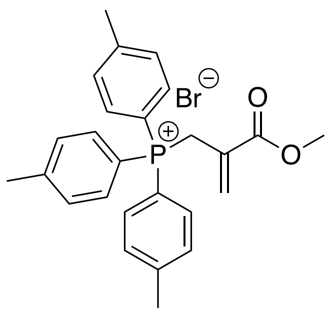

(2-(methoxycarbonyl)allyl)tri-p-tolylphenylphosphonium bromide

^{1}H NMR (500MHz, CDCl$_3$): δ 7.69-7.65 (m, 6H), 7.43-7.42 (m, 6H), 6.45 (d, *J*=5.5 Hz, 1H), 6.40 (d, *J*=5.5 Hz, 1H), 4.97 (d, *J*=15 Hz, 2H), 3.35 (s, 3H), 2.44 (s, 9H)

^{13}C NMR (125MHz, CDCl$_3$): δ 165.83 (d, J_{CP}=2.9 Hz), 146.25 (d, J_{CP}=2.8 Hz), 135.65 (d, J_{CP}=9.5 Hz), 134.06 (d, J_{CP}=10.5 Hz), 130.90 (d, J_{CP}=12.4 Hz), 127.60 (d, J_{CP}=8.6 Hz), 114.50 (d, J_{CP}=87.6 Hz), 52.27, 26.28 (d, J_{CP}=51.5 Hz), 21.81

HRMS (ESI) m/z: calc'd for $C_{26}H_{28}O_2P$ [M]$^+$: 403.1821, found 403.1835

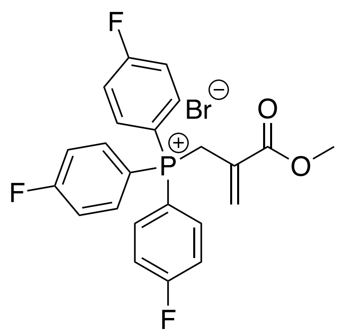

Tris(4-fluorophenyl)(2-(methoxycarbonyl)allyl)phosphonium bromide

^{1}H NMR (500MHz, CDCl$_3$): δ 7.85-7.84 (m, 6H), 7.30-7.26 (m, 6H), 6.41 (s, 2H), 5.20 (d, J=15.5 Hz, 2H), 3.36 (s, 3H)

^{13}C NMR (125MHz, CDCl$_3$): δ 167.88 (d, J_{CP}=3.8 Hz), 165.84 (dd, J_{CP}=2.9 Hz, J_{CF}=7.6 Hz), 137.23 (dd, J_{CP}=9.6 Hz, J_{CF}=12.5 Hz), 136.41 (d, J_{CP}=10.5 Hz), 127.11 (d, J_{CP}=10.5 Hz), 118.23 (dd, J_{CP}=21.9 Hz, J_{CF}=14.3 Hz), 113.34 (dd, J_{CP}=90.5 Hz, J_{CF}=2.8 Hz), 52.58, 26.61(d, J_{CP}=50.5 Hz)

HRMS (ESI) m/z: calc'd for $C_{23}H_{19}F_3O_2P$ $[M]^+$: 415.1069, found 415.1074

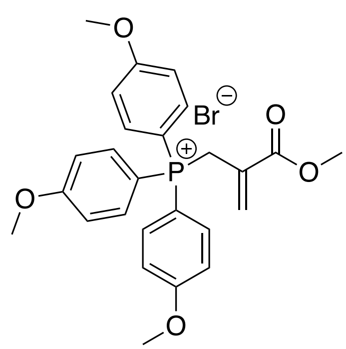

(2-(methoxycarbonyl)allyl)tris(4-methoxyphenyl)phosphonium bromide

^{1}H NMR (500MHz, CDCl$_3$): δ 7.71-7.67 (m, 6H), 7.12-7.10 (m, 6H), 6.44 (d, J=5.5 Hz, 1H), 6.33 (d, J=5.5 Hz, 1H), 4.84 (d, J=15.0 Hz, 2H), 3.87 (s, 9H), 3.39 (s, 3H)

^{13}C NMR (125MHz, CDCl$_3$): δ 165.88 (d, J_{CP}=1.9 Hz), 164.63 (d, J_{CP}=2.9 Hz), 136.04 (d, J_{CP}=11.5 Hz), 135.27 (d, J_{CP}=9.5 Hz), 127.93 (d, J_{CP}=9.5 Hz), 115.89 (d, J_{CP}=14.3 Hz), 108.37 (d, J_{CP}=94.4 Hz), 55.90, 52.36, 26.92 (d, J_{CP}=52.4 Hz)

HRMS (ESI) m/z: calc'd for $C_{26}H_{28}O_5P$ $[M]^+$: 451.1669, found 451.1681

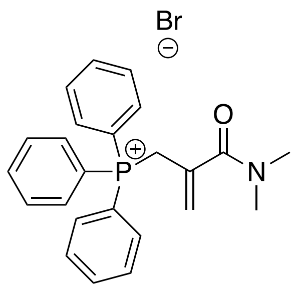

(2-(dimethylcarbamoyl)allyl)triphenylphosphonium bromide

^{1}H NMR (400MHz, CDCl$_3$): δ 7.95-7.90 (m, 6H), 7.77-7.74 (m, 3H), 7.67-7.66 (m, 6H), 5.80 (s, J=4.6 Hz, 1H), 5.41 (s, J=3.6 Hz, 1H), 5.07 (d, J=15 Hz, 2H), 3.12 (s, 3H), 2.64 (s, 3H)

^{13}C NMR (100MHz, CDCl$_3$): δ 168.87 (d, J_{CP}=2.4 Hz), 134.91 (d, J_{CP}=3.1 Hz), 134.44 (d, J_{CP}=10.0 Hz), 132.10 (d, J_{CP}=10.0 Hz), 130.15 (d, J_{CP}=12.8 Hz), 125.73 (d, J_{CP}=11.1 Hz), 118.78 (d, J_{CP}=86.4 Hz), 30.30 (d, J_{CP}=50.5 Hz)

HRMS (ESI) m/z: calc'd for $C_{24}H_{25}NOP$ $[M]^+$: 374.1668, found 374.1667

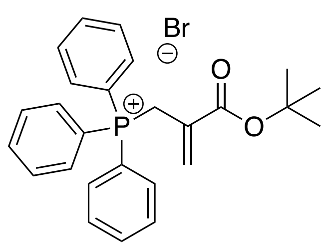

(2-(tert-butoxycarbonyl)allyl)triphenylphosphonium bromide

^{1}H NMR (400MHz, CDCl$_3$): δ 7.88-7.83 (m, 6H), 7.79-7.75 (m, 3H), 7.69-7.64 (m, 6H), 6.44 (d, *J*=5.7 Hz, 1H), 6.40 (d, *J*=5.2 Hz, 1H), 5.20 (d, *J*=15.1 Hz, 2H), 1.20 (s, 9H)

^{13}C NMR (100MHz, CDCl$_3$): δ 163.12 (d, J_{CP}=2.3 Hz), 133.61 (d, J_{CP}=3.3 Hz), 133.38 (d, J_{CP}=9.3 Hz), 132.94 (d, J_{CP}=10.3 Hz), 128.88 (d, J_{CP}=12.3 Hz), 127.49 (d, J_{CP}=10.0 Hz), 116.78 (d, J_{CP}=85.1 Hz), 80.57, 26.35, 24.34 (d, J_{CP}=51.0 Hz)

HRMS (ESI) m/z: calc'd for $C_{26}H_{28}O_2P$ $[M]^+$: 403.1821, found 403.1828

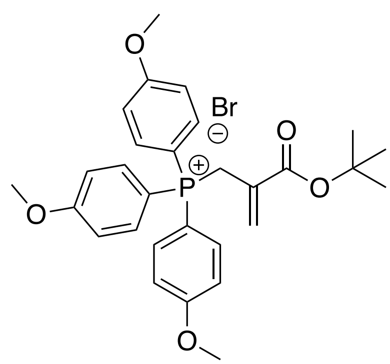

(2-(tert-butoxylcarbonyl)allyl)tris(4-methoxyphenyl)phosphonium bromide

^{1}H NMR (500MHz, CDCl$_3$): δ 7.77-7.73 (m, 6H), 7.15-7.14 (m, 6H), 6.43 (d, *J*=5.5 Hz, 1H), 6.31 (d, *J*=4.5 Hz, 1H), 4.91 (d, *J*=15.5 Hz, 2H), 3.91 (s, 9H), 1.25 (s, 9H)

^{13}C NMR (125MHz, CDCl$_3$): δ 164.59 (d, J_{CP}=2.9 Hz), 164.55, 136.11 (d, J_{CP}=11.5 Hz), 134.16 (d, J_{CP}=9.6 Hz), 129.36 (d, J_{CP}=9.5 Hz), 115.89 (d, J_{CP}=14.4 Hz), 108.79 (d, J_{CP}=93.5 Hz), 81.72, 55.88, 27.72, 26.49 (d, J_{CP}=53.4 Hz)

HRMS (ESI) m/z: calc'd for $C_{29}H_{34}O_5P$ $[M]^+$: 493.2138, found 493.2151

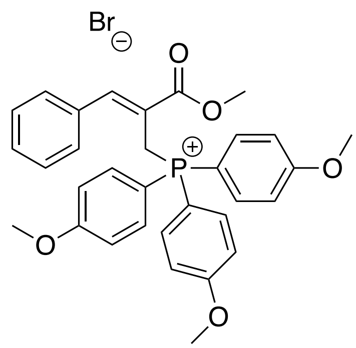

(*Z*)-(2-(methoxycarbonyl)-3-phenylallyl)tris(4-methoxyphenyl)phosphonium bromide

^{1}H NMR (500MHz, CDCl$_3$): δ 7.94 (d, *J*=4.5 Hz, 1H), 7.47-7.43 (m, 6H), 7.33-7.32 (m, 3H), 7.23-7.22 (m, 2H) 7.08-7.06 (m, 6H), 4.70 (d, *J*=15.5 Hz, 1H), 3.90 (s, 9H), 3.46 (s, 3H)

^{13}C NMR (125MHz, CDCl$_3$): δ 166.62 (d, J_{CP}=1.9 Hz), 164.62 (d, J_{CP}=2.9 Hz), 146.02 (d, J_{CP}=10.5 Hz), 135.83 (d, J_{CP}=11.5 Hz), 133.74 (d, J_{CP}=2.9 Hz), 129.54, 129.28, 128.54, 121.56 (d, J_{CP}=10.4 Hz), 115.91 (d, J_{CP}=14.3 Hz), 108.18 (d, J_{CP}=93.4 Hz), 56.07, 52.66, 25.33 (d, J_{CP}=53.4 Hz)

HRMS (ESI) m/z: calc'd for $C_{32}H_{32}O_5P$ $[M]^+$: 527.1982, found 527.1990

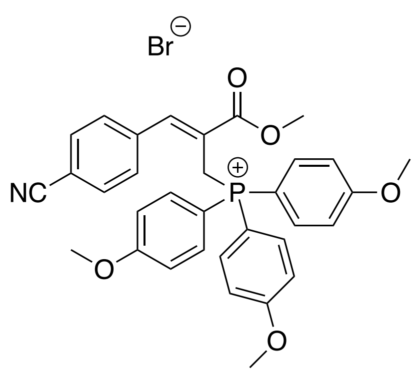

(*Z*)-(3-(4-cyanophenyl)-2-(methoxycarbonyl)allyl)tris(4-methoxyphenyl)phosphonium bromide

^{1}H NMR (500MHz, CDCl$_3$): δ 7.93 (d, *J*=5.5 Hz, 1H), 7.68-7.64 (m, 4H), 7.58-7.54 (m, 6H), 7.04-7.01 (m, 6H), 5.07 (d, *J*=15 Hz, 2H), 3.90 (s, 9H), 3.47 (s, 3H)

^{13}C NMR (125MHz, CDCl$_3$): δ 166.11, 164.56 (d, J_{CP}=2.9 Hz), 143.66 (d, J_{CP}=9.6 Hz), 138.11 (d, J_{CP}=2.8 Hz), 135.91 (d, J_{CP}=11.4 Hz), 132.85, 129.68 (d, J_{CP}=1.9 Hz), 123.93 (d, J_{CP}=10.5 Hz), 118.28, 115.71 (d, J_{CP}=14.4 Hz), 112.53, 108.16 (d, J_{CP}=93.4 Hz), 55.91, 52.79, 25.03 (d, J_{CP}=52.5 Hz)

HRMS (ESI) m/z: calc'd for $C_{33}H_{31}NO_5P$ $[M]^+$: 552.1934, found 552.1913

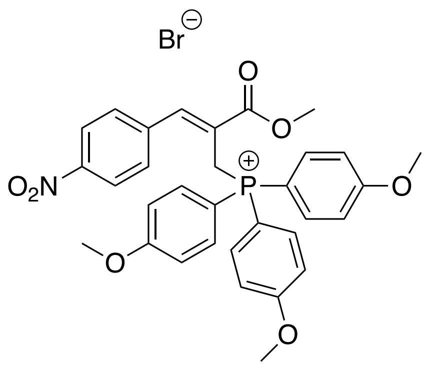

(*Z*)-(2-(methoxycarbonyl)-3-(4-nitrophenyl)allyl)tris(4-methoxyphenyl)phosphonium bromide (major isomer)

^{1}H NMR (500MHz, CDCl$_3$): δ 8.17 (d, *J*=9.0 Hz, 2H), 7.97 (d, *J*=6.0 Hz, 1H), 7.76 (d, *J*=8.5 Hz, 2H), 7.58-7.54 (m, 6H), 7.03-7.00 (m, 6H), 5.10 (d, *J*=15.5 Hz, 2H), 3.87 (s, 9H), 3.49 (s, 3H)

^{13}C NMR (125MHz, CDCl$_3$): δ 166.05, 164.58 (d, J_{CP}=2.9 Hz), 147.82, 143.27 (d, J_{CP}=10.5 Hz), 139.96 (d, J_{CP}=3.8 Hz), 135.92 (d, J_{CP}=11.4 Hz), 130.08 (d, J_{CP}=1.9 Hz), 124.35 (d, J_{CP}=9.6 Hz), 124.21, 115.71 (d, J_{CP}=13.4 Hz), 108.17 (d, J_{CP}=93.5 Hz), 55.87, 52.83, 25.25 (d, J_{CP}=52.5 Hz)

HRMS (ESI) m/z: calc'd for $C_{32}H_{31}NO_7P$ $[M]^+$: 572.1833, found 572.1858

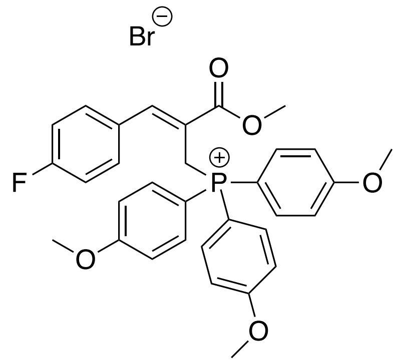

(Z)-(3-(4-fluorophenyl)-2-(methoxycarbonyl)allyl)tris(4-methoxyphenyl)phosphonium bromide

^{1}H NMR (500MHz, $CDCl_3$): δ 7.90 (d, J=5.0 Hz, 1H), 7.56-7.52 (m, 6H), 7.45-7.42 (m, 2H), 7.06-7.02 (m, 8H), 4.93 (d, J=15.0 Hz, 2H), 3.89 (s, 9H), 3.45 (s, 3H)

^{13}C NMR (125MHz, $CDCl_3$): δ 166.61, 164.53 (d, J_{CP}=2.9 Hz), 163.03 (d, J_{CF}=249.9 Hz), 144.86 (d, J_{CP}=9.5 Hz), 135.90 (d, J_{CP}=11.4 Hz), 131.11 (dd, J_{CP}=1.9 Hz, J_{CF}=8.6 Hz), 129.76 (d, J_{CP}=3.9 Hz), 121.25 (d, J_{CP}=9.6 Hz), 116.38 (d, J_{CP}= 21 Hz), 115.74 (d, J_{CP}=13.4 Hz), 108.38 (d, J_{CP}=93.5 Hz), 55.94, 52.59, 25.09 (d, J_{CP}=52.5 Hz)

HRMS (ESI) m/z: calc'd for $C_{32}H_{31}FO_5P$ $[M]^+$: 545.1888, found 545.1879

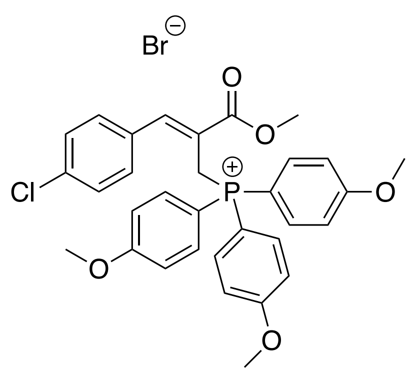

(Z)-(3-(4-chlorophenyl)-2-(methoxycarbonyl)allyl)tris(4-methoxyphenyl)phosphonium bromide (major isomer)

^{1}H NMR (500MHz, $CDCl_3$): δ 7.89 (d, J=5.0 Hz, 1H), 7.56-7.52 (m, 6H), 7.41 (d, J=8.5 Hz, 2H), 7.32 (d, J=8.5 Hz, 2H), 7.05-7.03 (m, 6H), 4.97 (d, J=15.0 Hz, 2H), 3.90 (s, 9H), 3.45 (s, 3H)

^{13}C NMR (125MHz, $CDCl_3$): δ 166.44 (d, J_{CP}=1.9 Hz), 164.53 (d, J_{CP}=2.9 Hz), 144.67 (d, J_{CP}=10.5 Hz), 135.88 (d, J_{CP}=11.4 Hz), 135.31, 132.16 (d, J_{CP}=2.9 Hz), 130.30 (d, J_{CP}=1.9 Hz), 129.44, 121.91 (d, J_{CP}=10.5 Hz), 115.71 (d, J_{CP}=13.4 Hz), 108.28 (d, J_{CP}=93.4 Hz), 55.93, 52.63, 24.96 (d, J_{CP}=52.4 Hz)

HRMS (ESI) m/z: calc'd for $C_{32}H_{31}ClO_5P$ $[M]^+$: 561.1592, found 561.1591

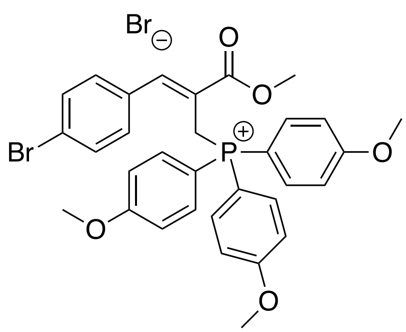

(Z)-(3-(4-bromophenyl)-2-(methoxycarbonyl)allyl)tris(4-methoxyphenyl)phosphonium bromide

(major isomer)

^{1}H NMR (500MHz, $CDCl_3$): 7.86 (d, J=5.5 Hz, 1H), 7.53-7.46 (m, 8H), 7.32 (d, J=8.5 Hz, 2H), 7.04-7.02 (m, 6H), 4.92 (d, J=15.0 Hz, 2H), 3.89 (s, 9H), 3.44 (s, 3H)

^{13}C NMR (125MHz, $CDCl_3$): δ 166.41 (d, J_{CP}=2.9 Hz), 164.53 (d, J_{CP}=3.8 Hz), 144.69 (d, J_{CP}=9.5 Hz), 135.85 (d, J_{CP}=11.5 Hz), 132.61 (d, J_{CP}=3.8 Hz), 132.37, 130.48 (d, J_{CP}=1.9 Hz), 123.66, 121.97 (d, J_{CP}=9.6 Hz), 115.72 (d, J_{CP}=13.3 Hz), 108.22 (d, J_{CP}=93.5 Hz), 55.95, 52.64, 24.88 (d, J_{CP}=52.5 Hz)

HRMS (ESI) m/z: calc'd for $C_{32}H_{31}BrO_5P$ $[M]^+$: 605.1087, found 605.1063

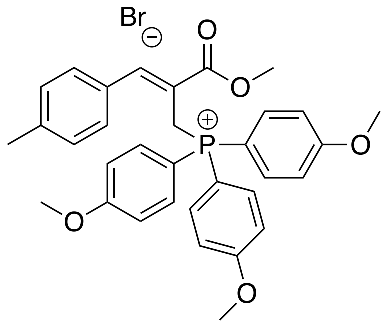

(*Z*)-(2-(methoxycarbonyl)-3-(*p*-tolyl)allyl)tris(4-methoxyphenyl)phosphonium bromide

^{1}H NMR (500MHz, CDCl$_3$): δ 7.91 (d, *J*=5.0 Hz, 1H), 7.52-7.48 (m, 6H), 7.17-7.12 (m, 4H), 7.09-7.07 (m, 6H), 4.74 (d, *J*=15.0 Hz, 2H), 3.91 (s, 9H), 3.47 (s, 3H), 2.35 (s, 3H)

^{13}C NMR (125MHz, CDCl$_3$): δ 166.85 (d, J_{CP}=1.9 Hz), 164.62 (d, J_{CP}=2.9 Hz), 146.13 (d, J_{CP}=10.5 Hz), 140.01, 135.90 (d, J_{CP}=11.4 Hz), 130.81 (d, J_{CP}=3.8 Hz), 129.94, 128.73 (d, J_{CP}=2.0 Hz), 120.54 (d, J_{CP}=10.4 Hz), 115.87 (d, J_{CP}=13.4 Hz), 108.39 (d, J_{CP}=93.4 Hz), 56.05, 52.59, 25.53 (d, J_{CP}=52.5 Hz), 21.41

HRMS (ESI) m/z: calc'd for $C_{32}H_{31}BrO_5P$ $[M]^+$: 605.2087, found 605.1063

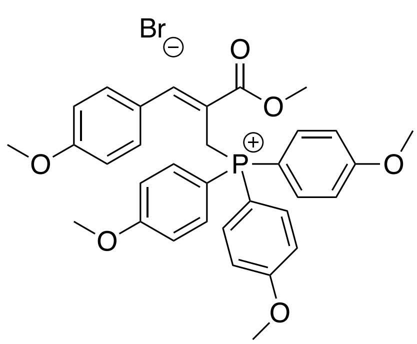

(*Z*)-(2-(methoxycarbonyl)-3-(4-methoxyphenylallyl)tris(4-methoxyphenyl)phosphonium bromide

^{1}H NMR (500MHz, CDCl$_3$): δ 7.86 (d, *J*=5.0 Hz, 1H), 7.54-7.50 (m, 6H), 7.30 (d, *J*=9.0 Hz, 2H), 7.08-7.06 (m, 6H), 6.85 (d, *J*=8.5 Hz, 2H), 4.79 (d, *J*=15.5 Hz, 2H), 3.89 (s, 9H), 3.82 (s, 3H), 3.45 (s, 3H)

^{13}C NMR (125MHz, CDCl$_3$): δ 167.04 (d, J_{CP}=1.9 Hz), 164.55 (d, J_{CP}=2.9 Hz), 160.71, 145.83 (d, J_{CP}=9.5 Hz), 135.90 (d, J_{CP}=11.4 Hz), 130.82 (d, J_{CP}=1.9 Hz), 125.93 (d, J_{CP}=3.9 Hz), 118.80 (d, J_{CP}=9.5 Hz), 115.81 (d, J_{CP}=14.3 Hz), 114.74, 108.42 (d, J_{CP}=93.5 Hz), 56.01, 55.59, 52.50, 25.50 (d, J_{CP}=52.5 Hz)

HRMS (ESI) m/z: calc'd for $C_{33}H_{34}O_6P$ $[M]^+$: 557.2088, found 557.2090

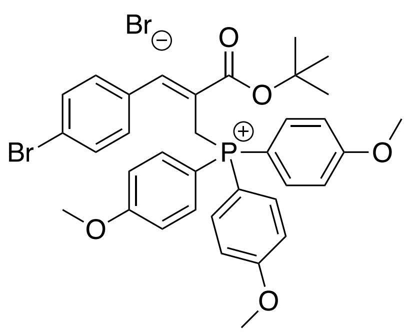

(*Z*)-(3-(4-bromophenyl)-2-(*tert*-butoxycarbonyl)allyl)tris(4-methoxyphenyl)phosphonium bromide (major isomer)

^{1}H NMR (500MHz, CDCl$_3$): δ 7.81 (d, *J*=5.5 Hz, 1H), 7.52-7.45 (m, 8H), 7.31 (d, *J*=8.0 Hz, 2H), 7.05-7.03 (m, 6H), 4.83 (d, *J*=15.0 Hz, 2H), 3.91 (s, 9H), 1.25 (s, 9H)

^{13}C NMR (125MHz, CDCl$_3$): δ 164.95, 164.50 (d, J_{CP}=3.9 Hz), 143.66 (d, J_{CP}=9.5 Hz), 135.89 (d, J_{CP}=11.5 Hz), 133.05, 132.37, 130.22, 123.96 (d, J_{CP}=10.5 Hz), 123.36, 115.74 (d, J_{CP}=14.3 Hz), 108.53 (d, J_{CP}=93.38 Hz), 82.47, 55.95, 27.71, 24.82 (d, J_{CP}=52.5 Hz)

HRMS (ESI) m/z: calc'd for $C_{35}H_{37}BrO_5P$ $[M]^+$: 647.1556, found 647.1556

CHAPTER 4: SUPPORTING INFORMATION

4.1 Appendices

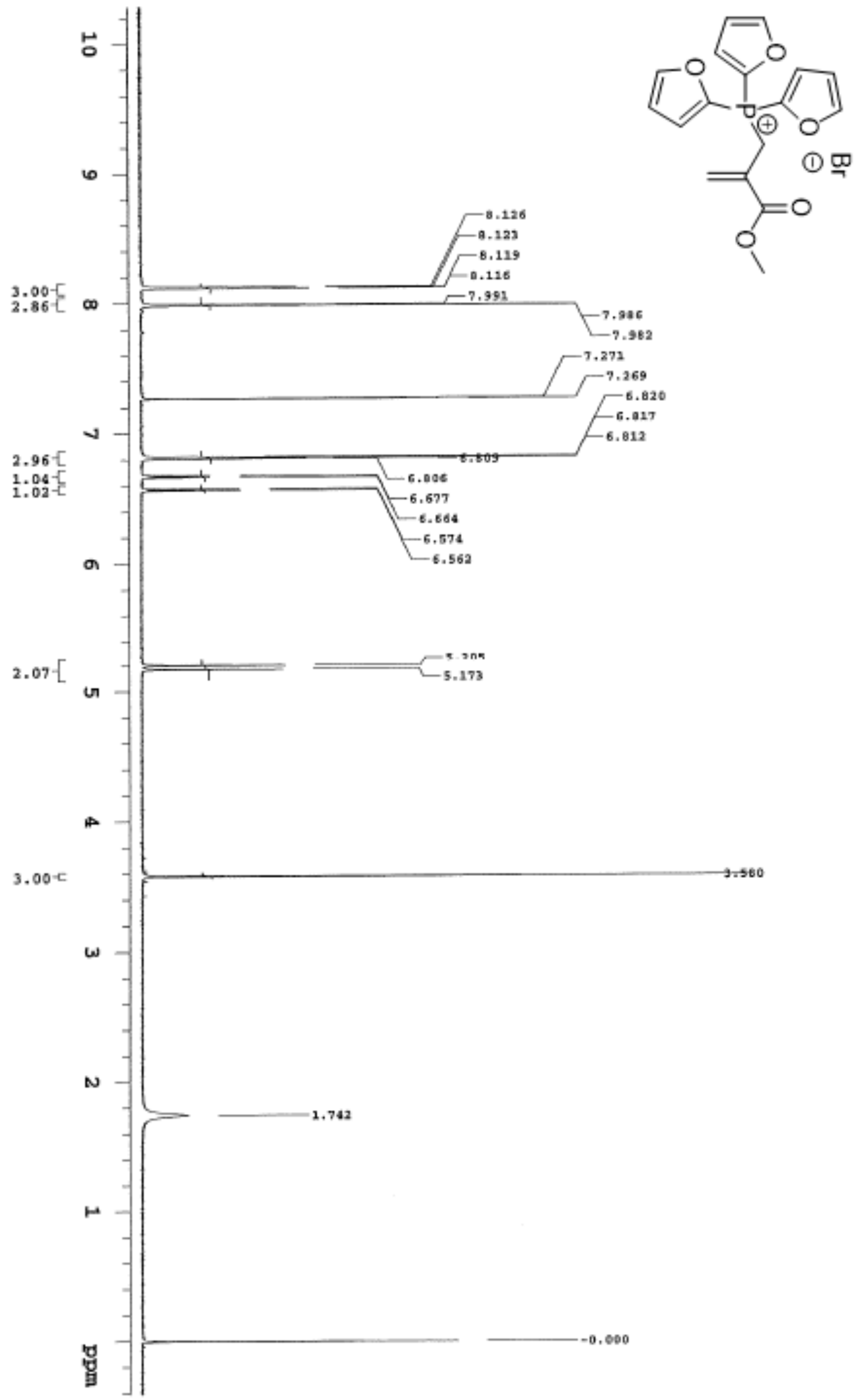

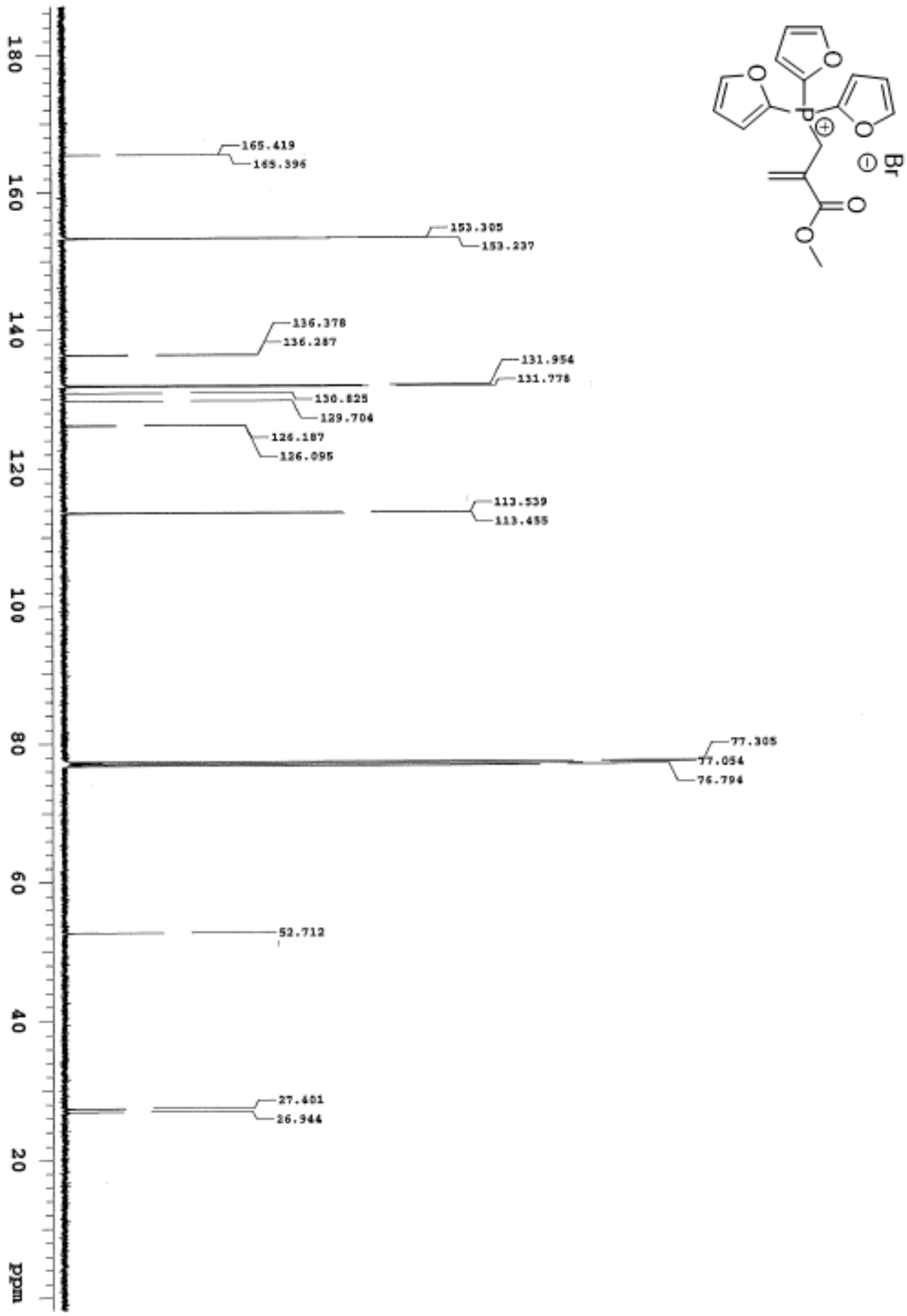

165.419
165.396
153.305
153.237
136.378
136.287
131.954
131.778
130.825
129.704
126.187
126.095
113.539
113.455
77.305
77.054
76.794
52.712
27.401
26.944
180
160
140
120
100
80
60
40
20
ppm
Br

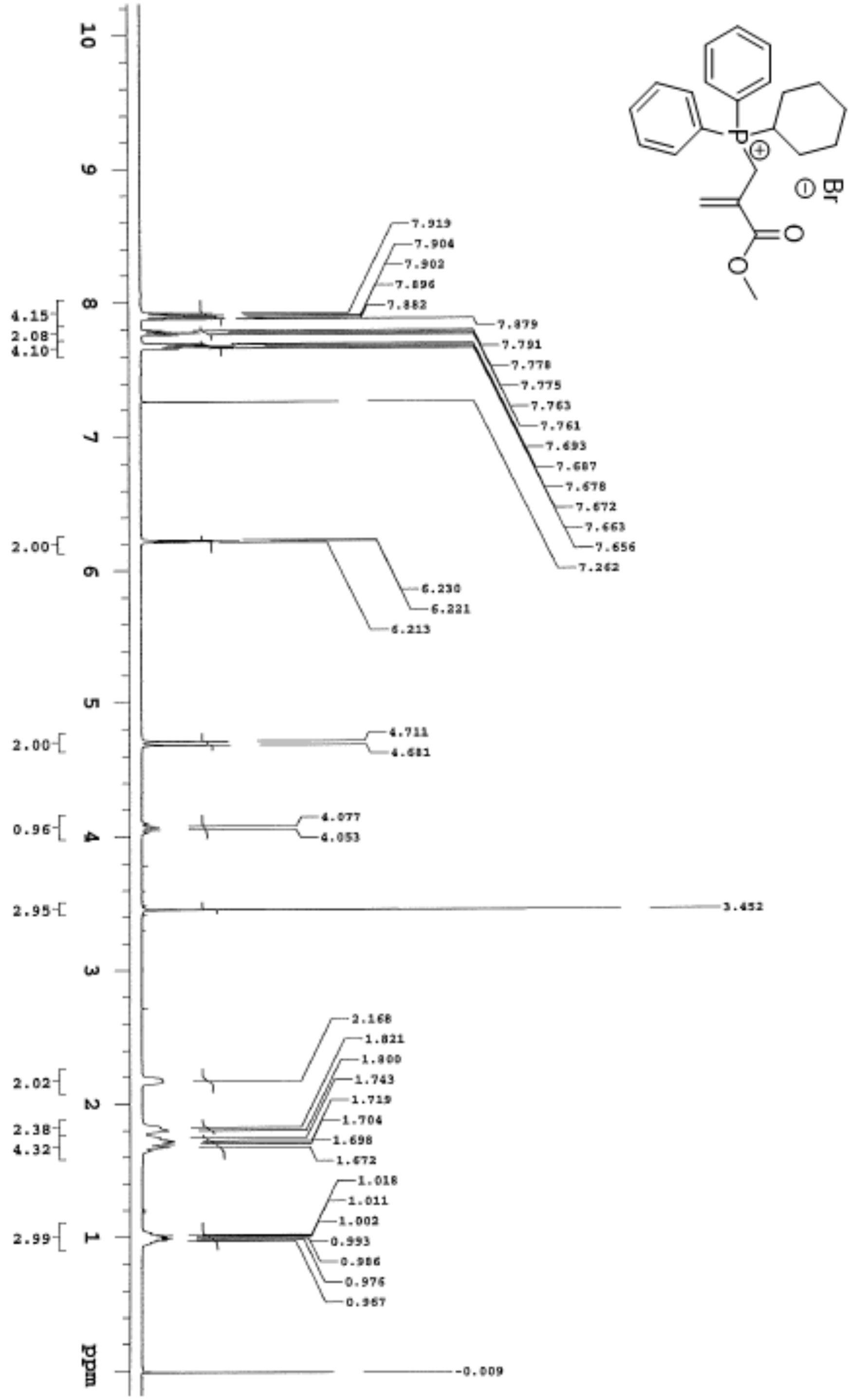
7.919
7.904
7.902
7.896
7.882
7.879
7.791
7.778
7.775
7.763
7.761
7.693
7.687
7.678
7.672
7.663
7.656
7.262
6.230
6.221
6.213
4.711
4.681
4.077
4.053
3.452
2.168
1.821
1.800
1.743
1.719
1.704
1.698
1.672
1.018
1.011
1.002
0.993
0.986
0.976
0.967
-0.009
4.15
2.08
4.10
2.00
2.00
0.96
2.95
2.02
2.38
4.32
2.99
ppm
P
Br
O

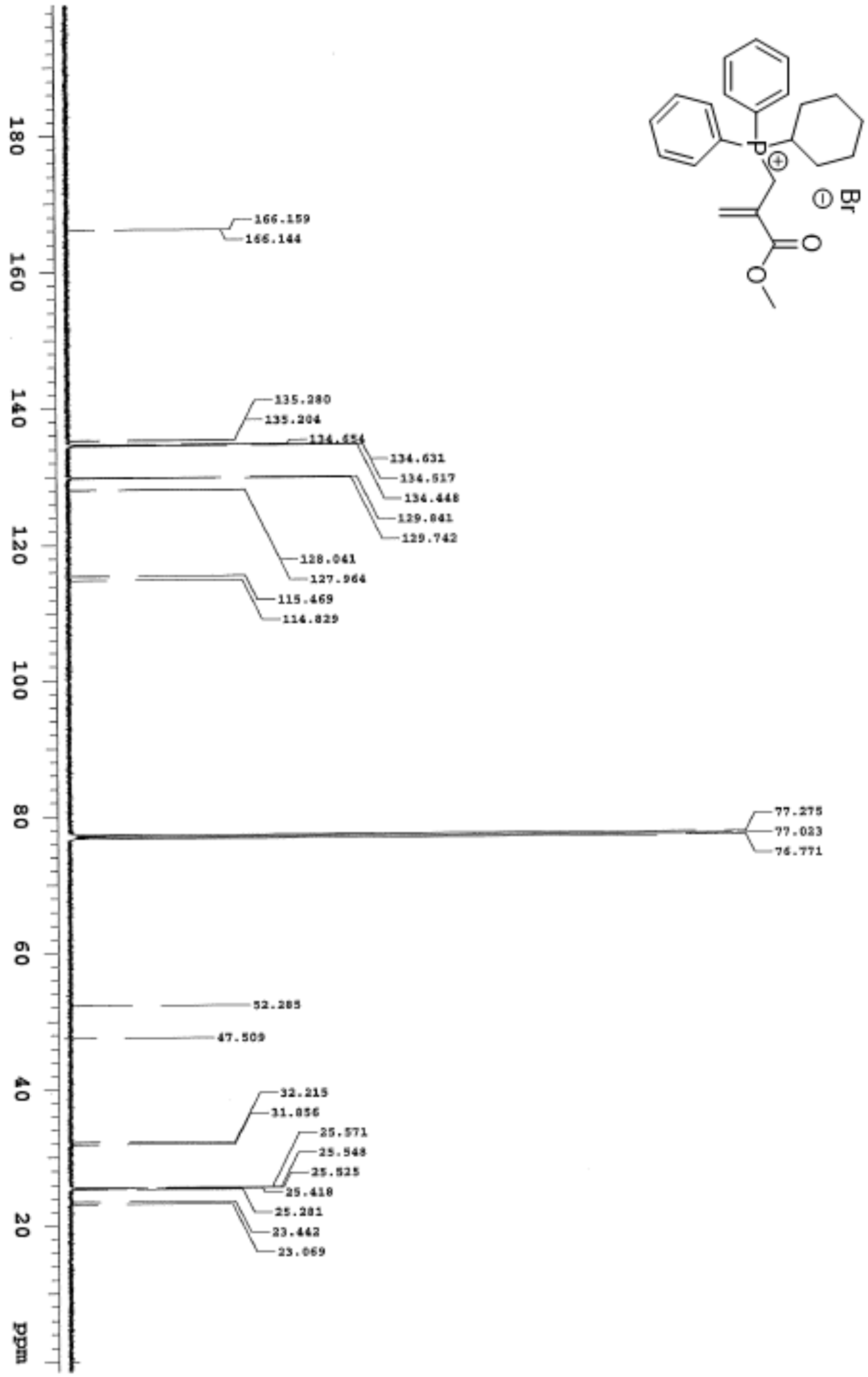

Br
166.159
166.144
135.280
135.204
134.654
134.631
134.517
134.448
129.841
129.742
128.041
127.964
115.469
114.829
77.275
77.023
76.771
52.285
47.509
32.215
31.856
25.571
25.548
25.525
25.418
25.281
23.442
23.069
180
160
140
120
100
80
60
40
20
ppm

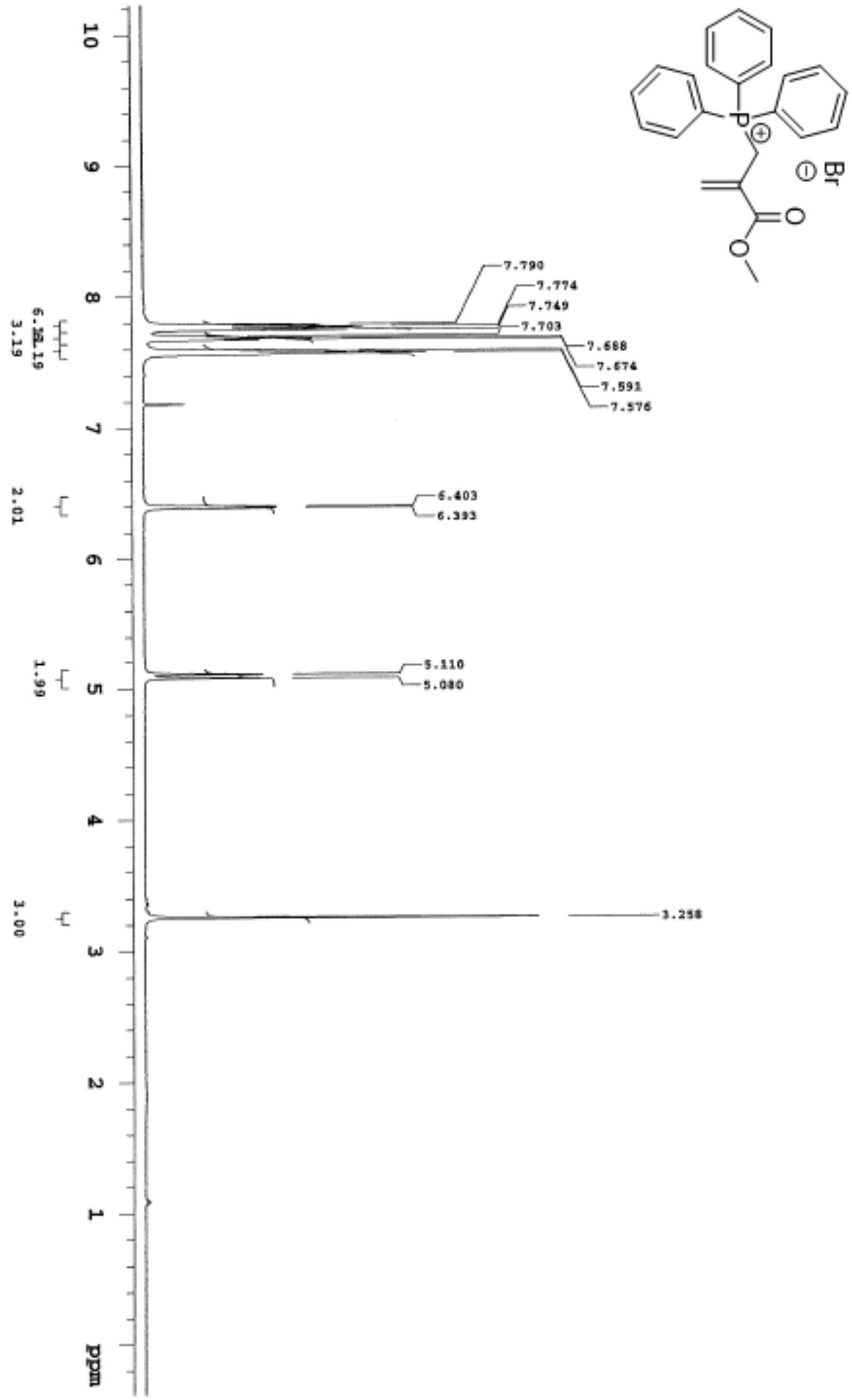
Br
7.790
7.774
7.749
7.703
7.688
7.674
7.591
7.576
6.403
6.393
5.110
5.080
3.258
3.19
2.01
1.99
3.00
10
9
8
7
6
5
4
3
2
1
ppm

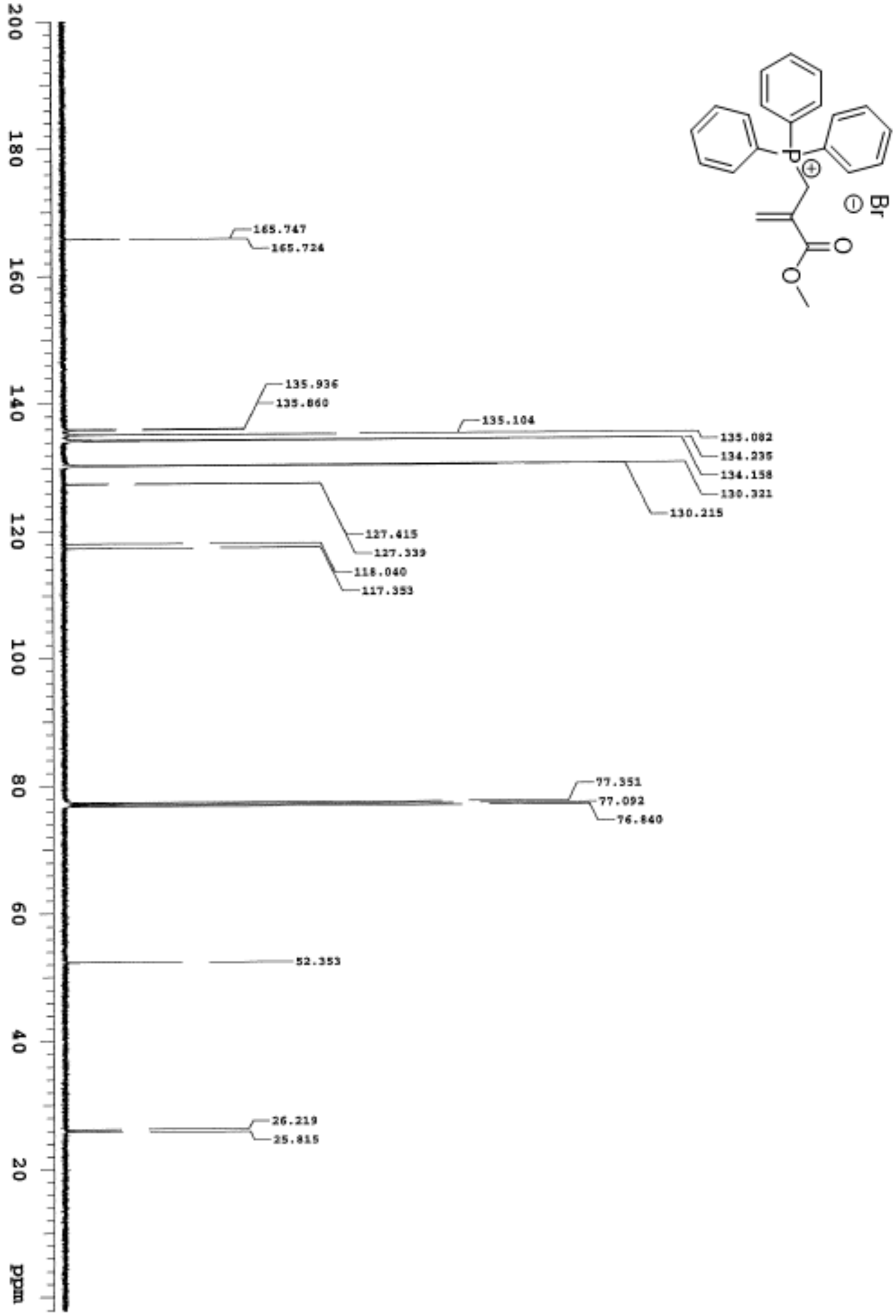
Br
165.747
165.724
135.936
135.860
135.104
135.082
134.235
134.158
130.321
130.215
127.415
127.339
118.040
117.353
77.351
77.092
76.840
52.353
26.219
25.815
200
180
160
140
120
100
80
60
40
20
ppm

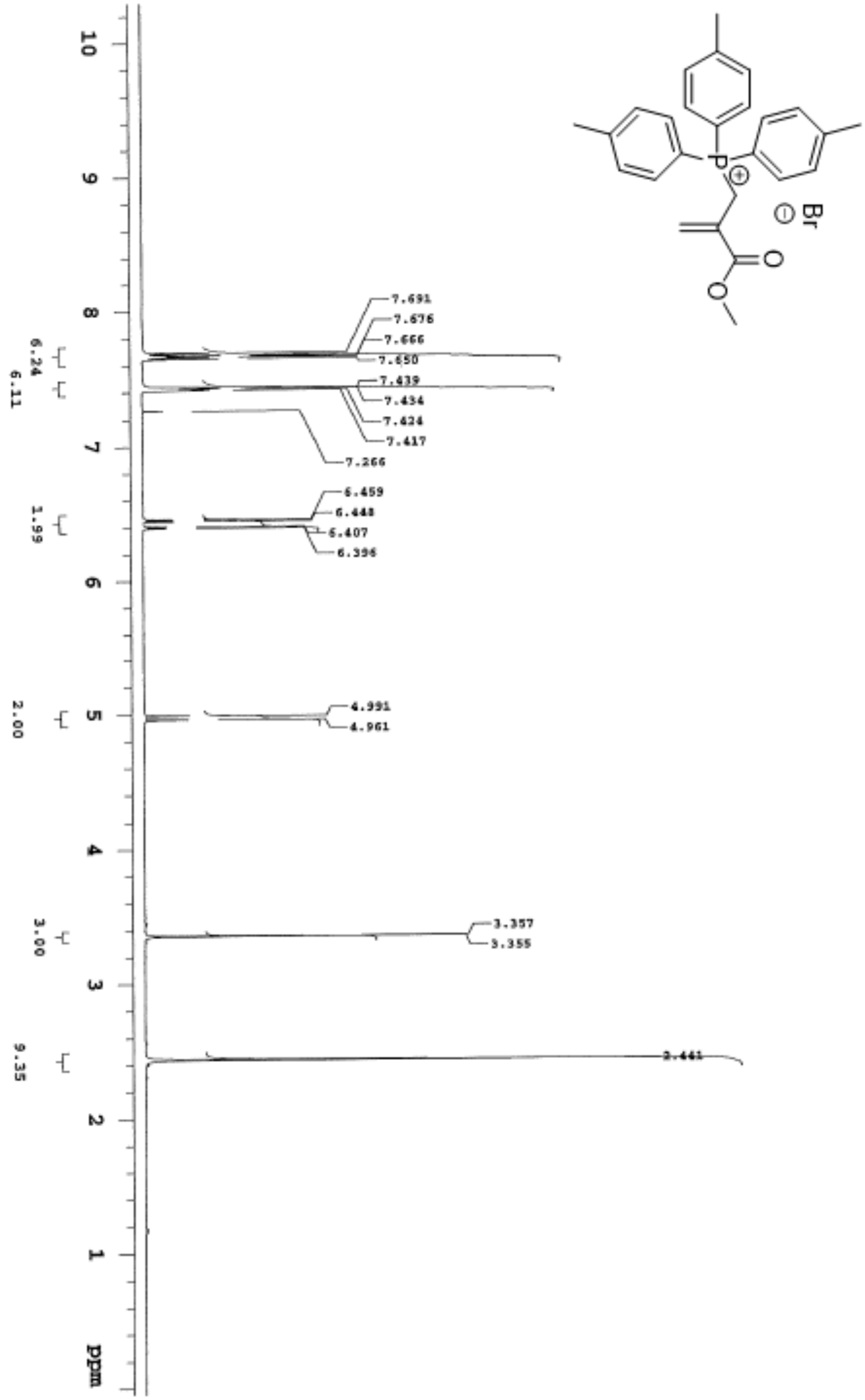
Br
7.691
7.676
7.666
7.650
7.439
7.434
7.424
7.417
7.266
6.459
6.448
6.407
6.396
4.991
4.961
3.357
3.355
2.441
6.24
6.11
1.99
2.00
3.00
9.35
10
9
8
7
6
5
4
3
2
1
ppm

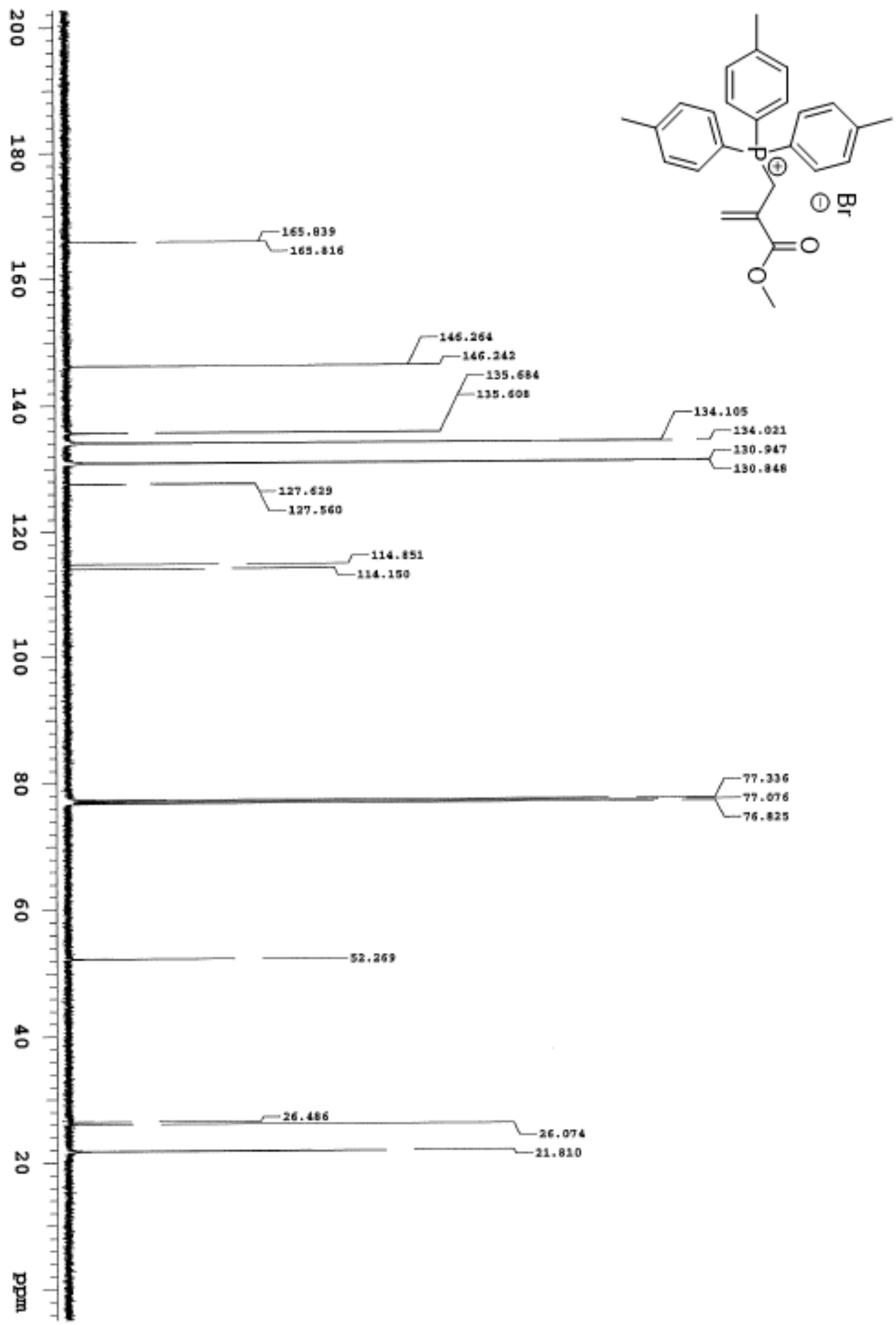
165.839
165.816
146.264
146.242
135.684
135.608
134.105
134.021
130.947
130.848
127.629
127.560
114.851
114.150
77.336
77.076
76.825
52.269
26.486
26.074
21.810
200
180
160
140
120
100
80
60
40
20
ppm
P
Br
O

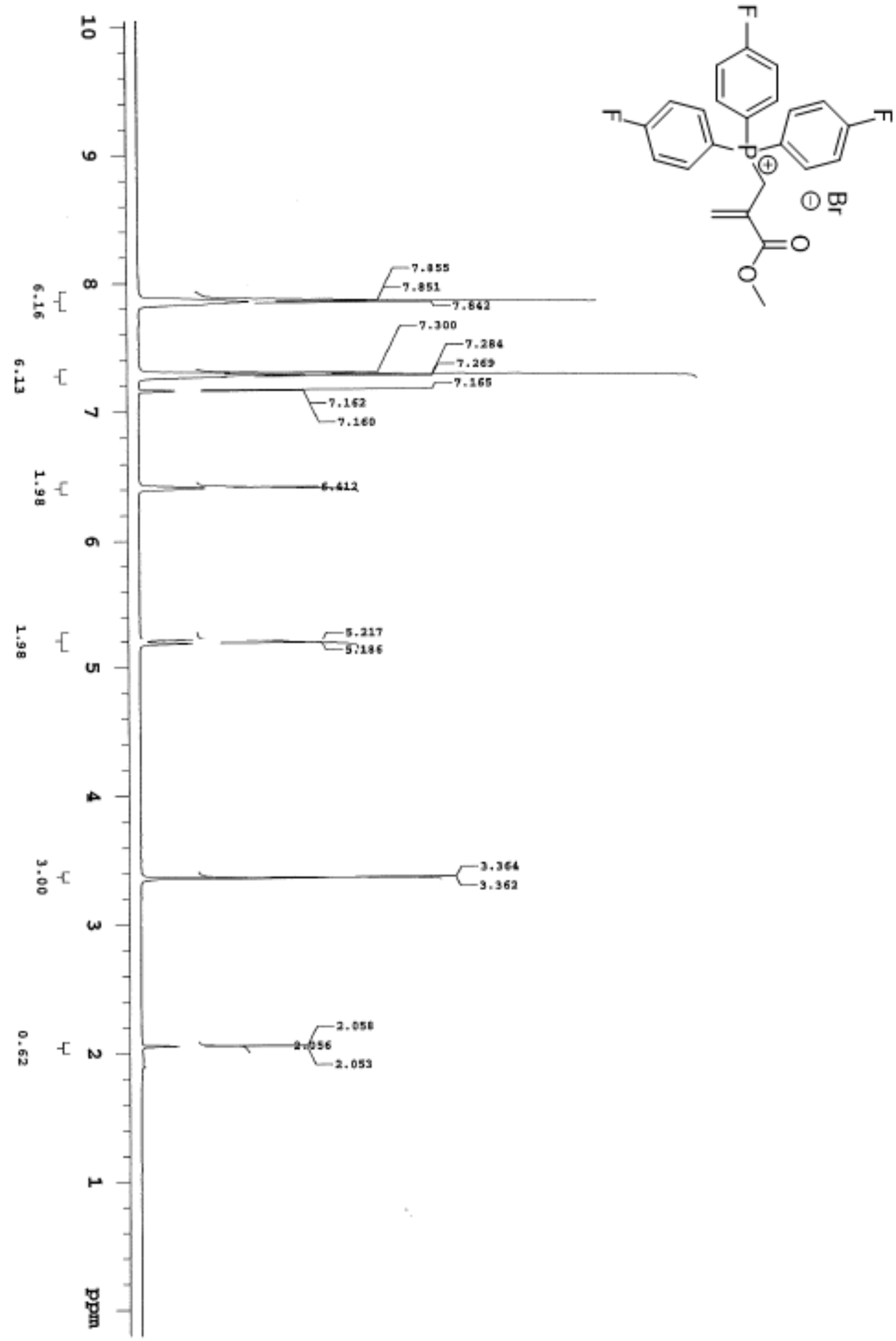

F
F
F
P
Br
O
7.855
7.851
7.842
7.300
7.284
7.269
7.165
7.162
7.160
6.412
5.217
5.186
3.364
3.362
2.058
2.056
2.053
6.16
6.13
1.98
1.98
3.00
0.62
10
9
8
7
6
5
4
3
2
1
ppm

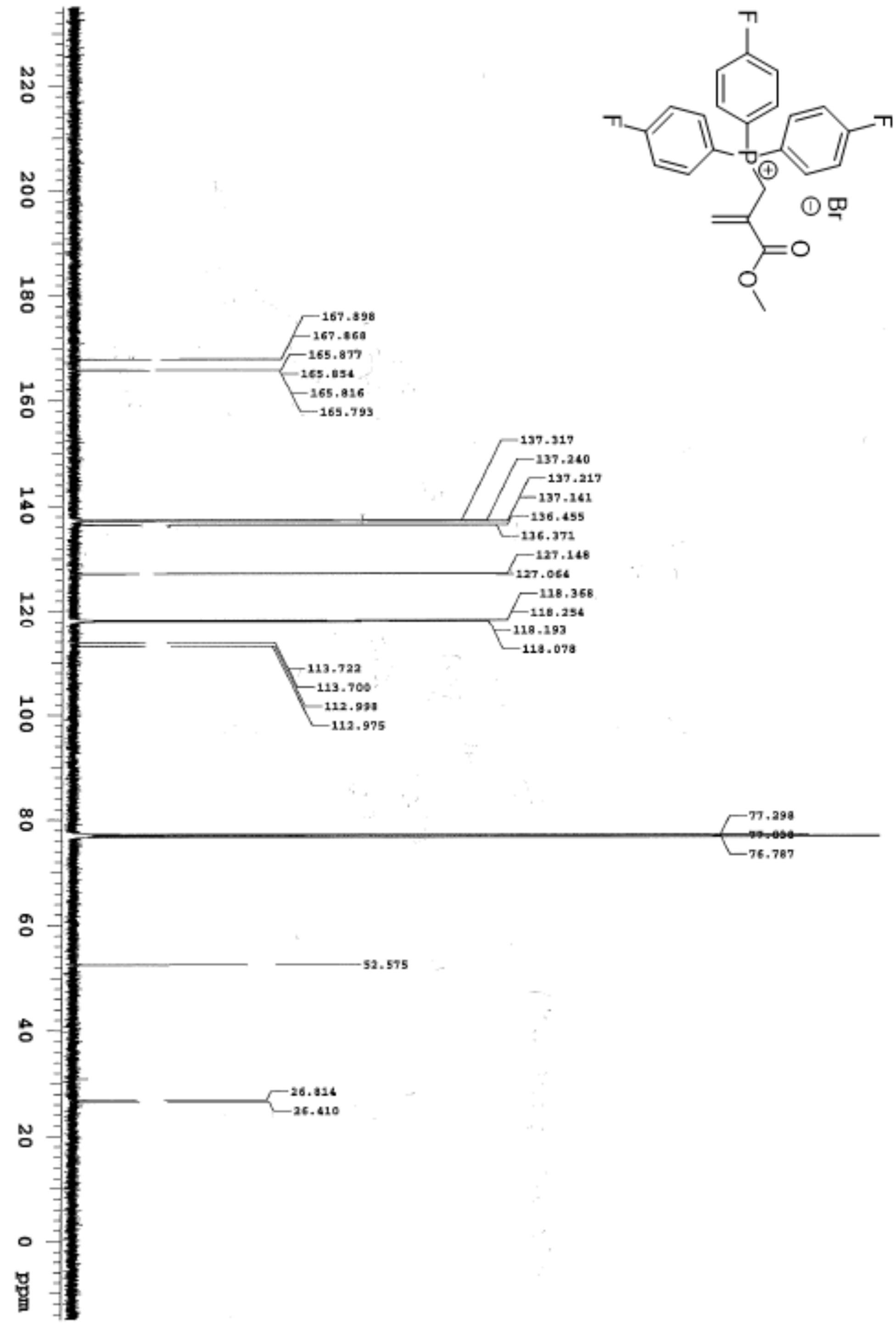

F
F
F
P
Br
O
O
167.898
167.868
165.877
165.854
165.816
165.793
137.317
137.240
137.217
137.141
136.455
136.371
127.148
127.064
118.368
118.254
118.193
118.078
113.722
113.700
112.998
112.975
77.298
76.787
52.575
26.814
26.410
220
200
180
160
140
120
100
80
60
40
20
0
ppm

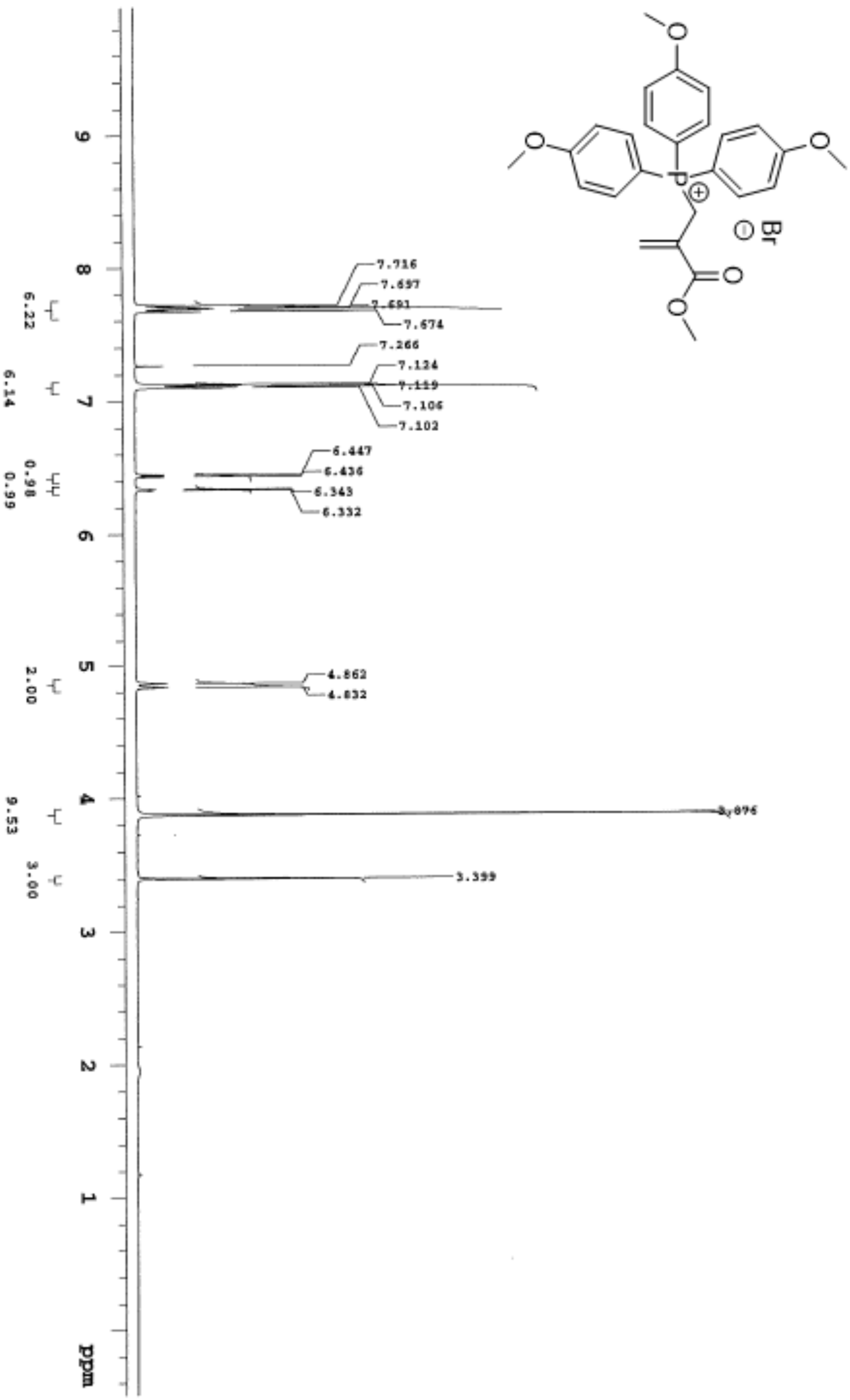
7.716
7.697
7.691
7.674
7.266
7.124
7.119
7.106
7.102
6.447
6.436
6.343
6.332
4.862
4.832
3.399
6.22
6.14
0.98
0.99
2.00
9.53
3.00
ppm
Br

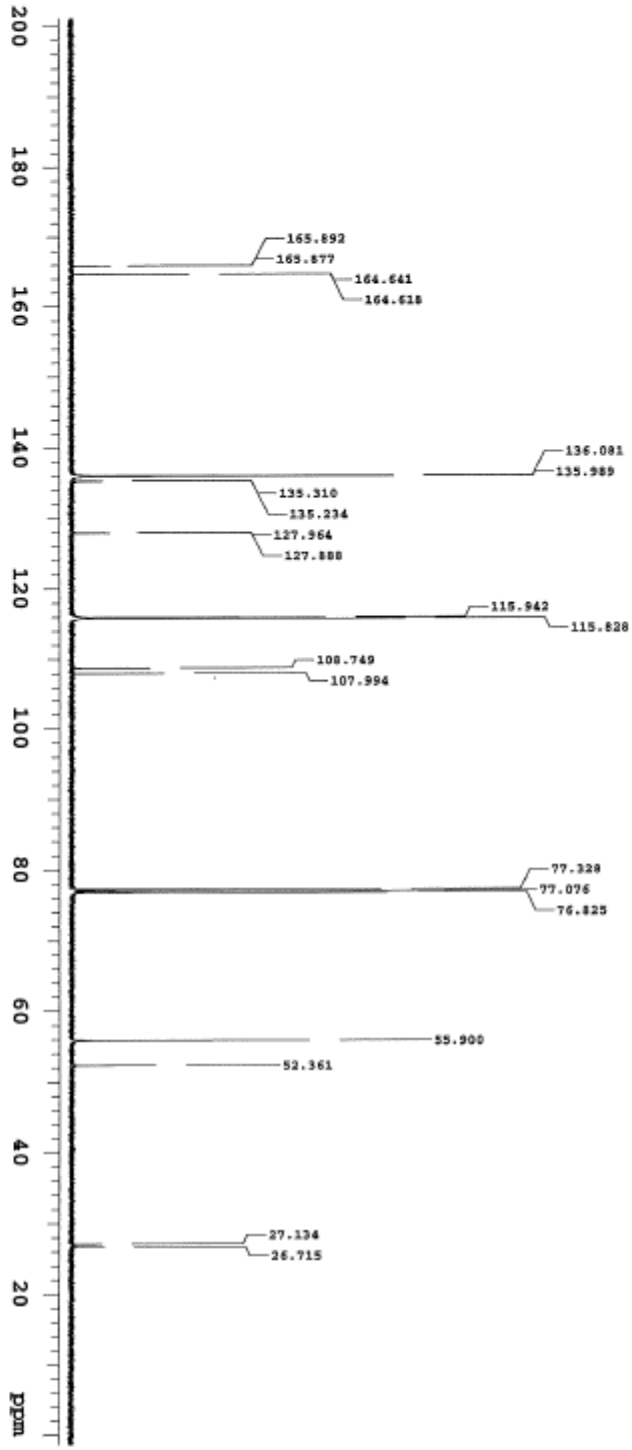
200
180
160
140
120
100
80
60
40
20
ppm
165.892
165.877
164.641
164.618
136.081
135.989
135.310
135.234
127.964
127.888
115.942
115.828
108.749
107.994
77.328
77.076
76.825
55.900
52.361
27.134
26.715

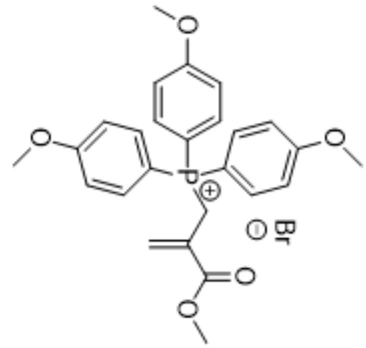
P
Br

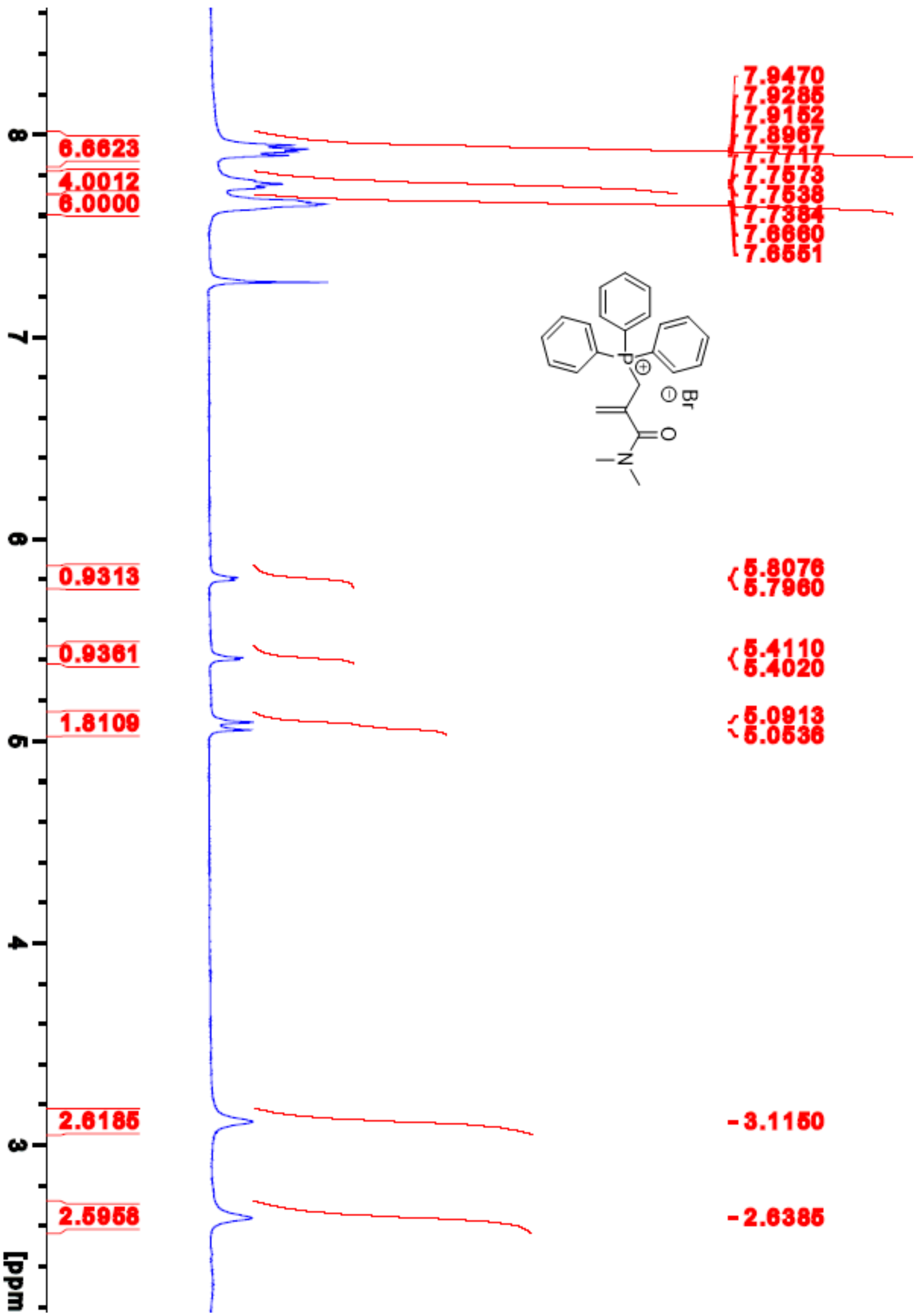
8
7
6
5
4
3
[ppm]
6.6623
4.0012
6.0000
0.9313
0.9361
1.8109
2.6185
2.5958
7.9470
7.9285
7.9152
7.8967
7.7717
7.7573
7.7538
7.7384
7.6660
7.6551
5.8076
5.7960
5.4110
5.4020
5.0913
5.0536
3.1150
2.6385
Br
O
N

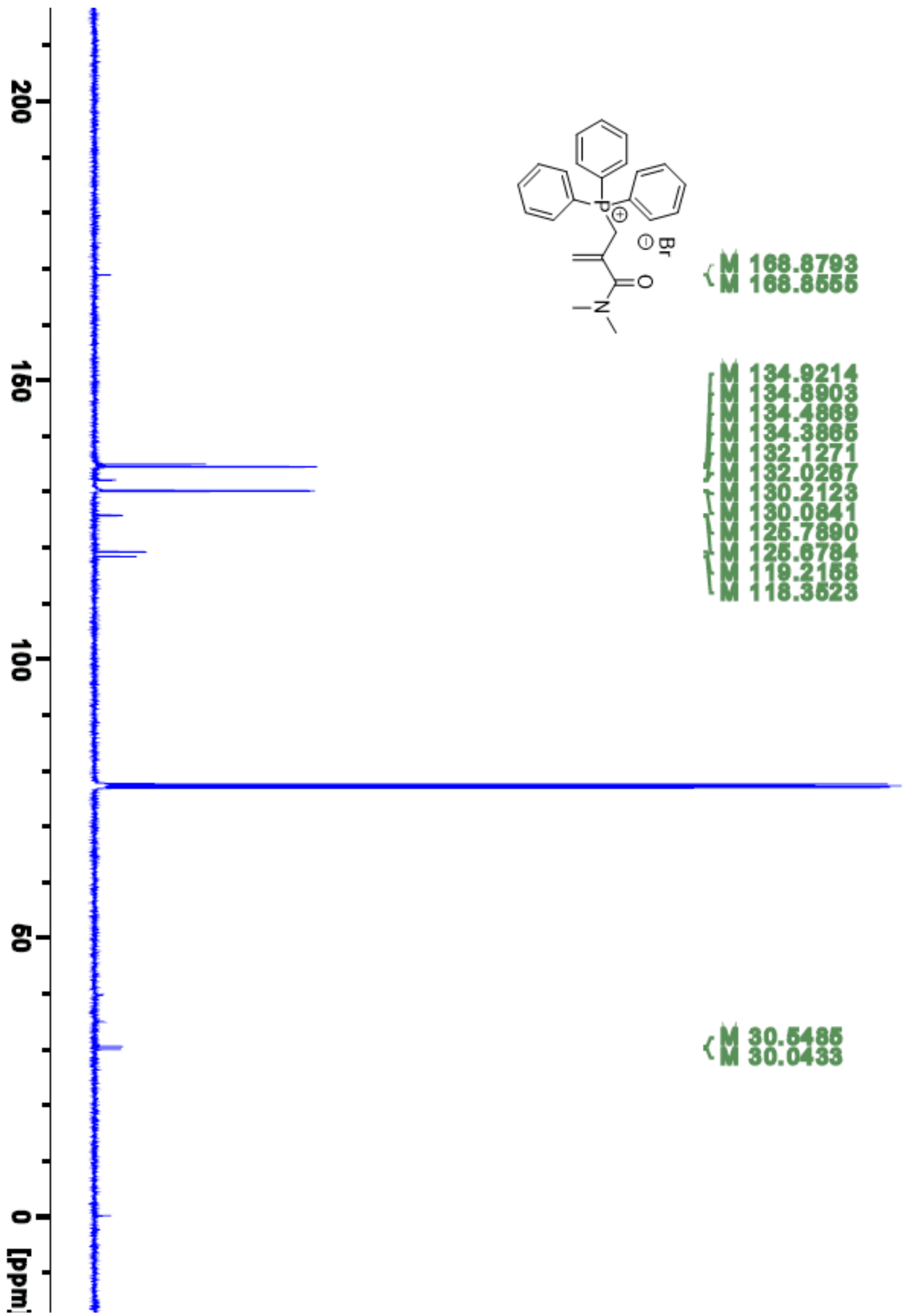
168.8793
168.8555
134.9214
134.8903
134.4869
134.3865
132.1271
132.0267
130.2123
130.0841
125.7890
125.6784
119.2158
118.3523
30.5485
30.0433
200
150
100
50
0
[ppm]
Br
O
N

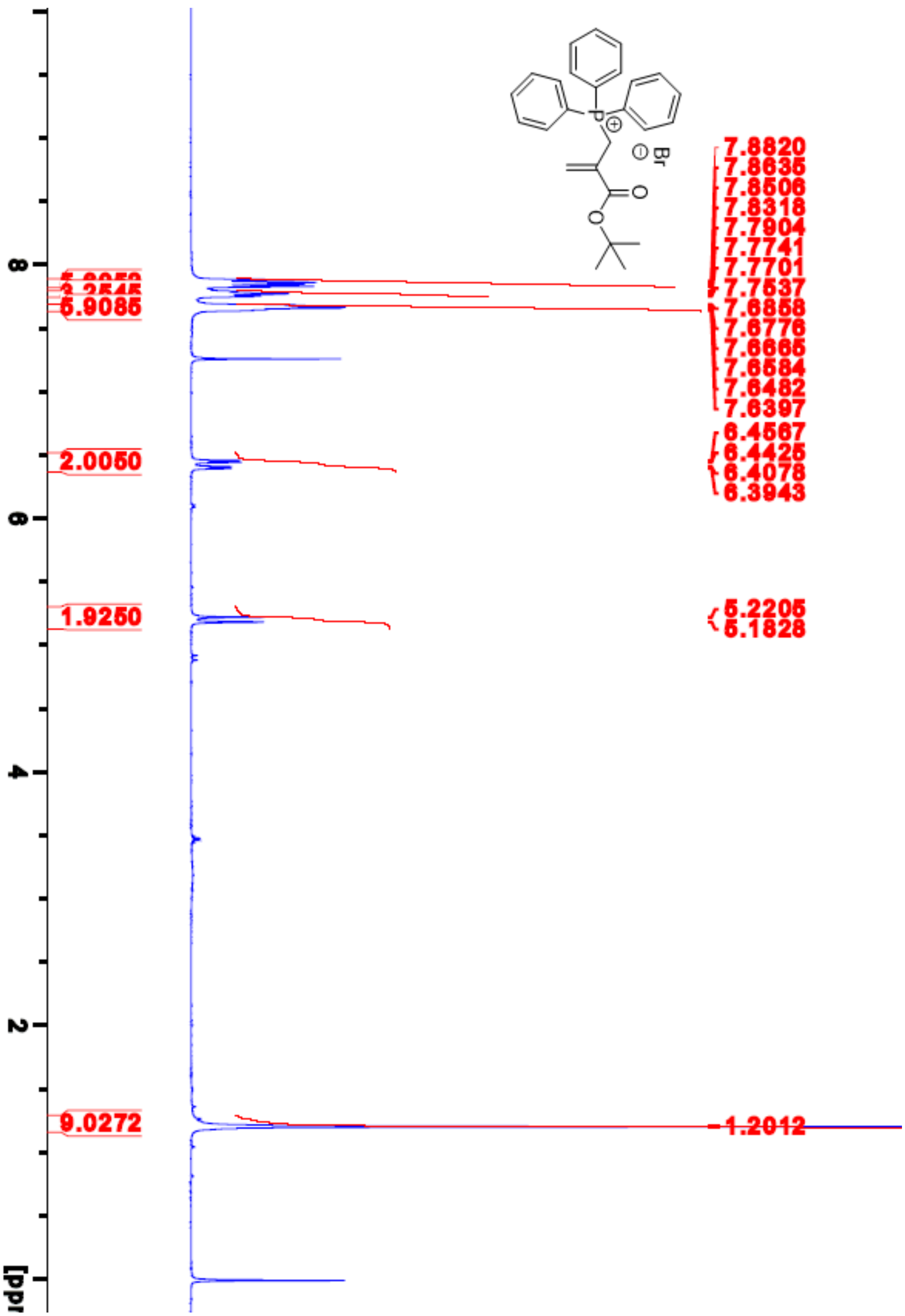

7.8820
7.8635
7.8506
7.8318
7.7904
7.7741
7.7701
7.7537
7.6858
7.6776
7.6665
7.6584
7.6482
7.6397
6.4567
6.4425
6.4078
6.3943
5.2205
5.1828
1.2012
6.9085
2.0050
1.9250
9.0272
Br
O
8
6
4
2

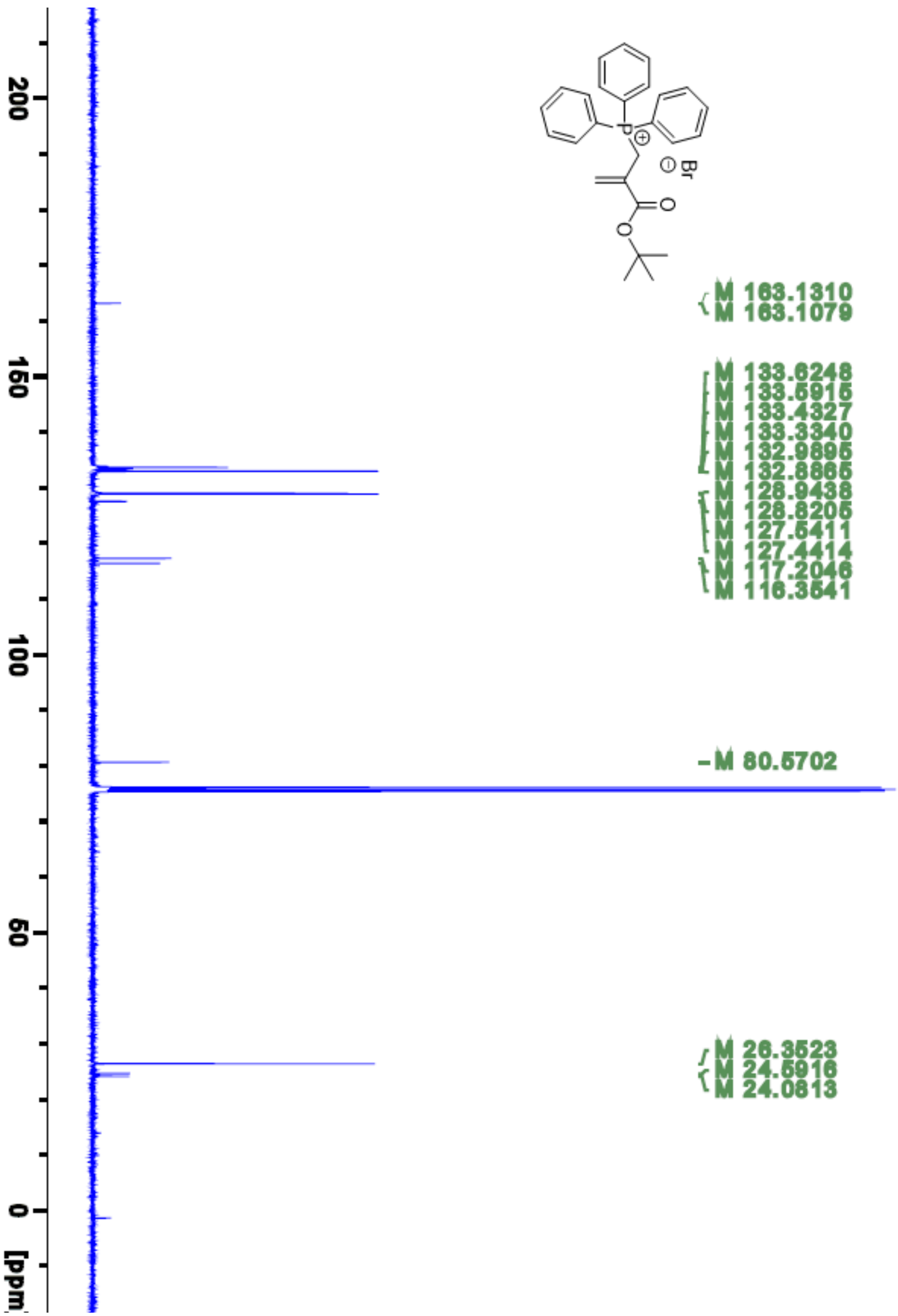

Br
M 163.1310
M 163.1079
M 133.6248
M 133.5915
M 133.4327
M 133.3340
M 132.9895
M 132.8865
M 128.9438
M 128.8205
M 127.5411
M 127.4414
M 117.2046
M 116.3541
M 80.5702
M 26.3523
M 24.5916
M 24.0813
200
150
100
50
0
[ppm]

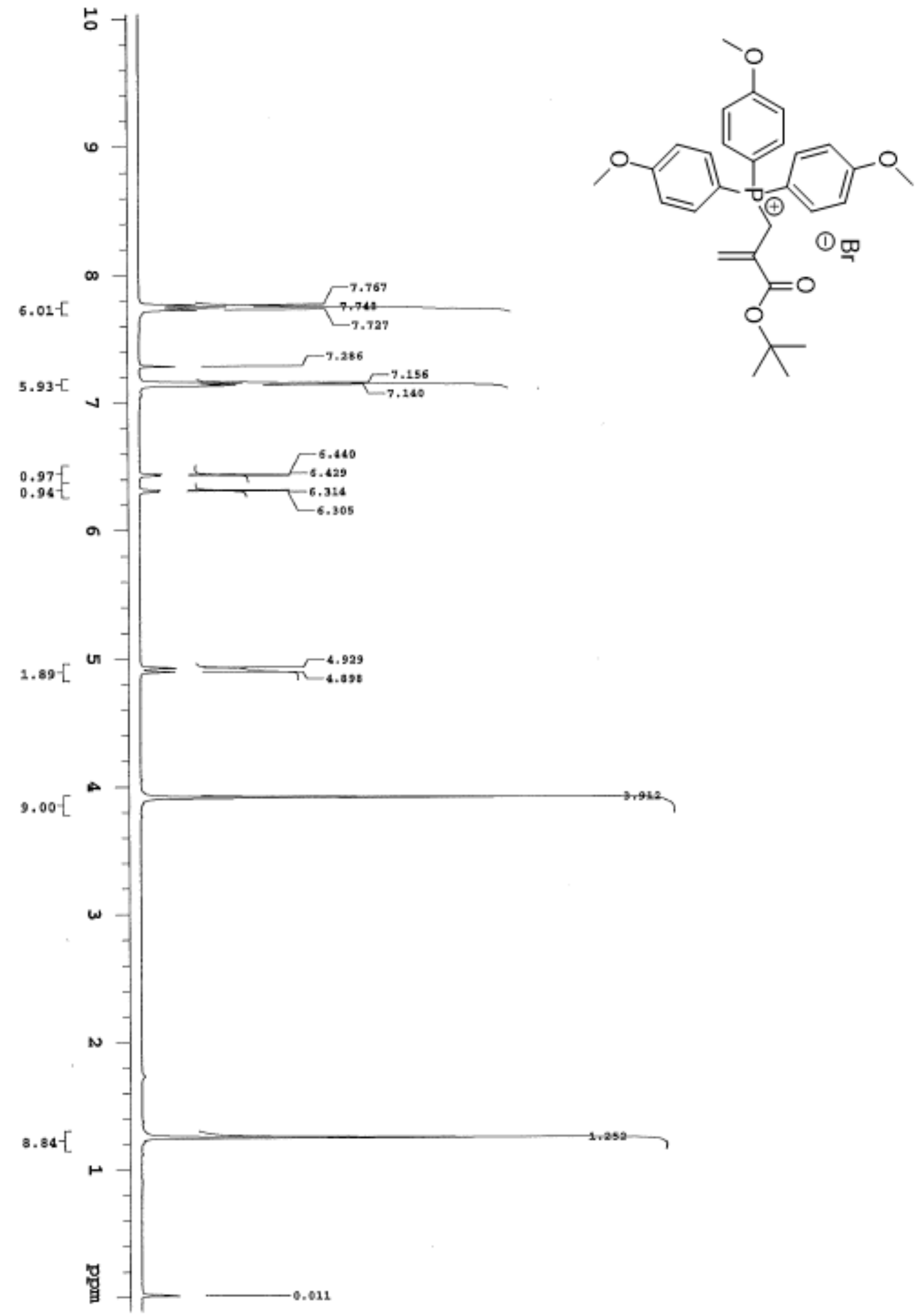
7.767
7.748
7.727
7.286
7.156
7.140
6.440
6.429
6.314
6.305
4.929
4.898
3.912
1.252
0.011
6.01
5.93
0.97
0.94
1.89
9.00
8.84
ppm
P
Br

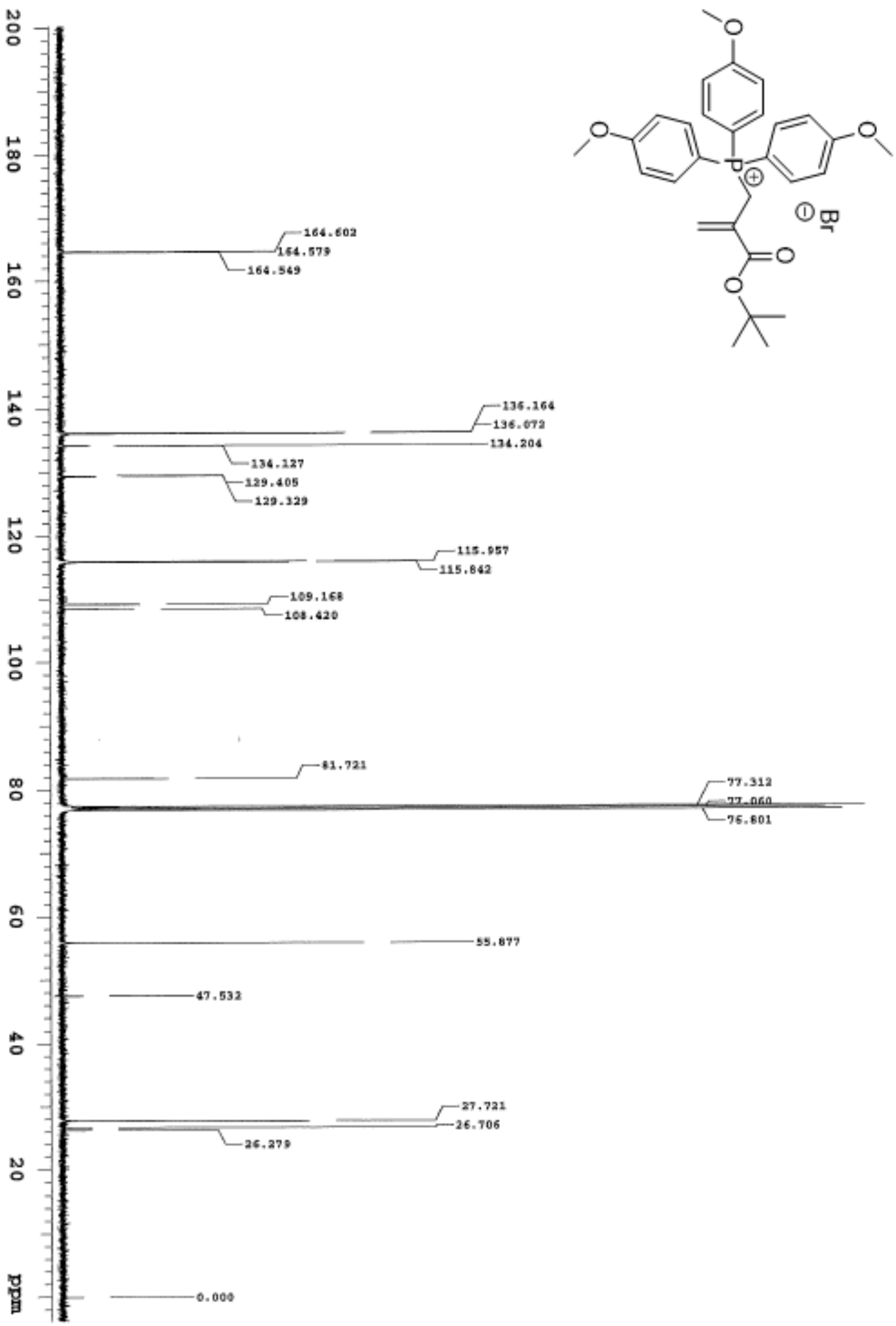

164.602
164.579
164.549
136.164
136.072
134.204
134.127
129.405
129.329
115.957
115.842
109.168
108.420
81.721
77.312
77.060
76.801
55.877
47.532
27.721
26.706
26.279
0.000
200
180
160
140
120
100
80
60
40
20
ppm
Br
P

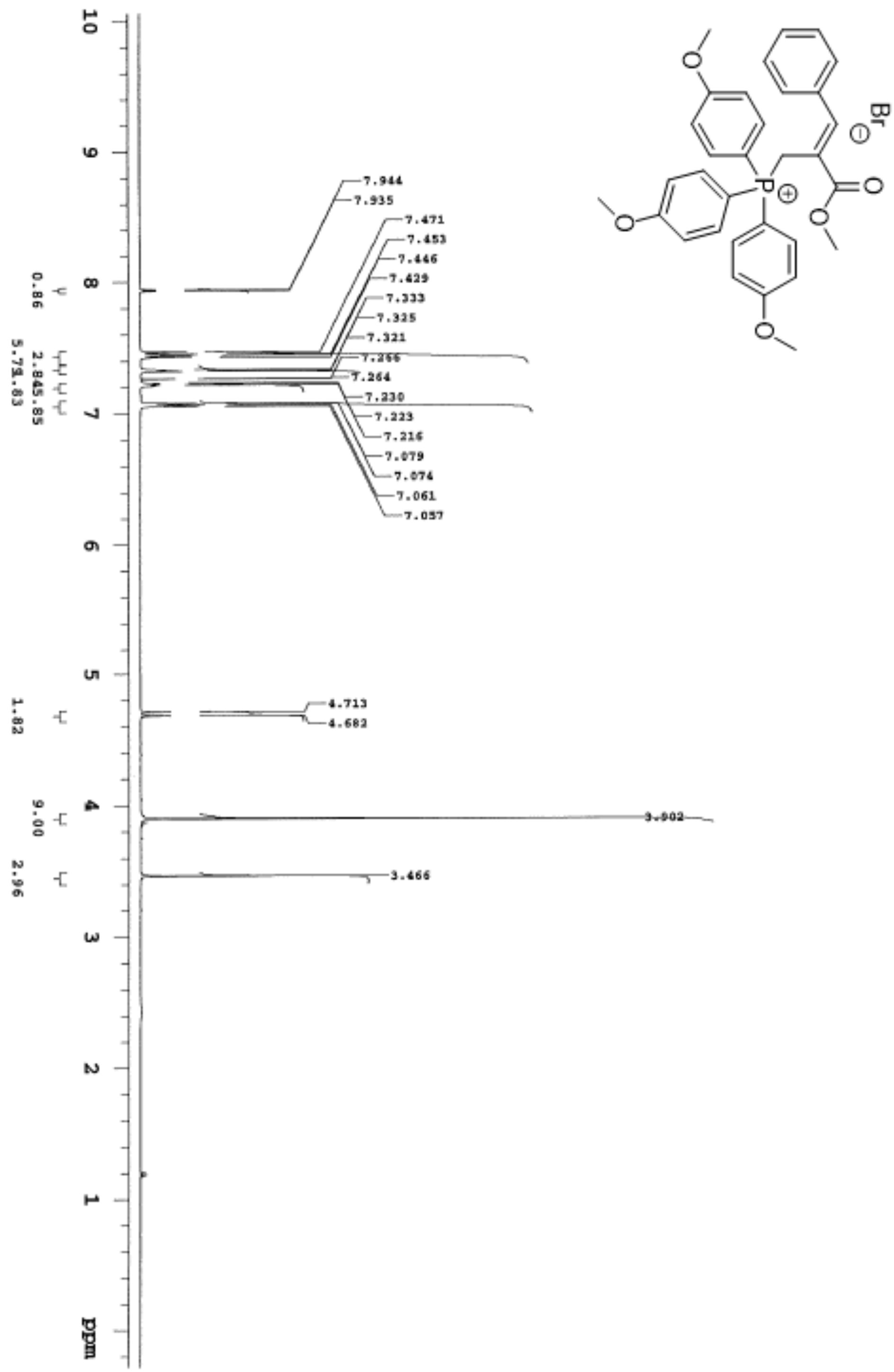
7.944
7.935
7.471
7.453
7.446
7.429
7.333
7.325
7.321
7.266
7.264
7.230
7.223
7.216
7.079
7.074
7.061
7.057
4.713
4.682
3.902
3.466
0.86
2.84
5.79
5.85
1.83
1.82
9.00
2.96
ppm
Br
P

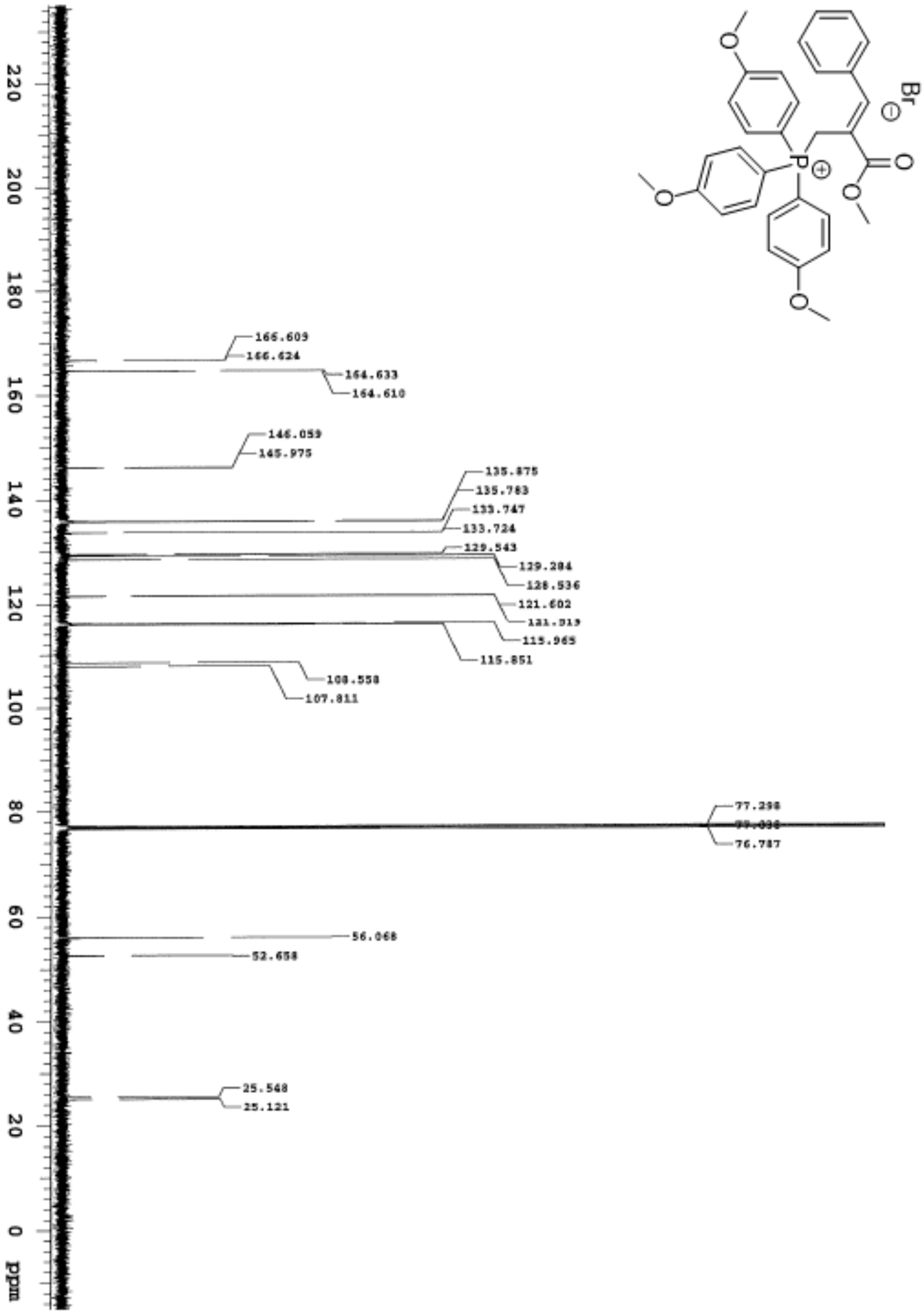
166.609
166.624
164.633
164.610
146.059
145.975
135.875
135.783
133.747
133.724
129.543
129.284
128.536
121.602
121.319
115.965
115.851
108.558
107.811
77.298
76.787
56.068
52.658
25.548
25.121
220
200
180
160
140
120
100
80
60
40
20
0
ppm
Br

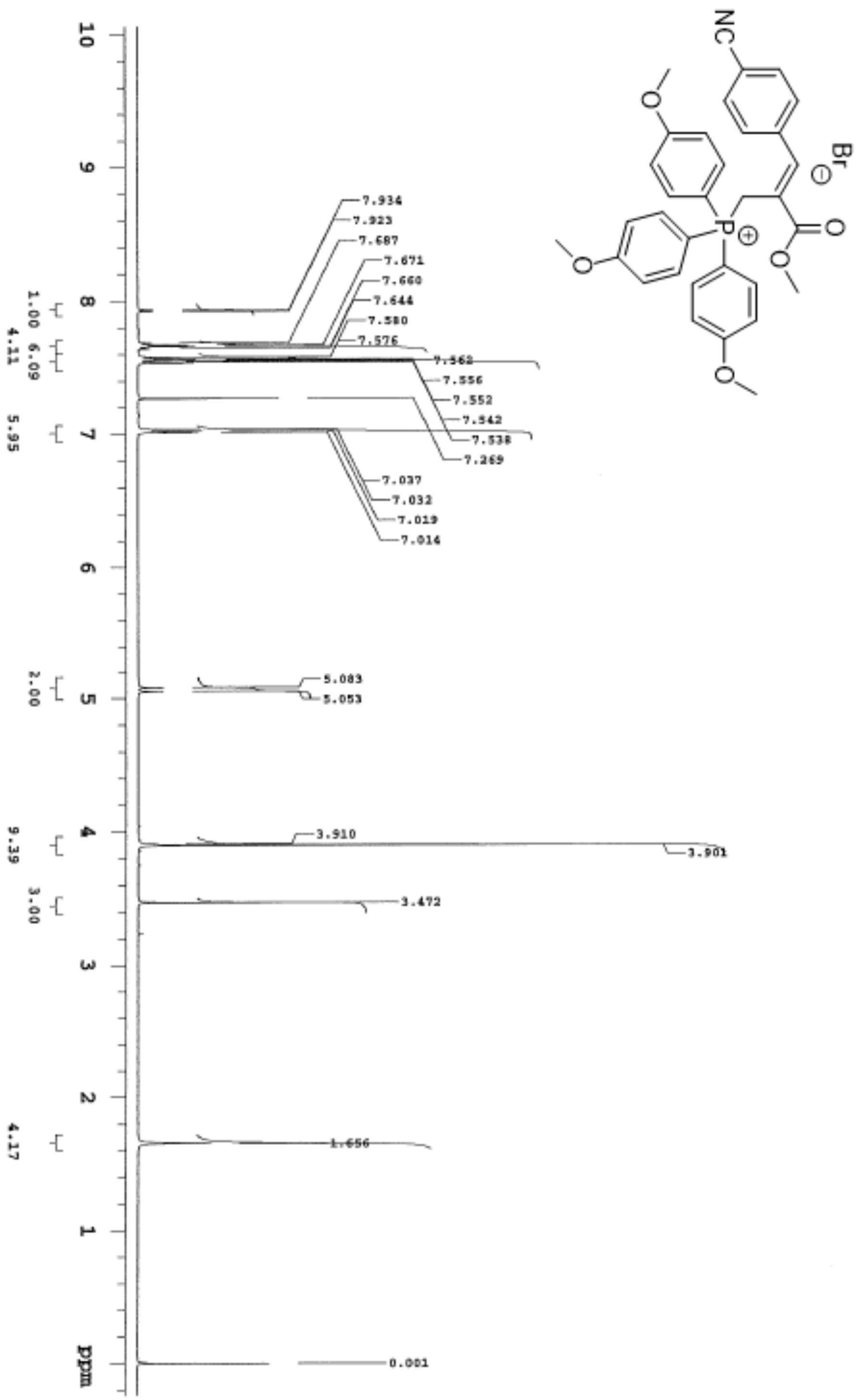
NC
Br
O
P
7.934
7.923
7.687
7.671
7.660
7.644
7.580
7.576
7.562
7.556
7.552
7.542
7.538
7.269
7.037
7.032
7.019
7.014
5.083
5.053
3.910
3.901
3.472
1.656
0.001
1.00
6.09
4.11
5.95
2.00
9.39
3.00
4.17
10
9
8
7
6
5
4
3
2
1
ppm

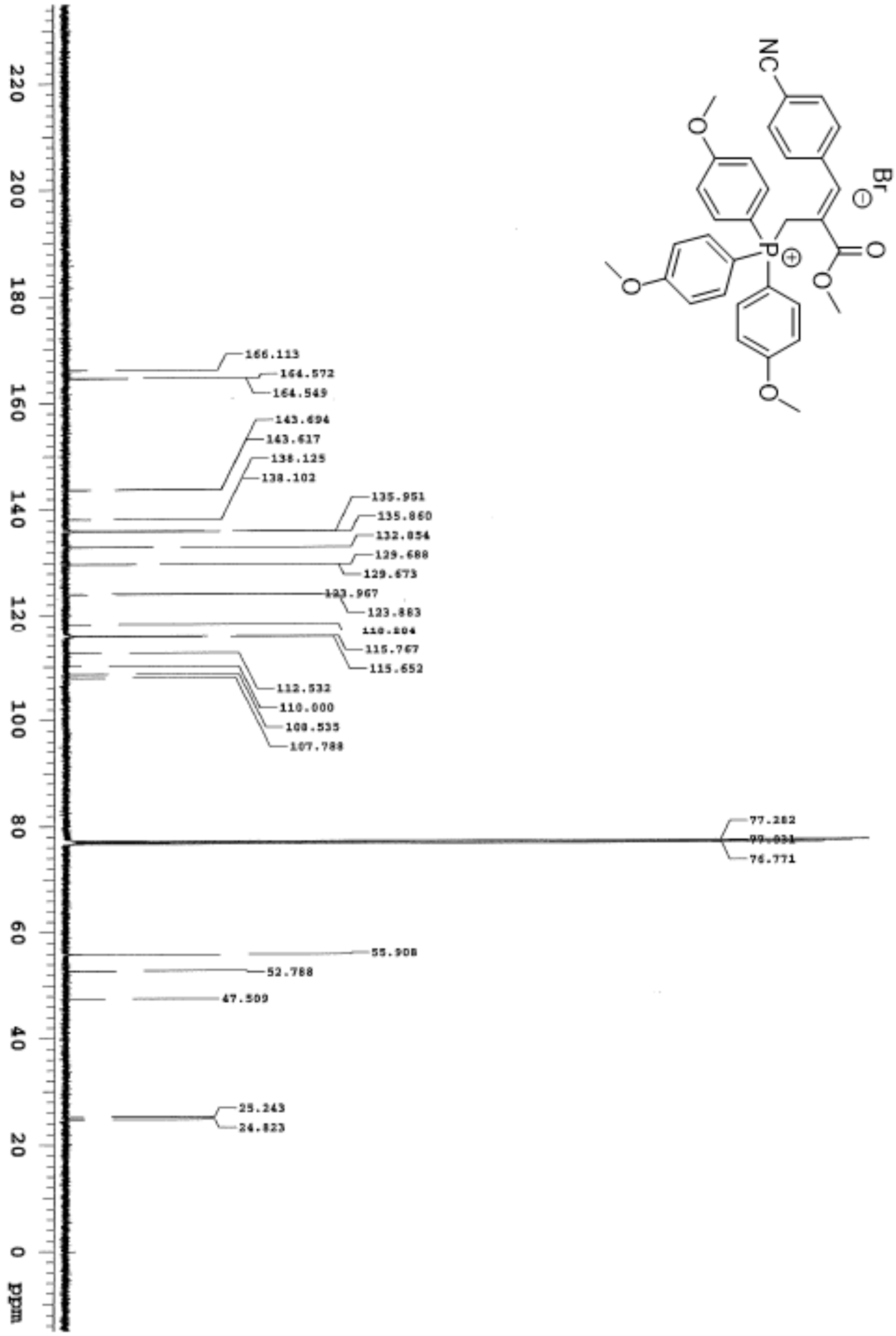
NC
Br
O
P
166.113
164.572
164.549
143.694
143.617
138.125
138.102
135.951
135.860
132.854
129.688
129.673
123.967
123.883
115.767
115.652
112.532
110.000
108.535
107.788
77.282
76.771
55.908
52.788
47.509
25.243
24.823
220
200
180
160
140
120
100
80
60
40
20
0
ppm

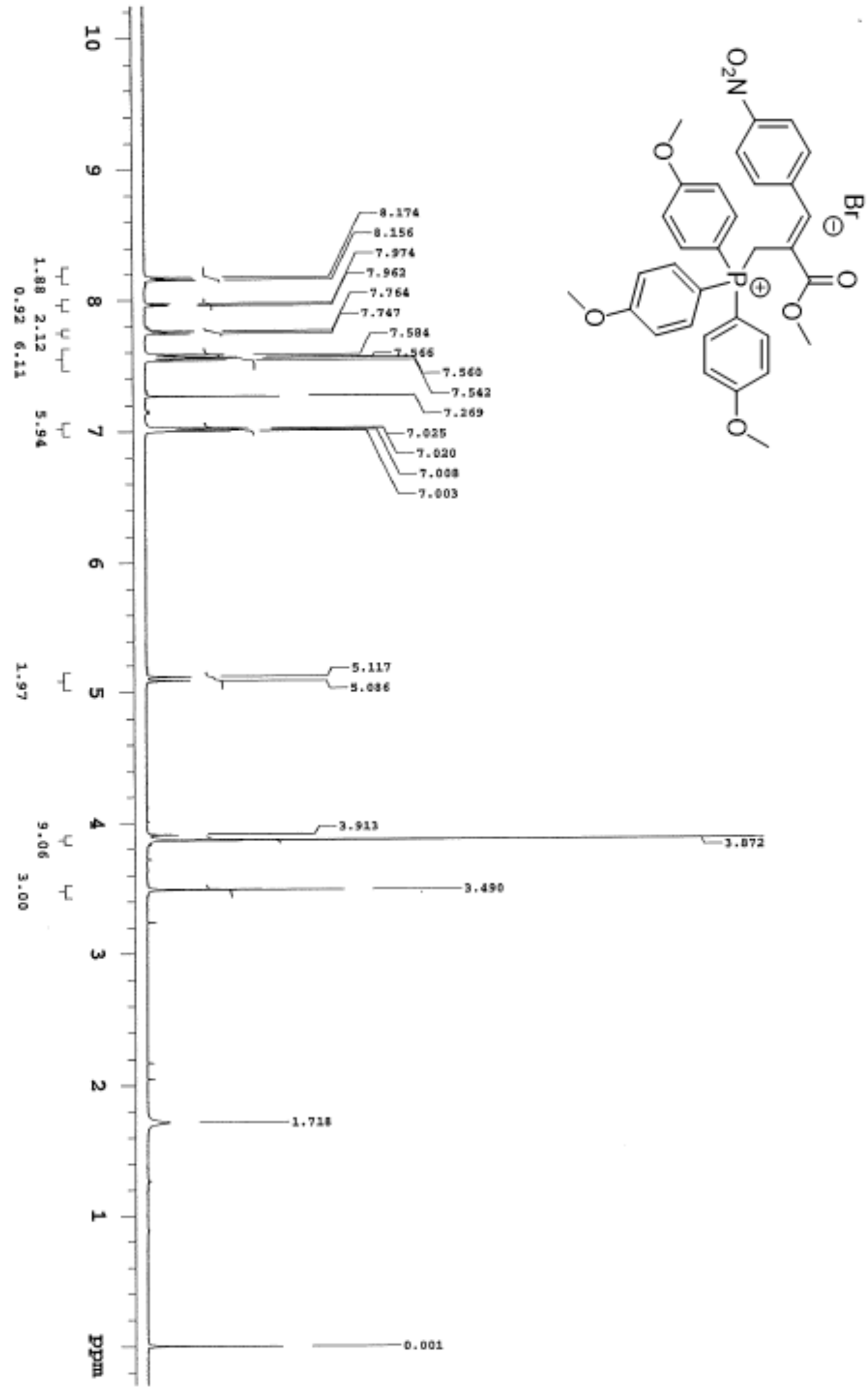
8.174
8.156
7.974
7.962
7.764
7.747
7.584
7.566
7.560
7.542
7.269
7.025
7.020
7.008
7.003
5.117
5.086
3.913
3.872
3.490
1.718
0.001
1.88
0.92
2.12
6.11
5.94
1.97
9.06
3.00
ppm
O_2N
Br
P

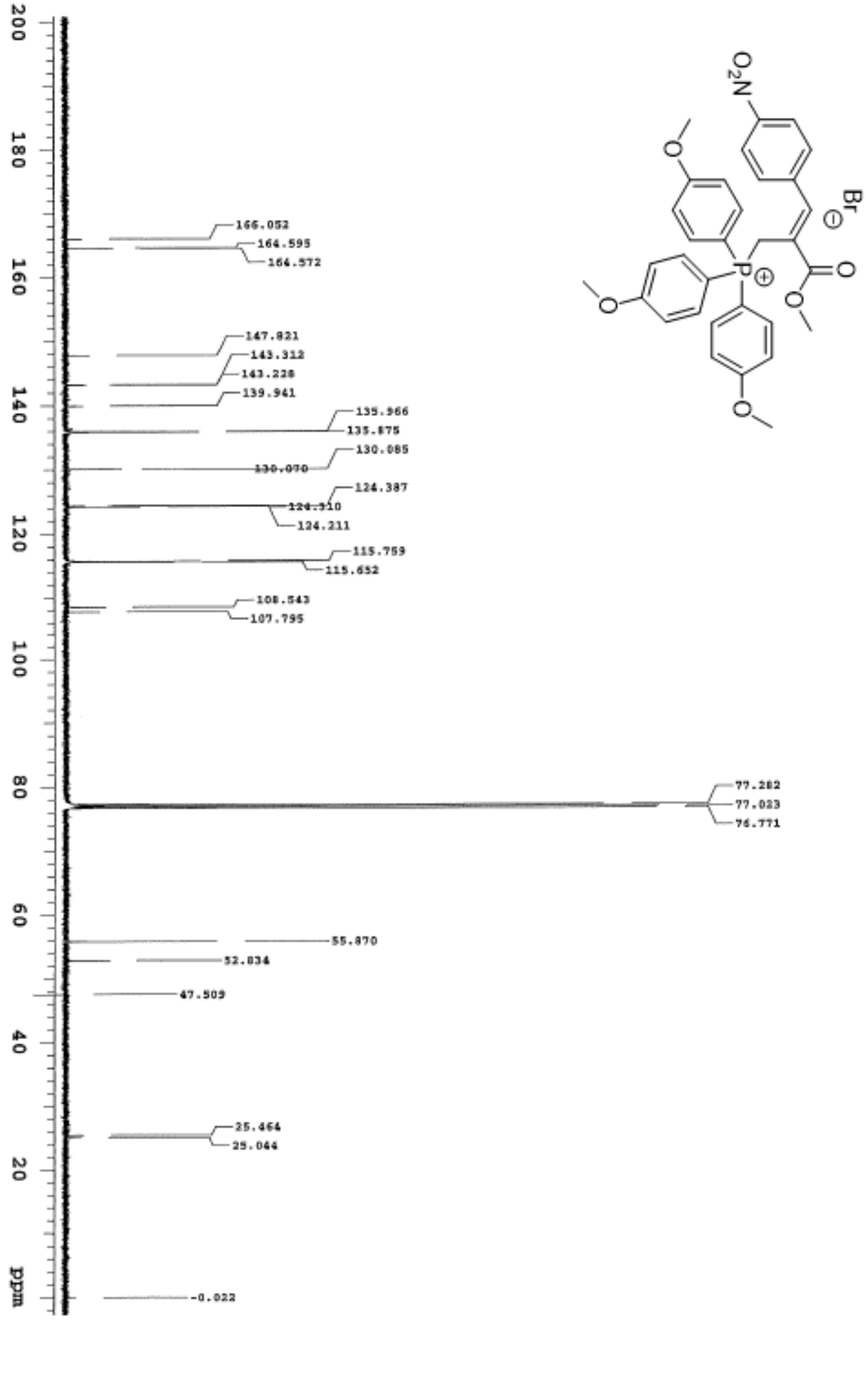
200
180
160
140
120
100
80
60
40
20
ppm
166.052
164.595
164.572
147.821
143.312
143.228
139.941
135.966
135.875
130.085
130.070
124.387
124.310
124.211
115.759
115.652
108.543
107.795
77.282
77.023
76.771
55.870
52.834
47.509
25.464
25.044
-0.022
O2N
Br
P

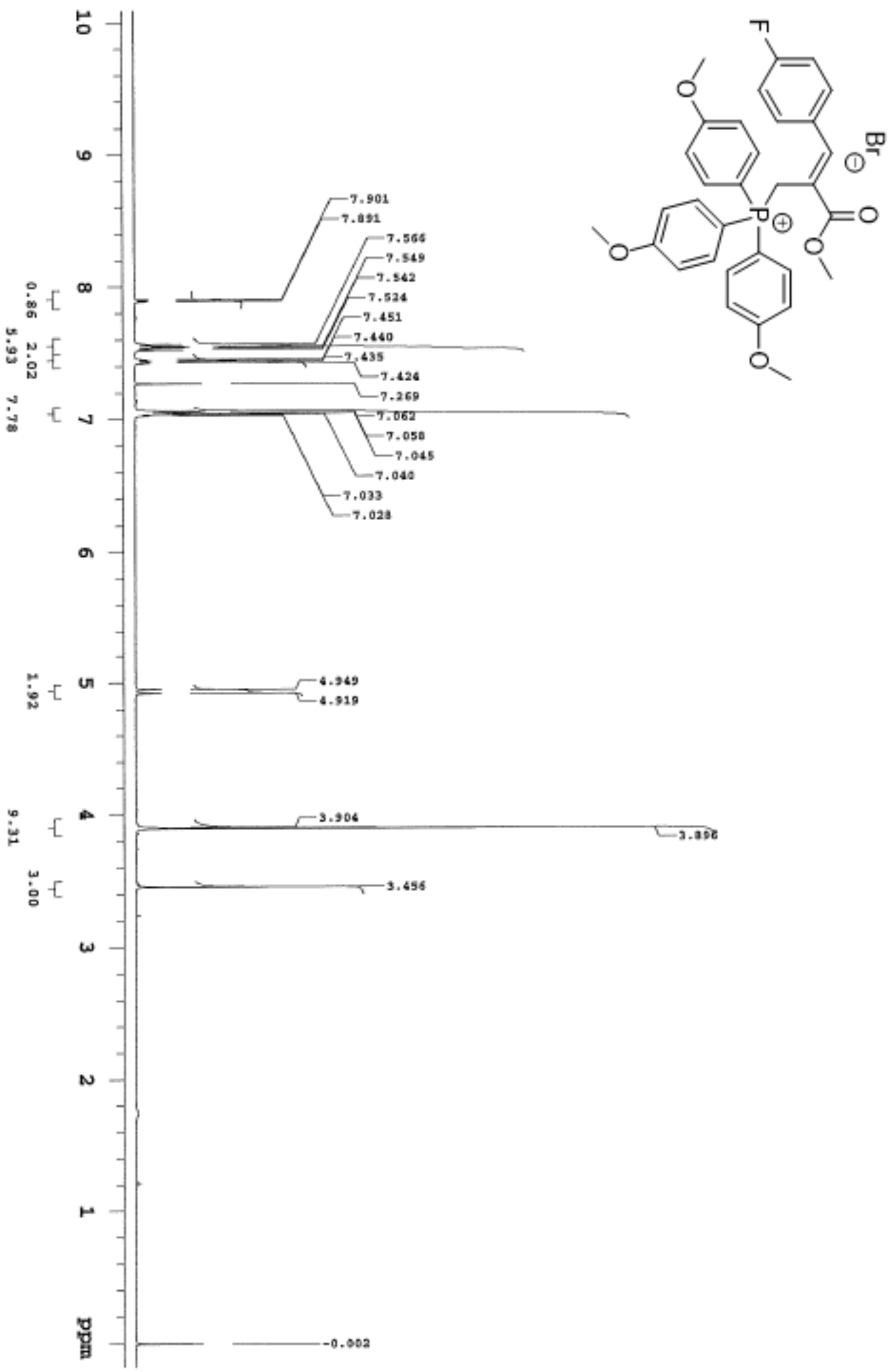

Br
F
P
O
7.901
7.891
7.566
7.549
7.542
7.524
7.451
7.440
7.435
7.424
7.269
7.062
7.058
7.045
7.040
7.033
7.028
4.949
4.919
3.904
3.898
3.496
-0.002
0.86
2.02
5.93
7.78
1.92
9.31
3.00
10
9
8
7
6
5
4
3
2
1
ppm

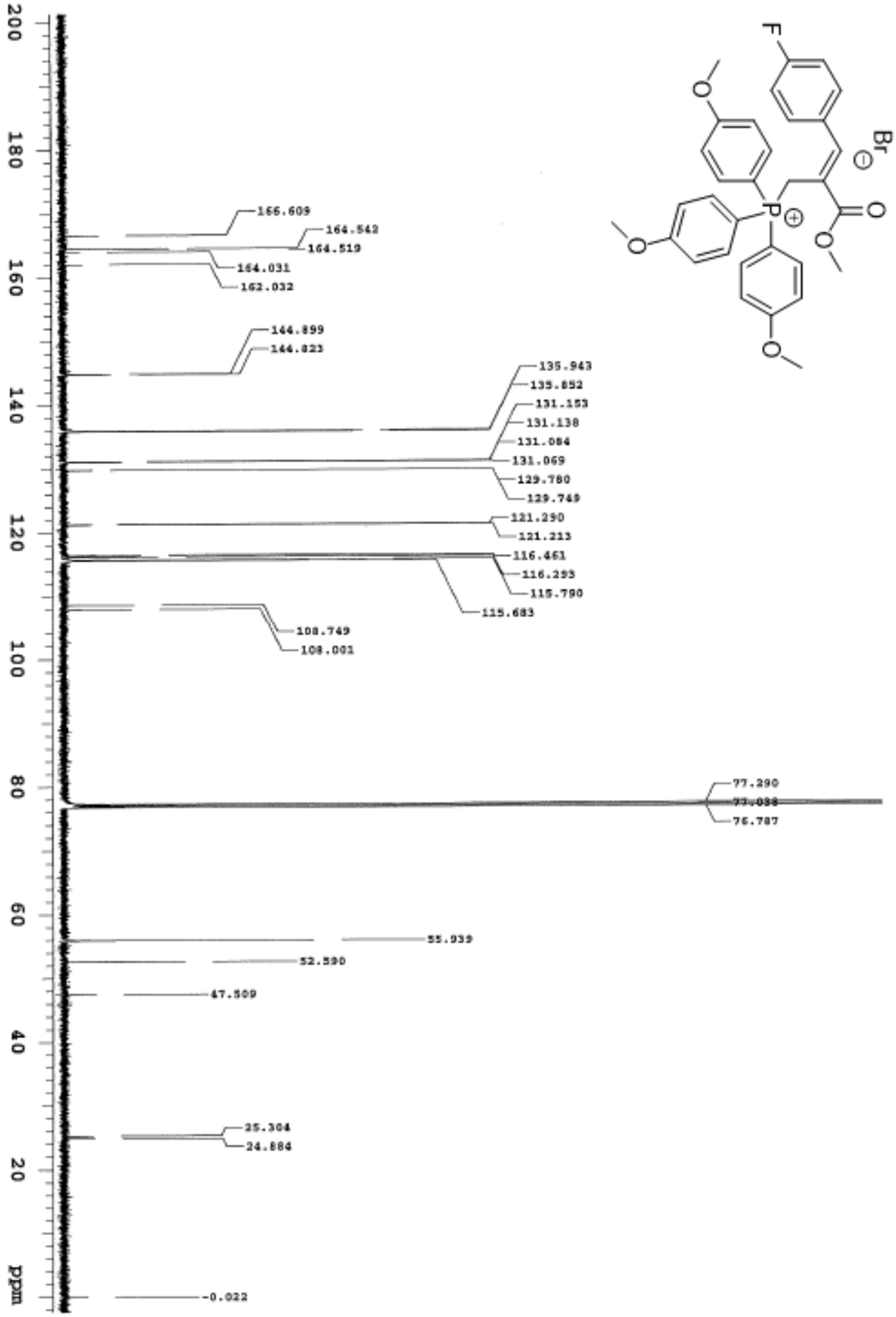
F
Br
P
200
180
160
140
120
100
80
60
40
20
ppm
166.609
164.542
164.519
164.031
162.032
144.899
144.823
135.943
135.852
131.153
131.138
131.084
131.069
129.780
129.749
121.290
121.213
116.461
116.293
115.790
115.683
108.749
108.001
77.290
77.038
76.787
55.939
52.590
47.509
25.304
24.884
-0.022

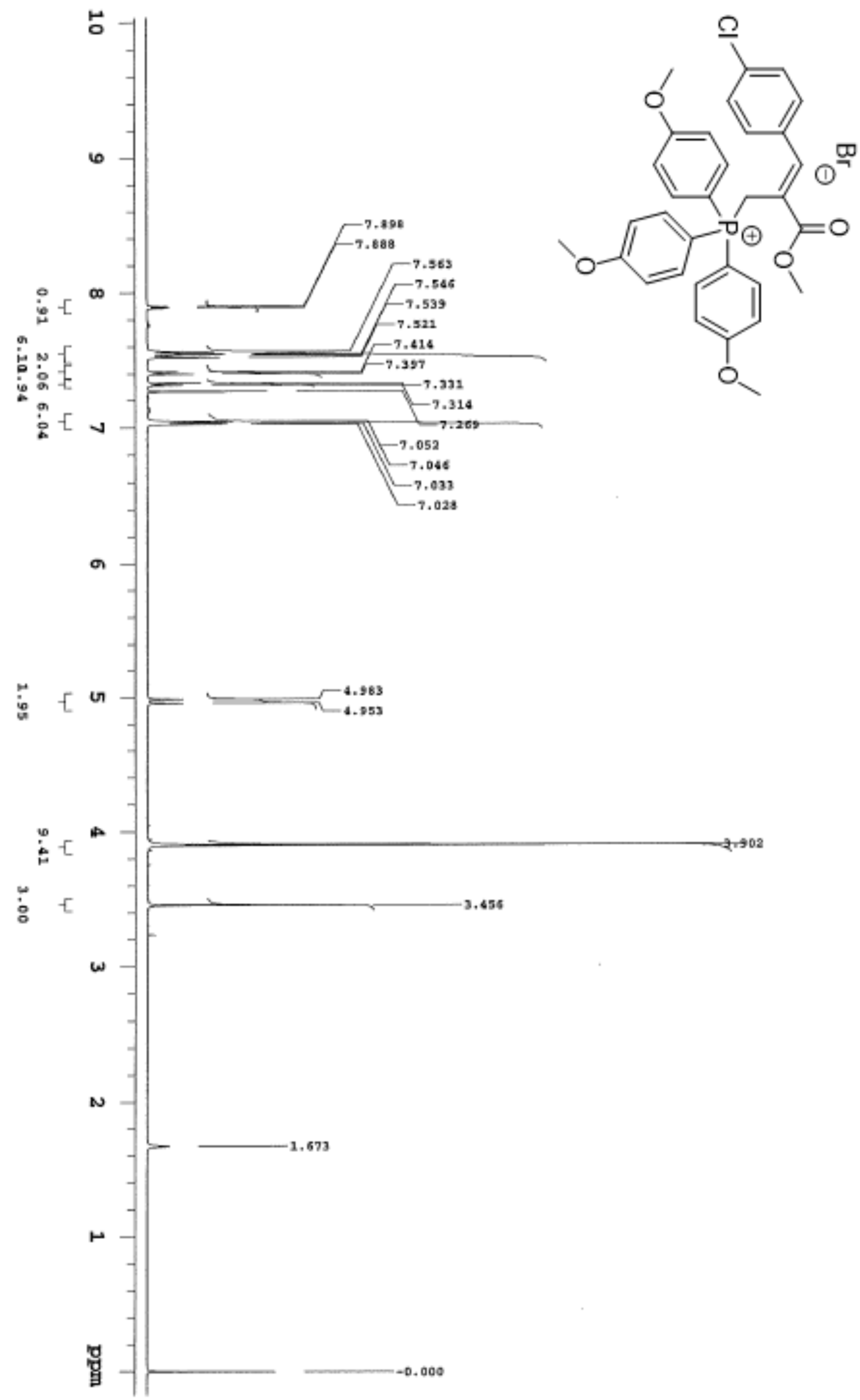
7.898
7.888
7.563
7.546
7.539
7.521
7.414
7.397
7.331
7.314
7.269
7.052
7.046
7.033
7.028
4.983
4.953
3.902
3.456
1.673
-0.000
0.91
2.06
6.04
6.10
.94
1.95
9.41
3.00
ppm
Cl
Br
P

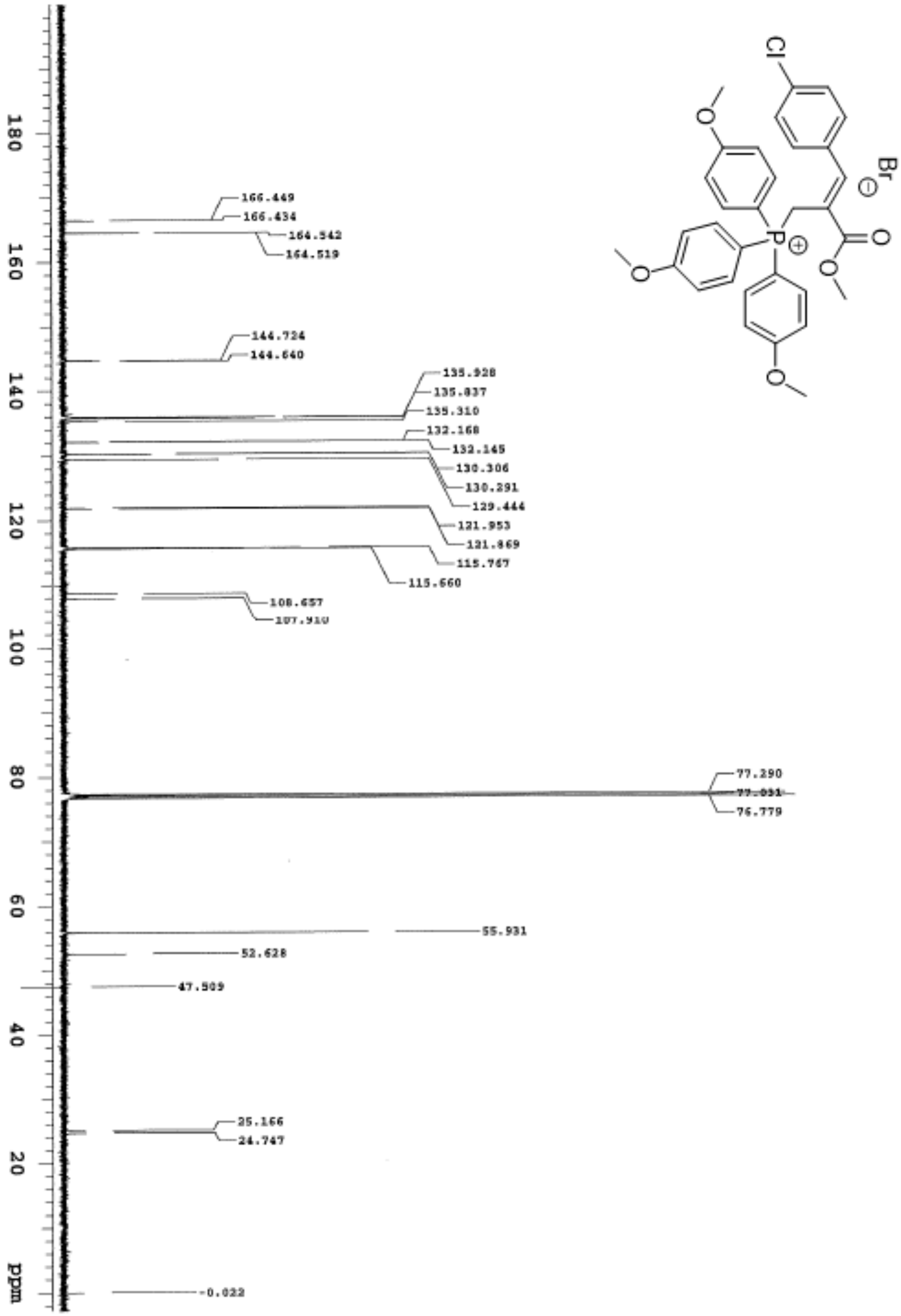
166.449
166.434
164.542
164.519
144.724
144.640
135.928
135.837
135.310
132.168
132.145
130.306
130.291
129.444
121.953
121.869
115.767
115.660
108.657
107.910
77.290
77.031
76.779
55.931
52.628
47.509
25.166
24.747
-0.022
180
160
140
120
100
80
60
40
20
ppm
Cl
Br
P
O

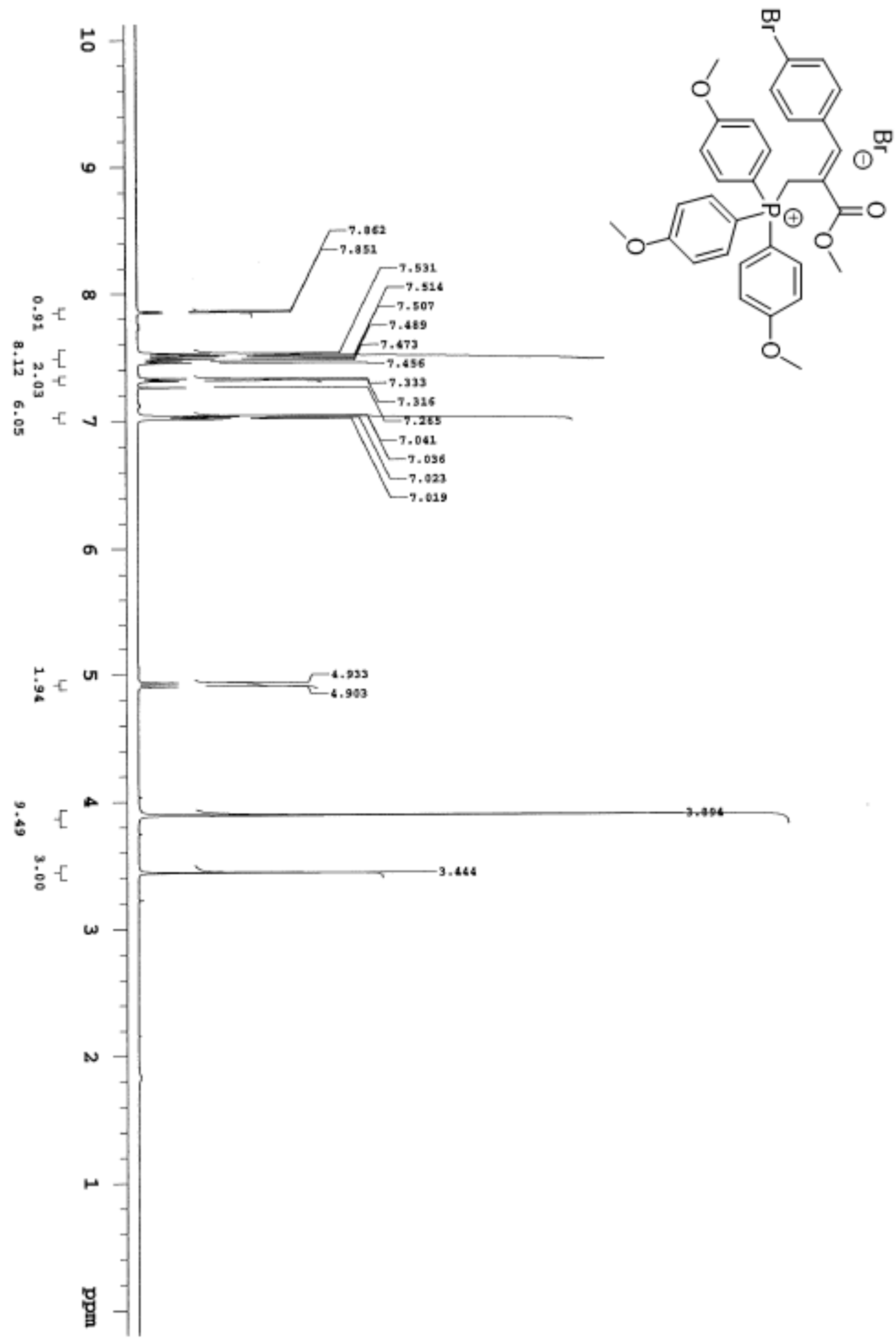
Br
Br
O
P
O
O
O
O
10
9
8
7
6
5
4
3
2
1
ppm
7.862
7.851
7.531
7.514
7.507
7.489
7.473
7.456
7.333
7.316
7.265
7.041
7.036
7.023
7.019
4.933
4.903
3.894
3.444
0.91
8.12
2.03
6.05
1.94
9.49
3.00

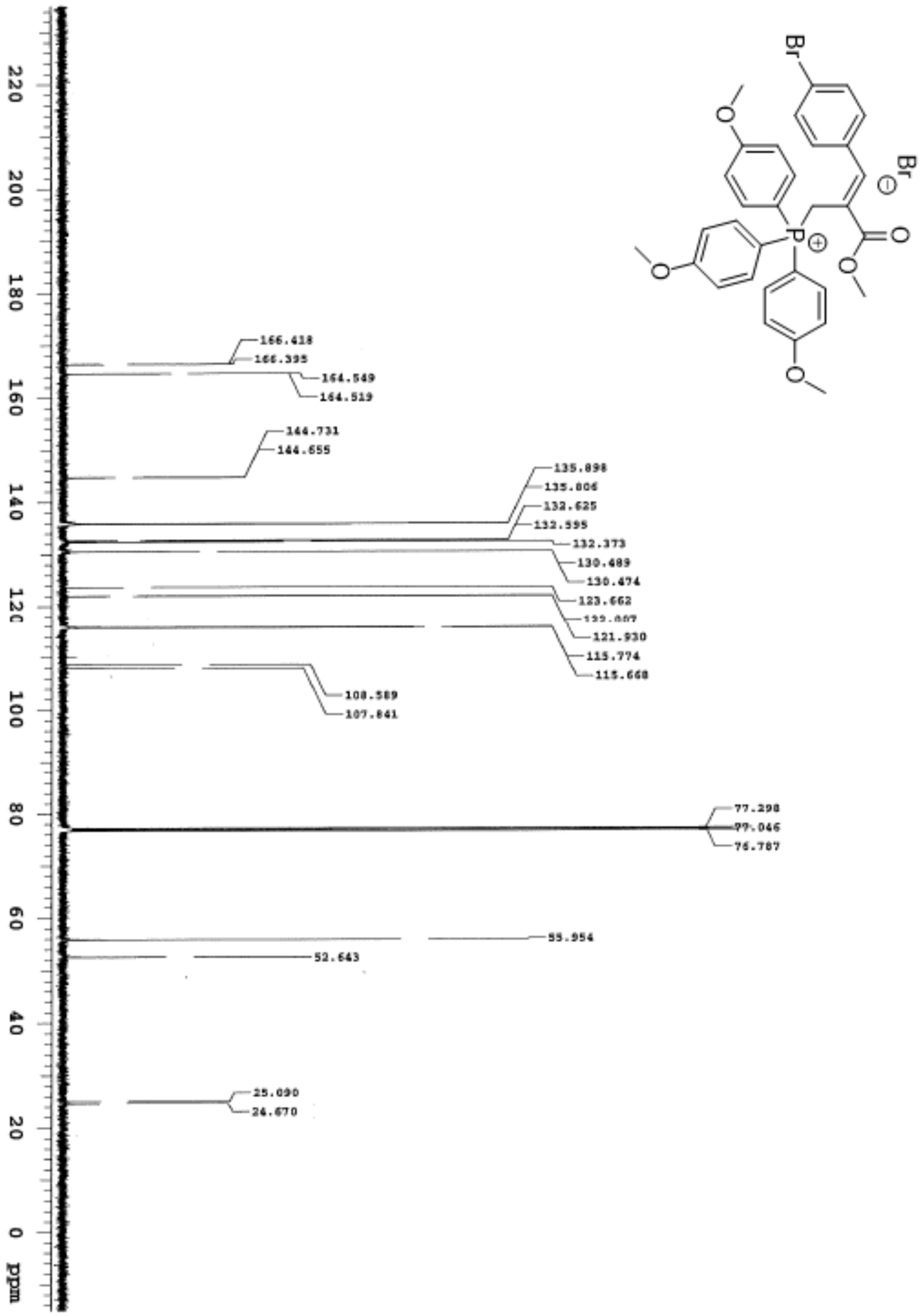
166.418
166.395
164.549
164.519
144.731
144.655
135.898
135.806
132.625
132.595
132.373
130.489
130.474
123.662
121.930
115.774
115.668
108.589
107.841
77.298
77.046
76.787
55.954
52.643
25.090
24.670
220
200
180
160
140
120
100
80
60
40
20
0
ppm
Br
Br
P
O

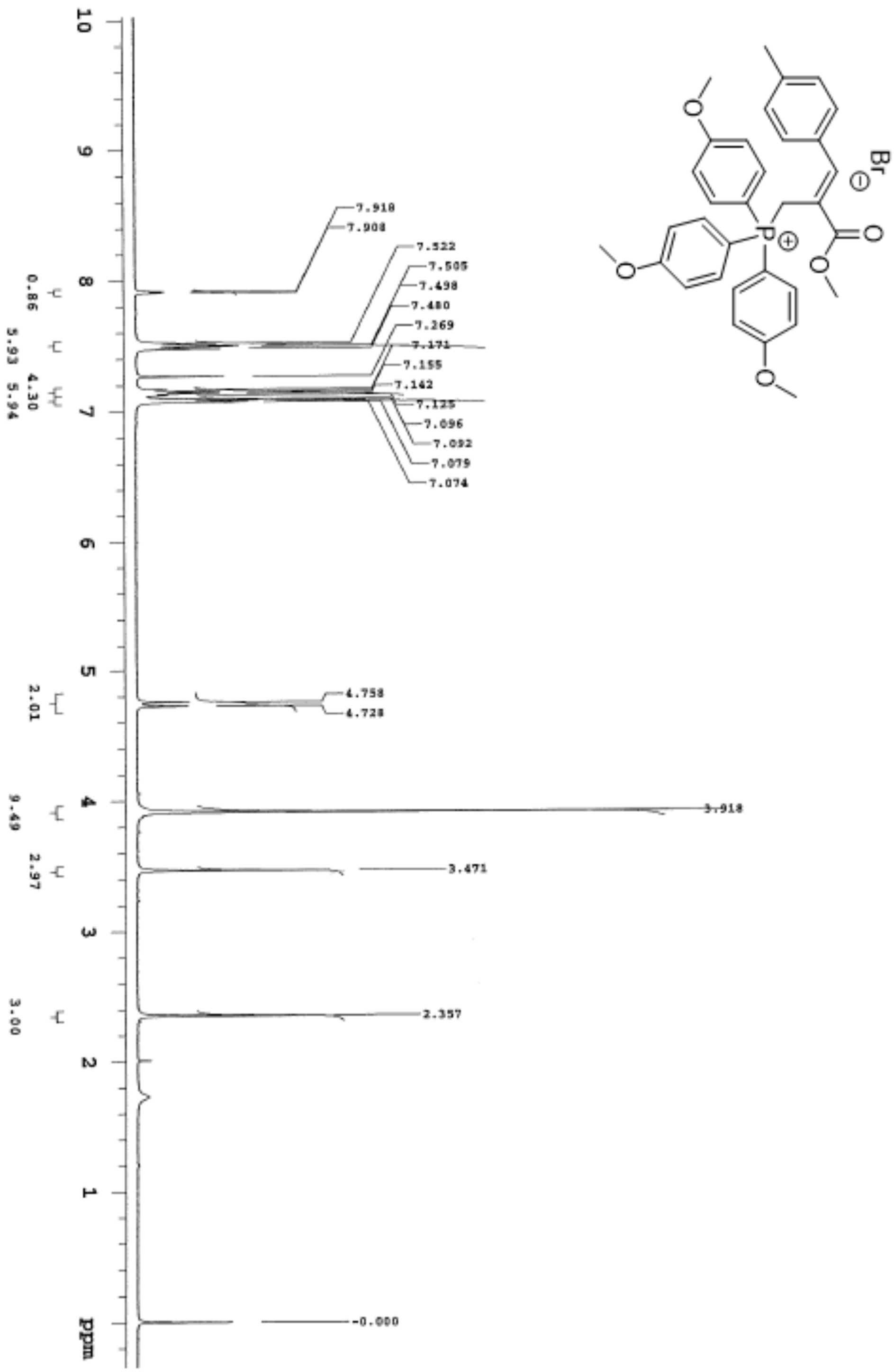

7.918
7.908
7.522
7.505
7.498
7.480
7.269
7.171
7.155
7.142
7.125
7.096
7.092
7.079
7.074
4.758
4.728
3.918
3.471
2.357
-0.000
0.86
5.93
4.30
5.94
2.01
9.49
2.97
3.00
10
9
8
7
6
5
4
3
2
1
ppm
Br
P
O

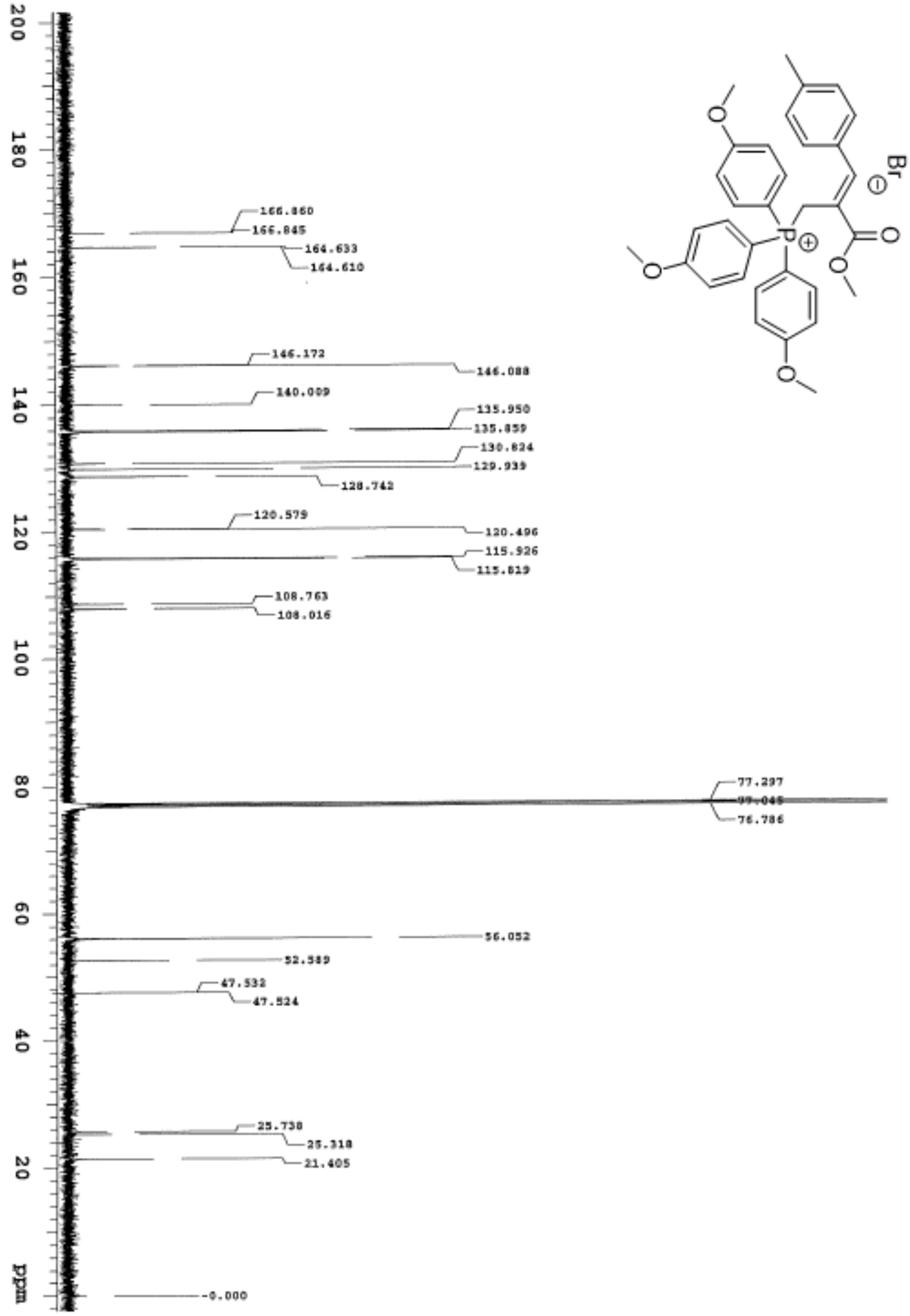

166.860
166.845
164.633
164.610
146.172
146.088
140.009
135.950
135.859
130.824
129.939
128.742
120.579
120.496
115.926
115.819
108.763
108.016
77.297
76.786
56.052
52.589
47.532
47.524
25.738
25.318
21.405
-0.000
200
180
160
140
120
100
80
60
40
20
ppm
Br

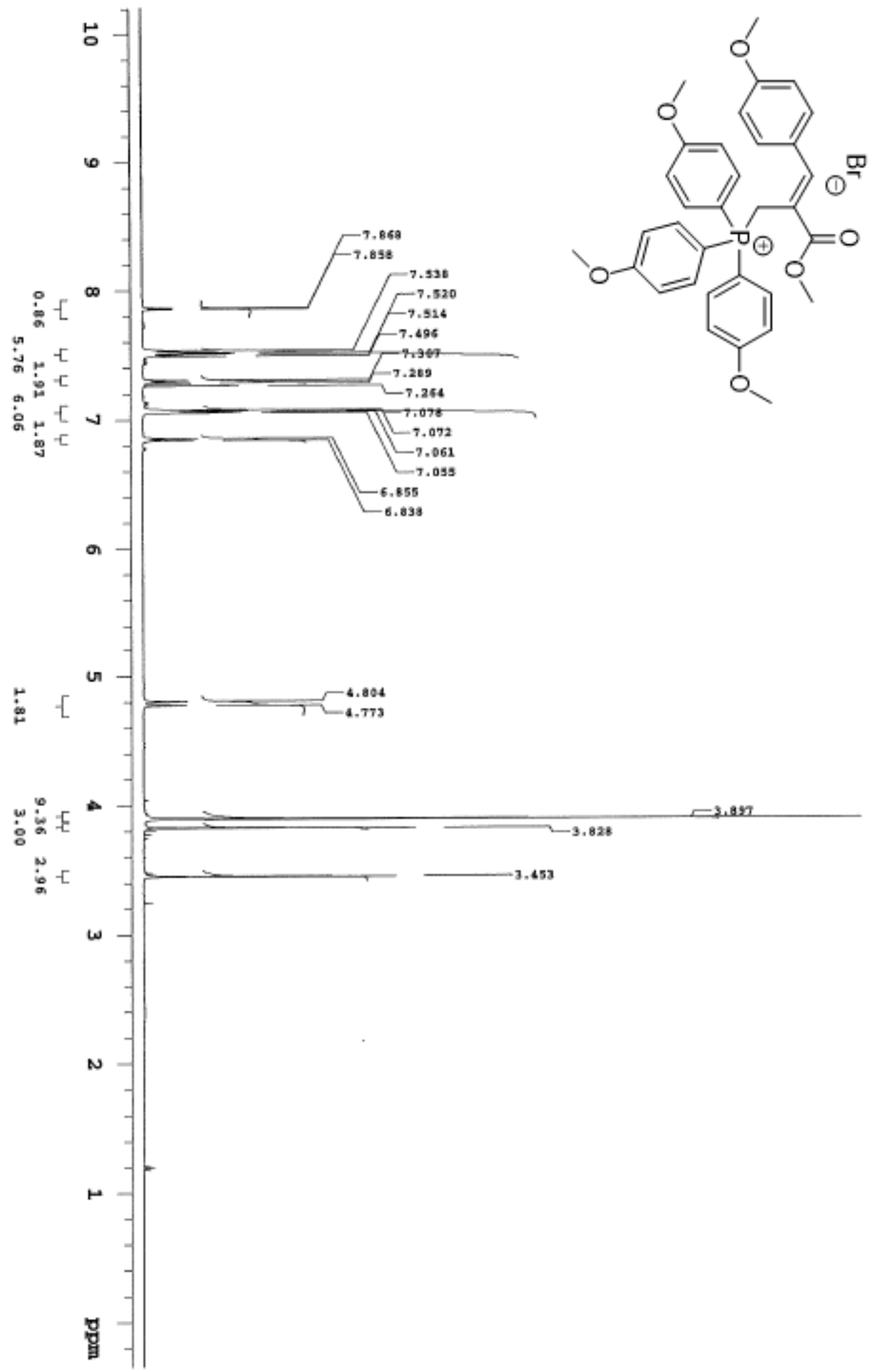
7.868
7.858
7.538
7.520
7.514
7.496
7.307
7.289
7.264
7.078
7.072
7.061
7.055
6.855
6.838
4.804
4.773
3.897
3.828
3.453
0.86
5.76
1.91
6.06
1.87
1.81
9.36
3.00
2.96
10
9
8
7
6
5
4
3
2
1
ppm
Br
P
O

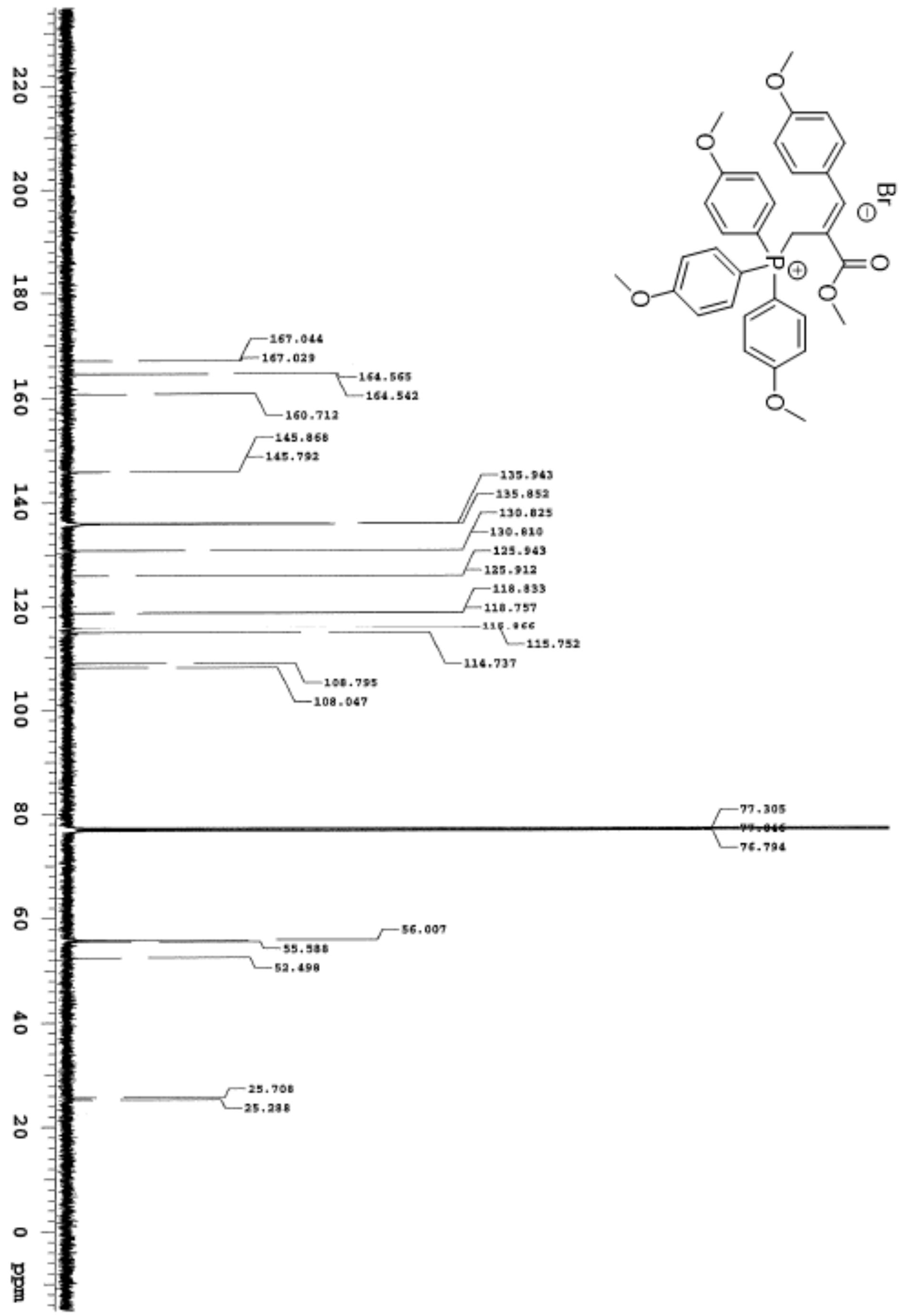
167.044
167.029
164.565
164.542
160.712
145.868
145.792
135.943
135.852
130.825
130.810
125.943
125.912
118.833
118.757
115.752
114.737
108.795
108.047
77.305
76.794
56.007
55.588
52.498
25.708
25.288
ppm
Br

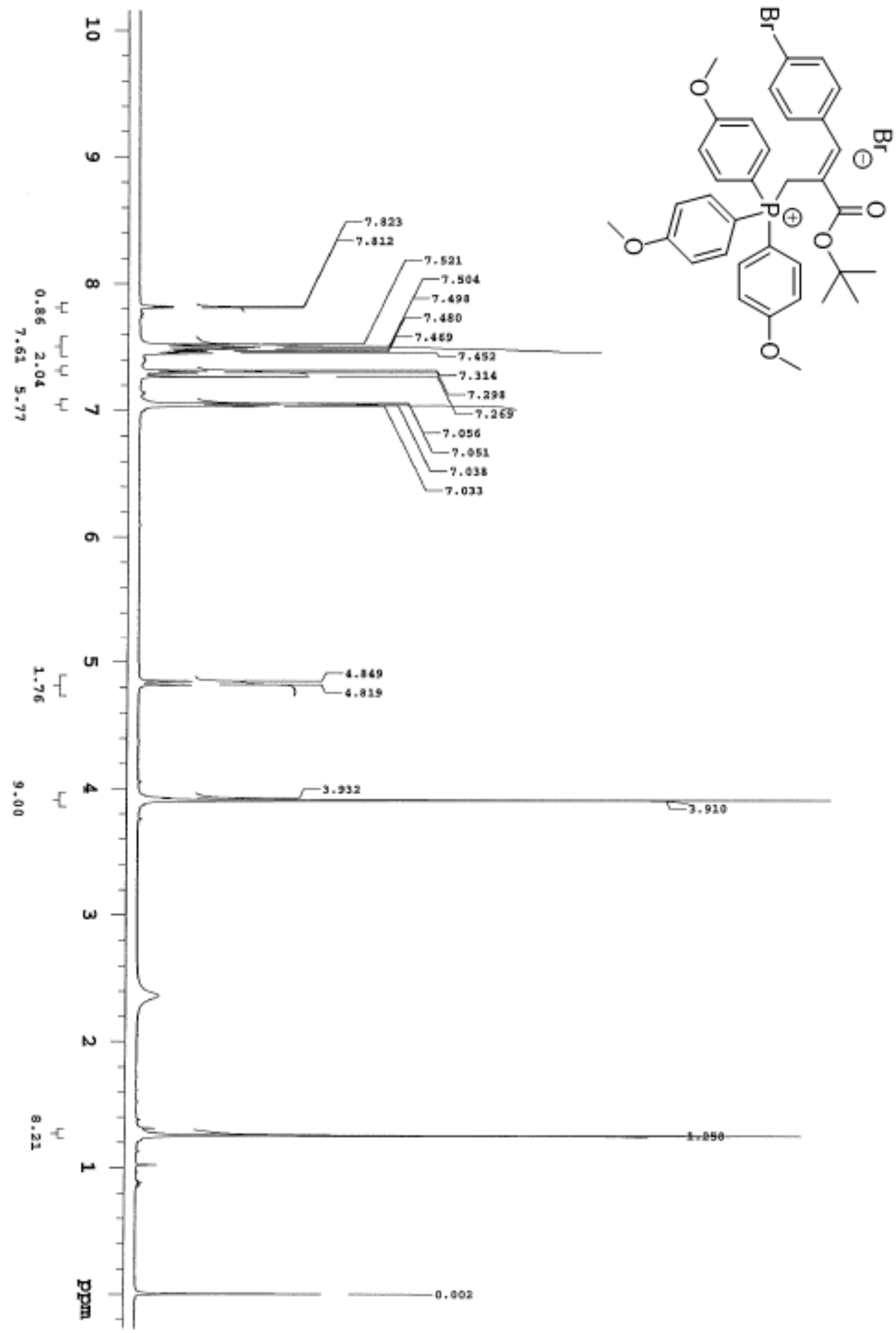
Br
Br
O
O
P
7.823
7.812
7.521
7.504
7.498
7.480
7.469
7.452
7.314
7.298
7.269
7.056
7.051
7.038
7.033
4.849
4.819
3.932
3.910
1.250
0.002
0.86
2.04
7.61
5.77
1.76
9.00
8.21
ppm

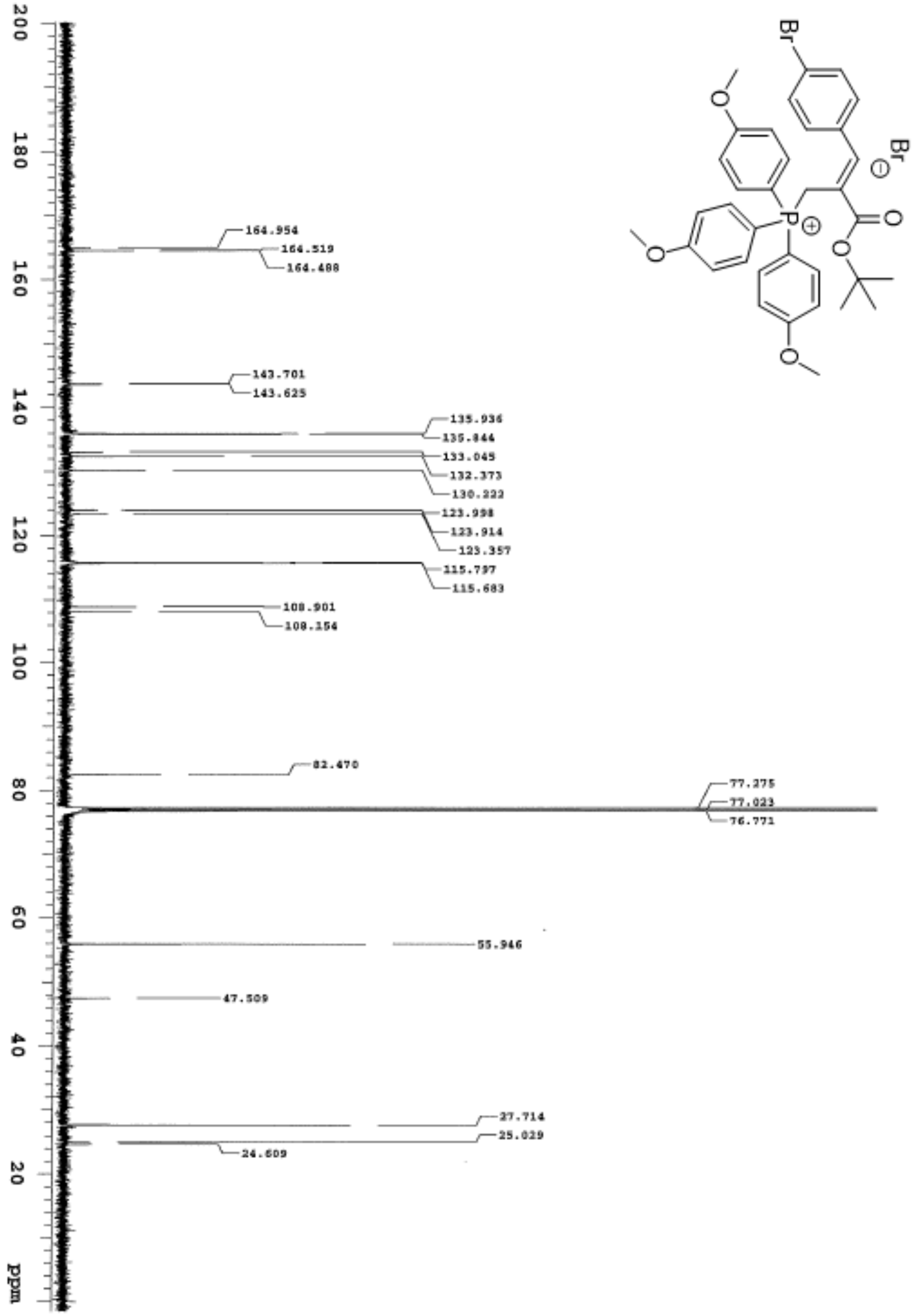
164.954
164.519
164.488
143.701
143.625
135.936
135.844
133.045
132.373
130.222
123.998
123.914
123.357
115.797
115.683
108.901
108.154
82.470
77.275
77.023
76.771
55.946
47.509
27.714
25.029
24.609
ppm
Br
Br

4.2 References

1. American Cancer Society. Surveillance Research. 5 (2019).
2. Tong, X. P. *et al.* Key autophagic targets and relevant small-molecule compounds in cancer therapy. *Cell Prolif.* **48**, 7–16 (2015).
3. Zhao, Y., Aguilar, A., Bernard, D. & Wang, S. Small-molecule inhibitors of the MDM2-p53 protein-protein interaction (MDM2 inhibitors) in clinical trials for cancer treatment. *J. Med. Chem.* **58**, 1038–1052 (2015).
4. Bai, L., Smith, D. C. & Wang, S. Small-molecule SMAC mimetics as new cancer therapeutics. *Pharmacol. Ther.* **144**, 82–95 (2014).
5. Maschinot, C. A., Pace, J. R. & Hadden, M. K. Synthetic Small Molecule Inhibitors of Hh Signaling As Anti-Cancer Chemotherapeutics. *Curr. Med. Chem.* **22**, 4033–4057 (2015).
6. Weinmann, H. Cancer Immunotherapy: Selected Targets and Small-Molecule Modulators. *ChemMedChem* **11**, 450–466 (2016).
7. Dozier, J., Zheng, H. & Adusumilli, P. S. Immunotherapy for malignant pleural mesothelioma: Current status and future directions. *Transl. Lung Cancer Res.* **6**, 315–324 (2017).
8. Grierson, P., Lim, K. H. & Amin, M. Immunotherapy in gastrointestinal cancers. *J. Gastrointest. Oncol.* **8**, 474–484 (2017).
9. Simpson, A. & Caballero, O. Monoclonal antibodies for the therapy of cancer. *BMC Proc.* **8**, O6 (2014).
10. van de Donk, N. W. C. J. *et al.* Monoclonal antibodies targeting CD38 in hematological malignancies and beyond. *Immunol. Rev.* **270**, 95–112 (2016).
11. Moussavou, G., Ko, K., Lee, J. H. & Choo, Y. K. Production of Monoclonal Antibodies in Plants for Cancer Immunotherapy. *Biomed Res. Int.* **2015**, (2015).
12. MR, P. Mechanism of Changes Balance Anaerobic Processes and Aerobic Processes in Cancer Metabolism Causing Warburg Effect Mechanism. *J. Biomol. Res. Ther.* **06**, 1–9 (2017).
13. Hamanaka, R. B. & Chandel, N. S. Targeting glucose metabolism for cancer therapy. *J. Exp. Med.* **209**, 211–215 (2012).
14. Nabi, K. & Le, A. *The intratumoral heterogeneity of cancer metabolism*. *Advances in Experimental Medicine and Biology* **1063**, (2018).
15. Cantor, J. R. & Sabatini, D. M. Cancer cell metabolism: One hallmark, many faces. *Cancer Discov.* **2**, 881–898 (2012).
16. Martinez-Outschoorn, U. E., Peiris-Pagés, M., Pestell, R. G., Sotgia, F. & Lisanti, M. P. Cancer metabolism: A therapeutic perspective. *Nat. Rev. Clin. Oncol.* **14**, 11–31 (2017).
17. Liberti, M. V. & Locasale, J. W. The Warburg Effect: How Does it Benefit Cancer Cells? *Trends Biochem. Sci.* **41**, 211–218 (2016).
18. Hanahan, D. & Weinberg, R. A. Hallmarks of cancer: The next generation. *Cell* **144**, 646–674 (2011).
19. Chen, K. W. & Pienta, K. J. Modeling invasion of metastasizing cancer cells to bone marrow utilizing ecological principles. *Theor. Biol. Med. Model.* **8**, 36 (2011).

20. Pantel, K. & Brakenhoff, R. H. Dissecting the metastatic cascade. *Nat. Rev. Cancer* **4**, 448–456 (2004).
21. Pascual, G., Domínguez, D. & Benitah, S. A. The contributions of cancer cell metabolism to metastasis. *DMM Dis. Model. Mech.* **11**, (2018).
22. Rankin, E. B., Giaccia, A. J. & Biology, C. Hyposis and Metastasis. **352**, 175–180 (2016).
23. Blacker, T. S. & Duchen, M. R. Investigating mitochondrial redox state using NADH and NADPH autofluorescence. *Free Radic. Biol. Med.* **100**, 53–65 (2016).
24. Fouad, Y. A. & Aanei, C. Revisiting the hallmarks of cancer. *Am. J. Cancer Res.* **7**, 1016–1036 (2017).
25. Ganapathy, V., Thangaraju, M. & Prasad, P. D. Nutrient transporters in cancer: Relevance to Warburg hypothesis and beyond. *Pharmacol. Ther.* **121**, 29–40 (2009).
26. Ashton, T. M., Gillies McKenna, W., Kunz-Schughart, L. A. & Higgins, G. S. Oxidative phosphorylation as an emerging target in cancer therapy. *Clin. Cancer Res.* **24**, 2482–2490 (2018).
27. Weinberg, S. E. & Chandel, N. S. Targeting mitochondria metabolism for cancer therapy. *Nat. Chem. Biol.* **11**, 9–15 (2015).
28. Sotgia, F. *et al.* Mitochondria 'fuel' breast cancer metabolism: Fifteen markers of mitochondrial biogenesis label epithelial cancer cells, but are excluded from adjacent stromal cells. *Cell Cycle* **11**, 4390–4401 (2012).
29. Martinez-Outschoorn, U. E. *et al.* Ketone bodies and two-compartment tumor metabolism: Stromal ketone production fuels mitochondrial biogenesis in epithelial cancer cells. *Cell Cycle* **11**, 3956–3963 (2012).
30. Jia, D., Park, J., Jung, K., Levine, H. & Kaipparettu, B. Elucidating the Metabolic Plasticity of Cancer: Mitochondrial Reprogramming and Hybrid Metabolic States. *Cells* **7**, 21 (2018).
31. Corbet, C. & Feron, O. Cancer cell metabolism and mitochondria: Nutrient plasticity for TCA cycle fueling. *Biochim. Biophys. Acta - Rev. Cancer* **1868**, 7–15 (2017).
32. Dong, L. F. *et al.* Mitochondrial targeting of vitamin E succinate enhances its pro-apoptotic and anti-cancer activity via mitochondrial complex II. *J. Biol. Chem.* **286**, 3717–3728 (2011).
33. Zielonka, J. *et al.* Mitochondria-Targeted Triphenylphosphonium-Based Compounds: Syntheses, Mechanisms of Action, and Therapeutic and Diagnostic Applications. *Chem. Rev.* **117**, 10043–10120 (2017).
34. Millard, M., Gallagher, J. D., Olenyuk, B. Z. & Neamati, N. A selective mitochondrial-targeted chlorambucil with remarkable cytotoxicity in breast and pancreatic cancers. *J. Med. Chem.* **56**, 9170–9179 (2013).
35. Zhang, X. Y. & Zhang, P. Y. Mitochondria targeting nano agents in cancer therapeutics (Review). *Oncol. Lett.* **12**, 4887–4890 (2016).
36. Ross, M. F. *et al.* Rapid and extensive uptake and activation of hydrophobic triphenylphosphonium cations within cells. *Biochem. J.* **411**, 633–645 (2008).
37. Millard, M. *et al.* Preclinical evaluation of novel triphenylphosphonium salts with

broad-spectrum activity. *PLoS One* **5**, (2010).
38. Michelakis, E. D., Webster, L. & Mackey, J. R. Dichloroacetate (DCA) as a potential metabolic-targeting therapy for cancer. *Br. J. Cancer* **99**, 989–994 (2008).
39. Kankotia, S. & Stacpoole, P. W. Dichloroacetate and cancer: New home for an orphan drug? *Biochim. Biophys. Acta - Rev. Cancer* **1846**, 617–629 (2014).
40. Pathak, R. K., Marrache, S., Harn, D. A. & Dhar, S. Mito-DCA: A mitochondria targeted molecular scaffold for efficacious delivery of metabolic modulator dichloroacetate. *ACS Chem. Biol.* **9**, 1178–1187 (2014).
41. Miles, J. M., Rule, A. D. & Borlaug, B. A. Use of metformin in diseases of aging. *Curr. Diab. Rep.* **14**, 1–16 (2014).
42. Boukalova, S. *et al.* Mitochondrial targeting of metformin enhances its activity against pancreatic cancer. *Mol. Cancer Ther.* **15**, 2875–2886 (2016).
43. Foretz, M., Guigas, B., Bertrand, L., Pollak, M. & Viollet, B. Metformin: From mechanisms of action to therapies. *Cell Metab.* **20**, 953–966 (2014).
44. Bridges, H. R., Jones, A. J. Y., Pollak, M. N. & Hirst, J. Effects of metformin and other biguanides on oxidative phosphorylation in mitochondria. *Biochem. J.* **462**, 475–487 (2014).
45. Liu, X., Romero, I. L., Litchfield, L. M., Lengyel, E. & Locasale, J. W. Metformin Targets Central Carbon Metabolism and Reveals Mitochondrial Requirements in Human Cancers. *Cell Metab.* **24**, 728–739 (2016).
46. Biasutto, L. *et al.* Development of mitochondria-targeted derivatives of resveratrol. *Bioorganic Med. Chem. Lett.* **18**, 5594–5597 (2008).
47. Reddy, C. A. *et al.* Mitochondrial-targeted curcuminoids: A strategy to enhance bioavailability and anticancer efficacy of curcumin. *PLoS One* **9**, (2014).
48. Han, M. *et al.* Mitochondrial delivery of doxorubicin via triphenylphosphine modification for overcoming drug resistance in MDA-MB-435/DOX cells. *Mol. Pharm.* **11**, 2640–2649 (2014).
49. Battogtokh, G., Cho, Y. Y., Lee, J. Y., Lee, H. S. & Kang, H. C. Mitochondrial-targeting anticancer agent conjugates and nanocarrier systems for cancer treatment. *Front. Pharmacol.* **9**, 1–20 (2018).
50. Basavaiah, D., Sharada, D. S., Kumaragurubaran, N. & Reddy, R. M. The Baylis-Hillman reaction: One-pot facile synthesis of 2,4-functionalized 1,4-pentadienes. *J. Org. Chem.* **67**, 7135–7137 (2002).
51. Bharadwaj, K. C. Intramolecular Morita-Baylis-Hillman and Rauhut-Currier reactions. A catalytic and atom economic route for carbocycles and heterocycles. *RSC Adv.* **5**, 75923–75946 (2015).
52. Wei, Y. & Shi, M. Recent advances in organocatalytic asymmetric morita-baylis-hillman/aza- morita-baylis-hillman reactions. *Chem. Rev.* **113**, 6659–6690 (2013).
53. Ma, G. N., Jiang, J. J., Shi, M. & Wei, Y. Recent extensions of the Morita-Baylis-Hillman reaction. *Chem. Commun.* 5496–5514 (2009). doi:10.1039/b909405a
54. Basavaiah, D., Venkateswara Rao, K. & Jannapu Reddy, R. The Baylis-Hillman reaction: A novel source of attraction, opportunities, and challenges in synthetic chemistry. *Chem. Soc. Rev.* **36**, 1581–1588 (2007).
55. Basavaiah, D. & Roy, S. Dimethyl sulfide induced [3 + 2] annulation strategy: An

efficient synthesis of functionalized dihydropyrazole derivatives using the Baylis-Hillman bromides. *Org. Lett.* **10**, 1819–1822 (2008).
56. Basavaiah, D. & Veeraraghavaiah, G. The Baylis-Hillman reaction: A novel concept for creativity in chemistry. *Chem. Soc. Rev.* **41**, 68–78 (2012).
57. Basavaiah, D., Reddy, K. R. & Kumaragurubaran, N. An expedient, facile and simple one-pot synthesis of 2-methylenealkanoates and alkanenitriles from the Baylis-Hillman bromides in aqueous media. *Nat. Protoc.* **2**, 2665–2676 (2007).
58. Baidya, M., Remennikov, G. Y., Mayer, P. & Mayr, H. SN2' versus SN2 reactivity: Control of regioselectivity in conversions of Baylis-Hillman adducts. *Chem. - A Eur. J.* **16**, 1365–1371 (2010).
59. Kaye, P. T. *Applications of the Morita–Baylis–Hillman Reaction in the Synthesis of Heterocyclic Systems*. *Advances in Heterocyclic Chemistry* **127**, (Elsevier Inc., 2019).
60. Suman, P. *et al.* Synthesis and cytotoxicity of Baylis-Hillman template derived betulinic acid-triazole conjugates. *Tetrahedron* **73**, 4214–4226 (2017).
61. Ronayne, C. T. *et al.* Synthesis and biological evaluation of 2-alkoxycarbonylallyl esters as potential anticancer agents. *Bioorganic Med. Chem. Lett.* **27**, 776–780 (2017).
62. Jonnalagadda, S. *et al.* Novel N,N-dialkyl cyanocinnamic acids as monocarboxylate transporter 1 and 4 inhibitors. *Oncotarget* **10**, 2355–2368 (2019).
63. Nicholas, D. *et al.* Advances in the quantification of mitochondrial function in primary human immune cells through extracellular flux analysis. *PLoS One* **12**, 1–19 (2017).
64. Decleer, M. *et al.* Oxygen consumption rate analysis of mitochondrial dysfunction caused by bacillus cereus cereulide in Caco-2 and hepG2 cells. *Toxins (Basel).* **10**, (2018).
65. Marchetti, P., Guerreschi, P., Mortier, L. & Kluza, J. Integration of Mitochondrial Targeting for Molecular Cancer Therapeutics. *Int. J. Cell Biol.* **2015**, (2015).
66. To, M. S. *et al.* Mitochondrial uncoupler FCCP activates proton conductance but does not block store-operated Ca2+ current in liver cells. *Arch. Biochem. Biophys.* **495**, 152–158 (2010).
67. Palorini, R., Simonetto, T., Cirulli, C. & Chiaradonna, F. Mitochondrial complex i inhibitors and forced oxidative phosphorylation synergize in inducing cancer cell death. *Int. J. Cell Biol.* **2013**, (2013).
68. Turunen, M., Olsson, J. & Dallner, G. Metabolism and function of coenzyme Q. *Biochim. Biophys. Acta - Biomembr.* **1660**, 171–199 (2004).
69. Walter, P. & Lardy, H. A. Effect of Antimycin A on Oxidative Phosphorylation with Ferricyanide as Electron Acceptor. *Biochemistry* **3**, 812–816 (1964).